

Numerical Modelling of a Deep Geological Repository Using the In-Floor Borehole Placement Method

NWMO TR-2007-14

December 2007

Ruiping Guo

Atomic Energy of Canada Limited

nwmo

NUCLEAR WASTE
MANAGEMENT
ORGANIZATION

SOCIÉTÉ DE GESTION
DES DÉCHETS
NUCLÉAIRES



Nuclear Waste Management Organization
22 St. Clair Avenue East, 6th Floor
Toronto, Ontario
M4T 2S3
Canada

Tel: 416-934-9814
Web: www.nwmo.ca

**Numerical Modelling of a Deep Geological Repository Using the In-Floor Borehole
Placement Method**

Report No.: NWMO TR-2007-14

December 2007

R. Guo
Atomic Energy of Canada Limited

Disclaimer:

This report does not necessarily reflect the views or position of the Nuclear Waste Management Organization, its directors, officers, employees and agents (the "NWMO") and unless otherwise specifically stated, is made available to the public by the NWMO for information only. The contents of this report reflect the views of the author(s) who are solely responsible for the text and its conclusions as well as the accuracy of any data used in its creation. The NWMO does not make any warranty, express or implied, or assume any legal liability or responsibility for the accuracy, completeness, or usefulness of any information disclosed, or represent that the use of any information would not infringe privately owned rights. Any reference to a specific commercial product, process or service by trade name, trademark, manufacturer, or otherwise, does not constitute or imply its endorsement, recommendation, or preference by NWMO.

ABSTRACT

Title: Numerical Modelling of a Deep Geological Repository Using the In-Floor Borehole Placement Method
Report No.: NWMO TR-2007-14
Author(s): R. Guo
Company: Atomic Energy of Canada Limited
Date: December 2007

Abstract

A series of three-dimensional finite element, thermal transient and thermal-mechanical stress analyses is performed to gain a better understanding of the behaviour of the plutonic rock mass in the near-field and far-field of a deep geological repository using an in-floor borehole placement method. For these analyses, the repository is conservatively assumed to be located at 1,000-m depth in granitic rock with characteristics similar to the sparsely fractured, highly stressed rock of the Whiteshell Research Area near Pinawa and Lac du Bonnet, Manitoba.

Three-dimensional near-field modelling using the thermal load corresponding to the gross thermal load and a far-field modelling using the dimensions of the in-room placement method are conducted using CODE_BRIGHT. The near-field and far field modelling results obtained in the present study appear to match reasonably well with those results from a previous modelling exercise performed using ABAQUS. Both results indicate that thermally acceptable repository layouts can be achieved using the in-floor borehole placement method.

Far-field thermal analyses are conducted for a repository with finite dimensions and for a repository with infinite horizontal dimensions, and the temperature results in the region of the placement room and borehole are compared. The differences in temperature between the far-field analyses are used to correct the temperatures from the near-field analyses, which simulate a repository with infinite horizontal dimensions. The temperature correction becomes significant about 1,000 years after container placement. Therefore, the results from near-field modelling using the boundary conditions for an infinite repository model can be used to represent the results for a finite repository for times less than 1,000 years.

Mechanical responses and stability of the rock around the placement room and the in-floor borehole are analysed by performing coupled thermal-mechanical near-field modelling. For the assumed depth, in situ stress and rock strength characteristics, and borehole diameter and spacing, the results imply that:

- excavation of the placement room will not cause failure in the rock, and
- drilling of the in-floor borehole may cause breakout and a zone of excavation damage near the in-floor borehole wall and in the rock on the placement room floor between adjacent boreholes.

Future conceptual designs for a deep geological repository using the in-floor borehole placement method will need to consider the physical and chemical characteristics of any proposed sites for long-term used fuel management.

TABLE OF CONTENTS

	<u>Page</u>
ABSTRACT	v
1. INTRODUCTION	1
2. DESCRIPTION OF PROPOSED DEEP GEOLOGICAL REPOSITORY	2
3. METHODS OF ANALYSES AND MATERIAL PROPERTIES.....	2
3.1 METHODS OF ANALYSES	2
3.2 ASSUMPTIONS.....	4
3.3 MATERIAL PROPERTIES.....	5
4. REPLICATION OF THE WORK CONDUCTED BY RWE NUKEM LIMITED	8
4.1 NEAR-FIELD MODELLING	8
4.1.1 Model Geometry, Thermal and Mechanical Boundary Conditions	8
4.1.1.1 Model Geometry	8
4.1.1.2 Thermal and Mechanical Boundary Conditions	8
4.1.2 Model Results from the Near-Field Modelling	12
4.2 FAR-FIELD MODELLING.....	13
4.2.1 Model Geometry, Thermal and Mechanical Boundary Conditions	13
4.2.1.1 Model Geometry	14
4.2.1.2 Thermal Boundary Conditions.....	15
4.2.1.3 Mechanical Boundary Conditions.....	16
4.2.2 Finite Element Discretization.....	16
4.2.3 Numerical Results from Far-Field Modelling	18
5. NUMERICAL RESULTS USING CODE_BRIGHT FOR A DEEP GEOLOGICAL REPOSITORY	19
5.1 FAR-FIELD MODELLING FOR A FINITE REPOSITORY	19
5.1.1 Far-Field Model Geometry	19
5.1.2 Far-Field Modelling Boundary Conditions	19
5.1.2.1 Far-Field Modelling Thermal Boundary Conditions	19
5.1.2.2 Far-Field Modelling Mechanical Boundary Conditions.....	19
5.1.3 Initial Conditions for the Far-Field Modelling	19
5.1.4 Far-Field Model Discretization.....	20
5.1.5 Far-Field Modelling Results	21
5.1.5.1 Thermal Results from the Far-Field Modelling	21
5.1.5.2 Mechanical Results from the Far-Field Modelling.....	26
5.2 INFLUENCE OF FINITE VERSUS INFINITE REPOSITORY MODEL ON THE CALCULATED THERMAL RESPONSE	44
5.3 NEAR-FIELD MODELLING	48
5.3.1 Thermal Near-Field Modelling.....	48
5.3.1.1 Model Geometry, Boundary Conditions and Initial Conditions.....	48
5.3.1.2 Thermal Near-Field Modelling Results	50
5.3.2 Thermal-Mechanical Near-field Modelling	56

5.3.2.1	Thermal-Mechanical Near-Field Model	56
5.3.2.2	Thermal Results from the Coupled Thermal-Mechanical Modelling	57
5.3.2.3	Near-Field Stresses	57
5.3.2.4	Near-Field Displacements.....	72
5.4	NEAR-FIELD STABILITY ANALYSES	75
6.	SUMMARY AND CONCLUSIONS.....	78
	ACKNOWLEDGEMENTS.....	79
	REFERENCES	81

LIST OF TABLES

	<u>Page</u>
Table 1: Heat Output of Containers of Reference Used CANDU Fuel at Different Times	6
Table 2: Thermal and Mechanical Parameters for the Materials Considered in the Modelling (RWE NUKEM Limited 2003b)	7
Table 3: Heat Output of Nuclear Waste per Container.....	12

LIST OF FIGURES

	<u>Page</u>
Figure 1: Sectional View of Placement Room using the In-Floor Placement Method	3
Figure 2: Placement Room showing General Arrangement of Sealign System Blocks and Used Fuel Containers	3
Figure 3: General Layout - Proposed Plan of In-Floor Borehole Method Deep Geological Repository	4
Figure 4: Finite Element Discretization of the Central Part of the Unit Cell for Near-Field Analyses.....	9
Figure 5: Thermal Boundary Conditions for Near-Field Unit Cell.....	10
Figure 6: Mechanical Boundary Conditions for Near-Field Unit Cell.....	11
Figure 7: Comparison of Near-field Modelling Temperature Results for an Infinite DGR using a Thermal Load Corresponding to the GTL	13
Figure 8: Perspective View of Far-Field Model of a DGR using the In-Room Placement Method	14
Figure 9: Thermal Boundary Conditions for Far-Field Model.....	15
Figure 10: Mechanical Boundary Conditions for Far-Field Model	16
Figure 11: Mesh for the Far-Field Thermal Model	17
Figure 12: Comparison of Simulated Temperatures from Far-Field Analyses using ABAQUS and CODE_BRIGHT for a Finite Repository	18
Figure 13: Geometric Model for the Far-Field Analyses of a DGR using the In-floor Borehole Placement Method.....	20
Figure 14: Far-Field Analyses Temperature Histories at Four Different Locations	21
Figure 15: Far-Field Analyses Temperature Profiles at Different Times along Horizontal Symmetric Line OR	22
Figure 16: Far-Field Analyses Temperature Rise Time Histories at Selected Points along the Vertical Line through the Repository Centre	22
Figure 17: Temperature Distributions along the Vertical Axis of the Repository	23
Figure 18: Temperature Profiles at Five Different Times.....	26
Figure 19: Profiles of Stresses in the X Direction along a Horizontal Line through the Repository Centre.....	27
Figure 20: Thermally Induced Stresses in the X Direction along a Horizontal Line through the Repository Centre.....	28
Figure 21: Profiles of Stresses in the Y Direction along a Horizontal Line through the Repository Centre.....	28
Figure 22: Thermally Induced Stresses in the Y Direction along a Horizontal Line through the Repository Centre.....	29

Figure 23: Profiles of Stresses in the Z Direction along a Horizontal Line through the Repository Centre.....	29
Figure 24: Thermally Induced Stresses in the Z Direction along a Horizontal Line through the Repository Centre	30
Figure 25: Profiles of Stresses in the X Direction along the Vertical Line through the Repository Centre.....	31
Figure 26: Thermally Induced Stresses in the X Direction along the Vertical Line through the Repository Centre	32
Figure 27: Profiles of Stresses in the Y Direction along the Vertical Line through the Repository Centre.....	32
Figure 28: Thermally Induced Stresses in the Y Direction along the Vertical Line through the Repository Centre	33
Figure 29: Profiles of Stresses in the Z Direction along the Vertical Line through the Repository Centre.....	33
Figure 30: Thermally Induced Stresses in the Z Direction along the Vertical Line through the Repository Centre	34
Figure 31: Thermally Induced Horizontal Stresses on the Ground Surface above the Repository Centre	35
Figure 32: Contours of Stresses in the X Direction on the Vertical Cross-Section through the Centre of the Repository at Four Different Times	36
Figure 33: Contours of Stresses in the Y Direction on the Vertical Cross-Section through the Centre of the Repository at Four Different Times	37
Figure 34: Contours of Stresses in the Z Direction on the Vertical Cross-Section through the Centre of the Repository at Four Different Times	38
Figure 35: Thermally Induced Maximum Principal Stresses at Different Times.....	39
Figure 36: Thermally Induced Minimum Principal Stresses at Different Times.....	40
Figure 37: Thermally Induced Vertical Displacements along the Vertical Line through the Repository Centre (Positive is upward)	41
Figure 38: Vertical Displacements along the Ground Surface	42
Figure 39: Thermally Induced Vertical Displacements with Time at Three Different Locations on the Ground Surface	42
Figure 40: Thermally Induced Vertical Displacements 8000 Years after Waste Placement with a Maximum Value of 0.203 m	43
Figure 41: Model Geometry for a Finite Repository with the Same Total Thermal Load without Considering the Auxiliary Unheated Spaces	44
Figure 42: Model Geometry for a Repository with Infinite Horizontal Dimensions and the Same Density of Thermal Load as a Repository with Finite Horizontal Dimensions	45
Figure 43: Comparison of the Central Temperature between a Finite Repository and an Infinite Repository and their Differences	46
Figure 44: Temperatures along Central Vertical Line for a Finite Repository	46
Figure 45: Temperatures along Vertical Axis for an Infinite Repository	47
Figure 46: Temperature Differences between an Infinite Repository Model and a Finite Repository Model	48
Figure 47: Locations for Presentation of Near-Field Modelling Results	49
Figure 48: Near-field Modelling Results for an Infinite DGR	50
Figure 49: Differences of Temperature at the Centre of a Repository between Infinite-Dimension Model and Finite-Dimension Model	51
Figure 50: Modified Results at Different Locations for a Finite Repository using a Thermal Load Corresponding to the PTL.....	52

Figure 51: Comparison of Original and Modified Near-field Temperatures at the Container Skin and Tunnel Crown for a Finite Repository using a Thermal Load Corresponding to the PTL.....	53
Figure 52: Modified Temperature Profiles along Line T at Different Times	53
Figure 53: Modified Temperature Profiles along Vertical Line through the Container Centre at Different Times	54
Figure 54: Temperature Contours in the Rock around a Container and the Tunnel at Four Different Times	55
Figure 55: Thermally Induced Stresses in the X Direction along Line M	57
Figure 56: Thermally Induced Stresses in the Y Direction along Line M.....	58
Figure 57: Thermally Induced Stresses in the Z Direction along Line M.....	58
Figure 58: Thermally Induced Stresses in the X Direction along Line L	59
Figure 59: Thermally Induced Stresses in the Y Direction along Line L	59
Figure 60: Thermally Induced Stresses in the Z Direction along Line L.....	60
Figure 61: Thermally Induced Stresses in the X Direction along Line T	60
Figure 62: Thermally Induced Stresses in the Y Direction along Line T	61
Figure 63: Thermally Induced Stresses in the Z Direction along Line T	61
Figure 64: Thermally Induced Stresses in the X Direction along Line N.....	62
Figure 65: Thermally Induced Stresses in the Y Direction along Line N.....	62
Figure 66: Thermally Induced Stresses in the Z Direction along Line N.....	63
Figure 67: Thermally Induced Stresses in the X Direction along Line CJ.....	63
Figure 68: Thermally Induced Stresses in the Y Direction along Line CJ	64
Figure 69: Profiles of Total Stresses in the X Direction along Line M.....	65
Figure 70: Profiles of Total Stresses in the Y Direction along Line M.....	65
Figure 71: Profiles of Total Stresses in the Z Direction along Line M.....	66
Figure 72: Profiles of Total Stresses in the X Direction along Line L.....	67
Figure 73: Profiles of Total Stresses in the Y Direction along Line L.....	67
Figure 74: Profiles of Total Stresses in the Z Direction along Line L.....	68
Figure 75: Profiles of Total Stresses in the X Direction along Line T.....	68
Figure 76: Profiles of Total Stresses in the Y Direction along Line T.....	69
Figure 77: Profiles of Total Stresses in the Z Direction along Line T.....	69
Figure 78: Profiles of Total Stresses in the X Direction along Line N	70
Figure 79: Profiles of Total Stresses in the Y Direction along Line N	70
Figure 80: Profiles of Total Stresses in the Z Direction along Line N	71
Figure 81: Profiles of Total Stresses in the X Direction along Line CJ	71
Figure 82: Profiles of Total Stresses in the Y Direction along Line CJ	72
Figure 83: Thermally Induced Displacements in the Z Direction along Line M	72
Figure 84: Thermally Induced Displacements in the X Direction along Line L.....	73
Figure 85: Thermally Induced Displacements in the X Direction along Line T.....	74
Figure 86: Thermally Induced Displacements in the Y Direction along Line N	74
Figure 87: Safety Factors along Line M at Four Different Times	75
Figure 88: Safety Factors along Line L at Four Different Times	76
Figure 89: Safety Factors along Line T at Four Different Times.....	76
Figure 90: Safety Factors along Line N at Four Different Times	77
Figure 91: Safety Factors along Line CJ at Four Different Times.....	78

1. INTRODUCTION

The Adapted Phased Management (APM) approach proposed by the Nuclear Waste Management Organization (NWMO) and accepted by the Government of Canada (NRCAN 2007) for long term management of Canada's used nuclear fuel (NWMO 2005) includes eventual interment of the waste in engineered excavations 500 to 1,000 m deep in plutonic rock (AECL 1994) or sedimentary rock. A design concept for deep geological placement of used CANDU fuel was first developed by Atomic Energy of Canada Limited (AECL) during the period of 1978 to 1996, under the Canadian Nuclear Fuel Waste Management Program. The waste owners and the NWMO have continued to develop the deep geological repository (DGR) concept for the long-term safe management of used fuel. An updated conceptual design and cost estimate for a DGR based on an in-room placement method was prepared in 2002 (CTECH 2002). The Canadian DGR concept using the in-floor borehole placement method for used fuel containers was developed by RWE NUKEM Limited (2003a) based on the Swedish SKB KBS-3V design (Birgersson et al. 2001).

In the past, a series of conceptual design studies for a deep geological repository have been carried out (Acres et al. 1985, 1993; Golder Associates Ltd. 1993; Tsai 1986; Tsui and Tsai 1982; 1985; 1994a, b, c). These studies include two-dimensional and three-dimensional thermal transient and thermal-mechanical analyses for the far-field and near-field of a repository. RWE NUKEM Limited (2003b) also conducted thermal and mechanical analyses for in-floor placement of spent nuclear fuel in a DGR using ABAQUS (a finite element computer program) as part of the assessment of the updated conceptual design for in-floor placement of spent nuclear fuel in a DGR.

In order to further develop the technology, a new assessment of the structural performance of a DGR using the in-floor borehole placement is presented in this report and is compared to the RWE NUKEM Limited analyses. This assessment consists of the thermal and mechanical modelling of a DGR using the in-floor placement method for used fuel containers including the following tasks.

- Far-field, three-dimensional thermal and thermal-mechanical analyses for one quarter of a rectangular parallelepiped-shaped repository with model dimensions of 4.2 m x 695 m x 725 m, which includes all the non-heat-generating areas of the overall DGR area, and with the thermal load corresponding to the gross thermal load (GTL).
- Far-field, three-dimensional thermal analyses for one quarter of a finite-dimensional rectangular parallelepiped-shaped repository with model dimensions of 4.2 m x 560 m x 600 m and with the thermal load corresponding to the panel thermal load (PTL), which is calculated based on a smaller derived DGR area with the non-heat-generating areas removed.
- Far-field, three-dimensional thermal analyses for a horizontally infinite-dimensional rectangular parallelepiped-shaped repository with thermal load corresponding to the PTL.
- Near-field, three-dimensional mechanical analyses for an excavated condition under ambient temperature.
- Near-field, three-dimensional thermal analyses for the sealed condition under elevated temperature.
- Near-field, three-dimensional thermal-mechanical analyses for the sealed condition under elevated temperature.

This report includes the following contents.

- Description of the modelled DGR scenarios.
- Material properties.
- Replication of the numerical work conducted by RWE NUKEM Limited (RWE NUKEM Limited uses COMPASS and the replication in this report is done using CODE_BRIGHT).
- Numerical modelling results using CODE_BRIGHT for an in-floor DGR.
- Summary and Conclusions.

2. DESCRIPTION OF PROPOSED DEEP GEOLOGICAL REPOSITORY

The modelled deep geological repository (DGR) layout consists of an array of horizontal, elliptically shaped placement rooms with an aspect ratio (width to height) of approximately 1.7 (Figure 1) (RWE NUKEM Limited 2003b). The placement room is set at 4.05 m high and 6.89 m wide. The placement rooms are connected by access tunnels for moving excavated rock, waste containers and backfilling materials. These rooms are arranged into four distinct sections. Each section consists of 40 rooms (spaced at 30 m centre-to-centre), each containing 70 in-floor boreholes. Each container is placed in a borehole positioned along the centreline of the placement room floor at a spacing of 4 m (Figure 2). Each container is 3,867 mm long with a diameter of 1,168 mm and will accommodate 324 fuel bundles. The container design consists of a 25-mm-thick copper outer corrosion-barrier and an inner, carbon steel load-bearing component (Maak 2006). A DGR has a maximum total capacity of 11,232 used fuel containers (UFCs) or 3,639,168 intact fuel bundles.

Stresses around elliptical placement rooms are influenced by the ratio of the major and minor axes of the ellipse and the orientation of the ellipse to the major and minor principal stresses in the rock mass. In order to minimize the tangential stress concentrations around the room, the placement room should be oriented such that its axis is parallel to the maximum principal stress direction and the major axis of the elliptical cross section is parallel to the intermediate principal stress direction. The overall dimensions of the UFC placement area are 1,434 m by 1,390 m as shown in Figure 3. The repository is located in granite rock at a depth of 1,000 m with geological and hydrogeologic conditions similar to those of the sparsely fractured rock of the Whiteshell Research Area near Pinawa, Manitoba.

3. METHODS OF ANALYSES AND MATERIAL PROPERTIES

3.1 METHODS OF ANALYSES

This study is performed using CODE_BRIGHT, a coupled thermo-hydro-mechanical (THM) finite element computer program. CODE_BRIGHT is developed by Universidad Polit cnica de Catalu a (UPC) (Olivella et al. 1996). CODE_BRIGHT is a commercial finite-element program for modelling coupled THM processes in geological media, including moisture transfer in unsaturated soils. GiD is used for pre-processing and post-processing the CODE_BRIGHT input and output data. GiD is a commercial graphical user interface, developed by the International Centre for Numerical Methods in Engineering, for the definition, preparation and visualization of the data related to numerical simulations.

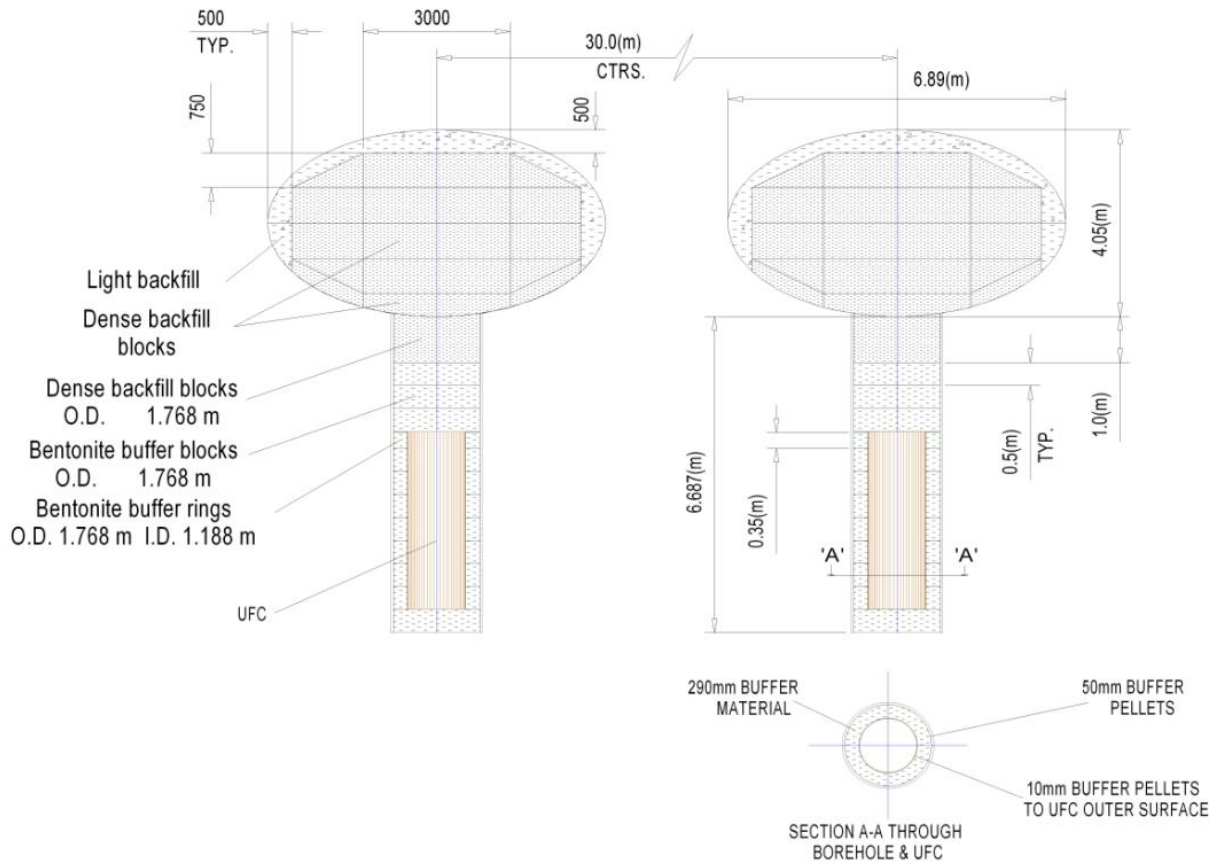


Figure 1: Sectional View of Placement Room using the In-Floor Placement Method (RWE NUKEM Limited 2003b)

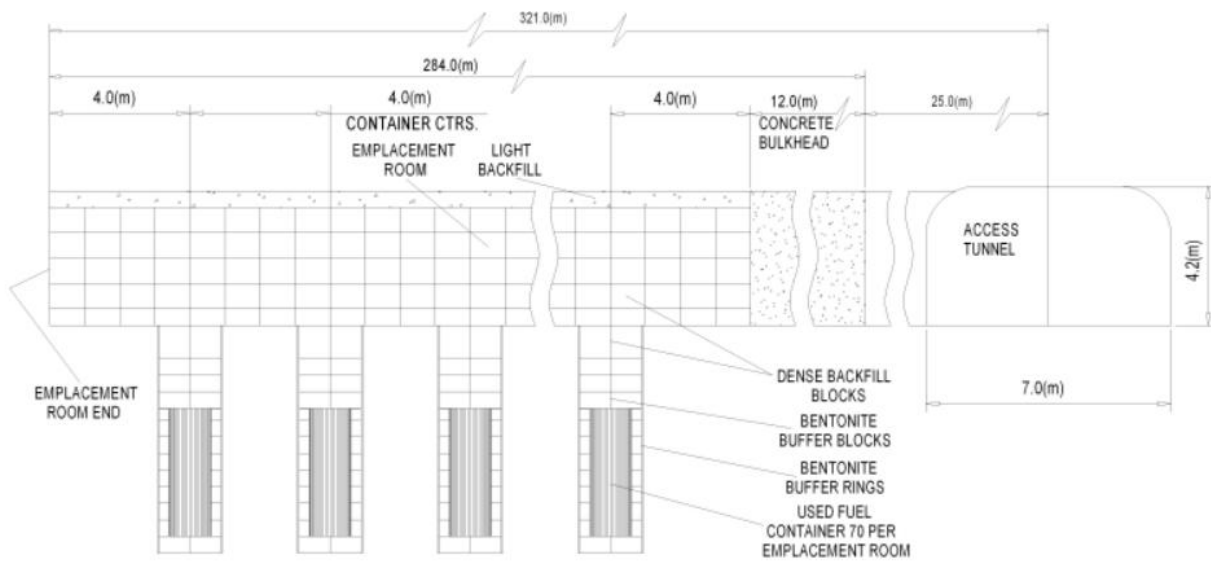


Figure 2: Placement Room showing General Arrangement of Sealing System Blocks and Used Fuel Containers (RWE NUKEM Limited 2003b)

3.2 ASSUMPTIONS

In this study, all of the materials included in the modelling are assumed to be homogeneous, isotropic and linearly elastic within each type of material. The thermal and mechanical properties of all of these materials are further assumed to be temperature-independent. The rock mass around the DGR is assumed to be infinite in the horizontal extent.

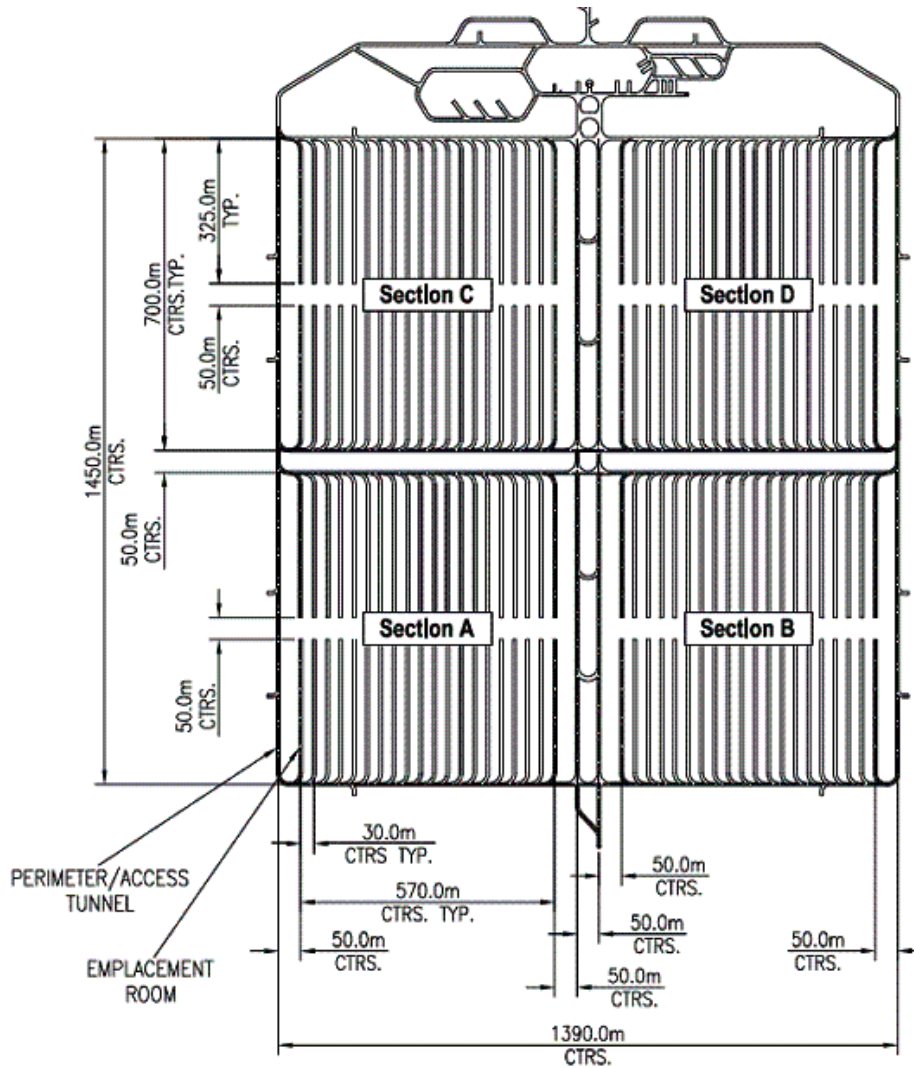


Figure 3: General Layout - Proposed Plan of In-Floor Borehole Method Deep Geological Repository (RWE NUKEM Limited 2003a)

The Hoek and Brown empirical failure criterion (Hoek and Brown 1980 and 1988) is adopted to evaluate the stability of the rock mass near the placement tunnel and the in-floor borehole. The empirical equation of the Hoek and Brown failure criterion is given by:

$$\sigma_{1f} = \sigma_3 + (m \cdot \sigma_c \cdot \sigma_3 + s \cdot \sigma_c^2)^{\frac{1}{2}} \quad (1)$$

where σ_{1f} is the major principal stress at failure;

σ_3 is the minor principal stress;

σ_c is the uniaxial compressive strength of the intact rock materials from which the rock mass is made up; and

m and s are empirical constants.

There are two sets of parameters used in the Hoek and Brown's failure criterion as first used by Baumgartner et al. (1995). The first set of parameters, applied during excavation, is for a condition below which no damage occurs to the rock. They are: $m = 16.6$, $s = 1$ and $\sigma_c = 100$ MPa. The second set of parameters is used for the peak strength of the undamaged rock under the full thermal-mechanical loads. These strength parameters can only be applied if the rock excavation stresses do not exceed the initial design parameters during excavation. They are: $m = 25$, $s = 1$ and $\sigma_c = 150$ MPa (Baumgartner et al. 1995).

3.3 MATERIAL PROPERTIES

USED FUEL PROPERTIES

Each DGR has a maximum total capacity of 11,232 UFCs. The heat output from the used fuel in each UFC is as shown in Table 1. All of used fuel is assumed to undergo an initial cooling period of 30 years in surface facilities prior to placement within the DGR.

Table 1: Heat Output of Containers of Reference Used CANDU Fuel at Different Times

Time out of reactor (years)	Container heat output (W) 324 bundles per container
30	1138.61
40	961.40
50	821.06
60	708.48
75	580.06
100	440.84
150	310.88
200	258.73
300	221.19
500	180.99
1,000	125.27
10,000	44.48
100,000	2.55
1,000,000	0.92
10,000,000	0.62

(Table 1 concluded)

ROCK MASS PROPERTIES

The material properties of the rock mass are based on measurements from Lac du Bonnet granite at the Underground Research Laboratory (Martin 1993) and are included in Table 2.

SEALING MATERIAL PROPERTIES

There are four bentonite clay-based sealing materials for the in-room placement design: buffer material, dense backfill, light backfill and buffer pellets. For the in-floor placement method, the buffer is placed around the container in the form of close-fitting, pre-compacted rings. The 10-mm gap between the UFC and the buffer rings, and the 50-mm gap between the rings and the rock formation will be filled using a pelleted form of the buffer material. The specifications for the basic physical properties of clay-based sealing materials are presented in Table 2.

Table 2: Thermal and Mechanical Parameters for the Materials Considered in the Modelling (RWE NUKEM Limited 2003b)

Property	Lac du Bonnet Granite ¹	Buffer	Buffer Pellets	Dense backfill	Light backfill
Composition	N/A ²	100% bentonite	100% bentonite	70:25:5 aggregate, clay, bentonite	50:50 bentonite, crushed granite sand
Thermal conductivity (W/m°C)	3.00	1.10	0.5	2.00	0.70
Specific heat (J/kg°C)	845	1320	910	1100	1280
Bulk Density (kg/m ³)	2650	1860	1410	2280	1400
Dry Density (kg/m ³)	2650	1610	1410	2120	1240
Porosity (%)	N/A	41	49	22	55
Saturation Level (%)	N/A	65	6	80	33
Moisture content (Gravimetric, %)	N/A	17	2	8.5	15
Young's modulus (GPa)	50	0.10	0.10	0.20	0.10
Poisson's ratio	0.10	0.10	0.10	0.10	0.10
Coefficient of thermal expansion (10 ⁻⁶ /°C)	10	N/A	N/A	N/A	N/A

¹ P. Baumgartner *et al* "The in-room emplacement method for a used fuel disposal facility – preliminary design consideration", AECL TR-655, COG-94-533, 1995

² not applicable.

4. REPLICATION OF THE WORK CONDUCTED BY RWE NUKEM LIMITED

For the purpose of comparison of numerical results using CODE_BRIGHT with numerical results from the modelling performed by RWE NUKEM Limited using ABAQUS, the numerical model described in this section has the same dimensions and the same heat input as those used in the RWE NUKEM Limited report (2003b).

4.1 NEAR-FIELD MODELLING

4.1.1 Model Geometry, Thermal and Mechanical Boundary Conditions

4.1.1.1 Model Geometry

The finite element discretization of a unit cell using the in-floor borehole method for the near-field modelling is shown in Figure 4. There are six kinds of materials: granite rock; light backfill, dense backfill blocks, bentonite buffer blocks, container and bentonite pellets. The dimensions of the tunnel and the in-floor borehole are the same as shown in Figure 1. The horizontal dimensions of a unit cell are 15 m x 2 m. The vertical dimension of the model unit cell is 10,000 m. The depth of the crown of the tunnel is 1,000 m. There are 25,948 nodes and 21,895 eight-noded solid elements in this numerical model. The elements are more densely distributed in the region of interest as shown in Figure 4 (near the placement tunnel room and the in-floor borehole). Dimensions of a typical solid element around the in-floor borehole are approximately 0.15 m x 0.18 m x 0.28 m.

4.1.1.2 Thermal and Mechanical Boundary Conditions

Thermal Boundary Conditions shown in Figure 5 are as follows.

- On the top surface (ground surface), the temperature is 5°C for the first 10,000 years. After 10,000 years, the temperature is 0°C.
- On the bottom of the model, an isothermal condition is applied with a temperature of 125°C.
- On the four side surfaces, an adiabatic condition is applied.
- At the nodes (11 nodes) located on the central line corresponding to the location of the axis of the container, a uniform thermal load is applied. The total thermal load applied on the 11 nodes is equivalent to the GTL of a far-field model. This thermal load is the ratio of the panel area to ¼ of overall repository area, which is 0.82, multiplied by 1/4 of the container thermal load, which is the heat emitted into the model quadrant for a horizontal unit area of 15 m x 2 m as shown in Table 3.

Mechanical Boundary Conditions shown in Figure 6 are as follows.

- The ground surface is free to move in the vertical direction.
- The four side surfaces are fixed in the horizontal direction.
- The bottom surface is fixed in the vertical direction.

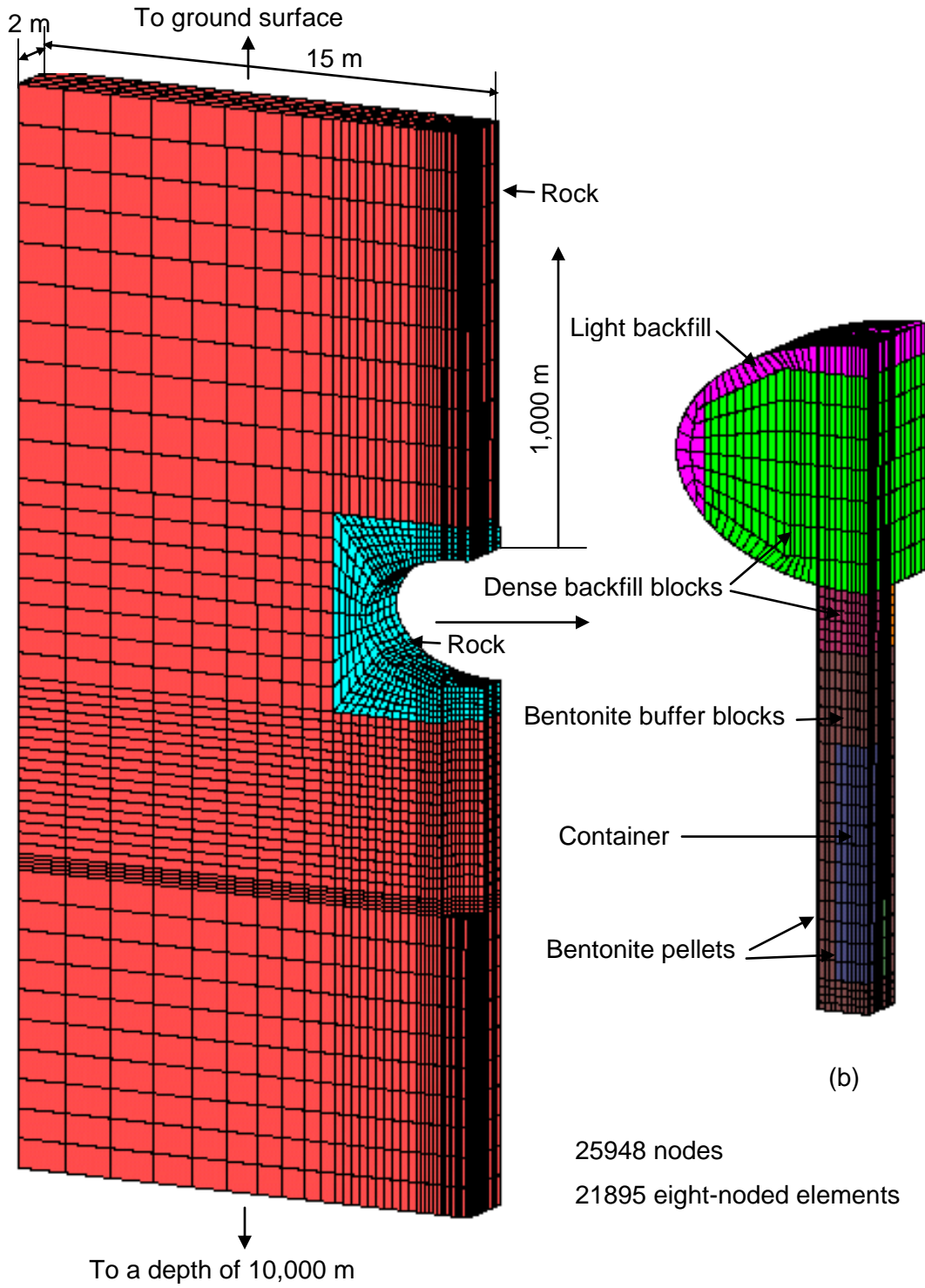


Figure 4: Finite Element Discretization of the Central Part of the Unit Cell for Near-Field Analyses

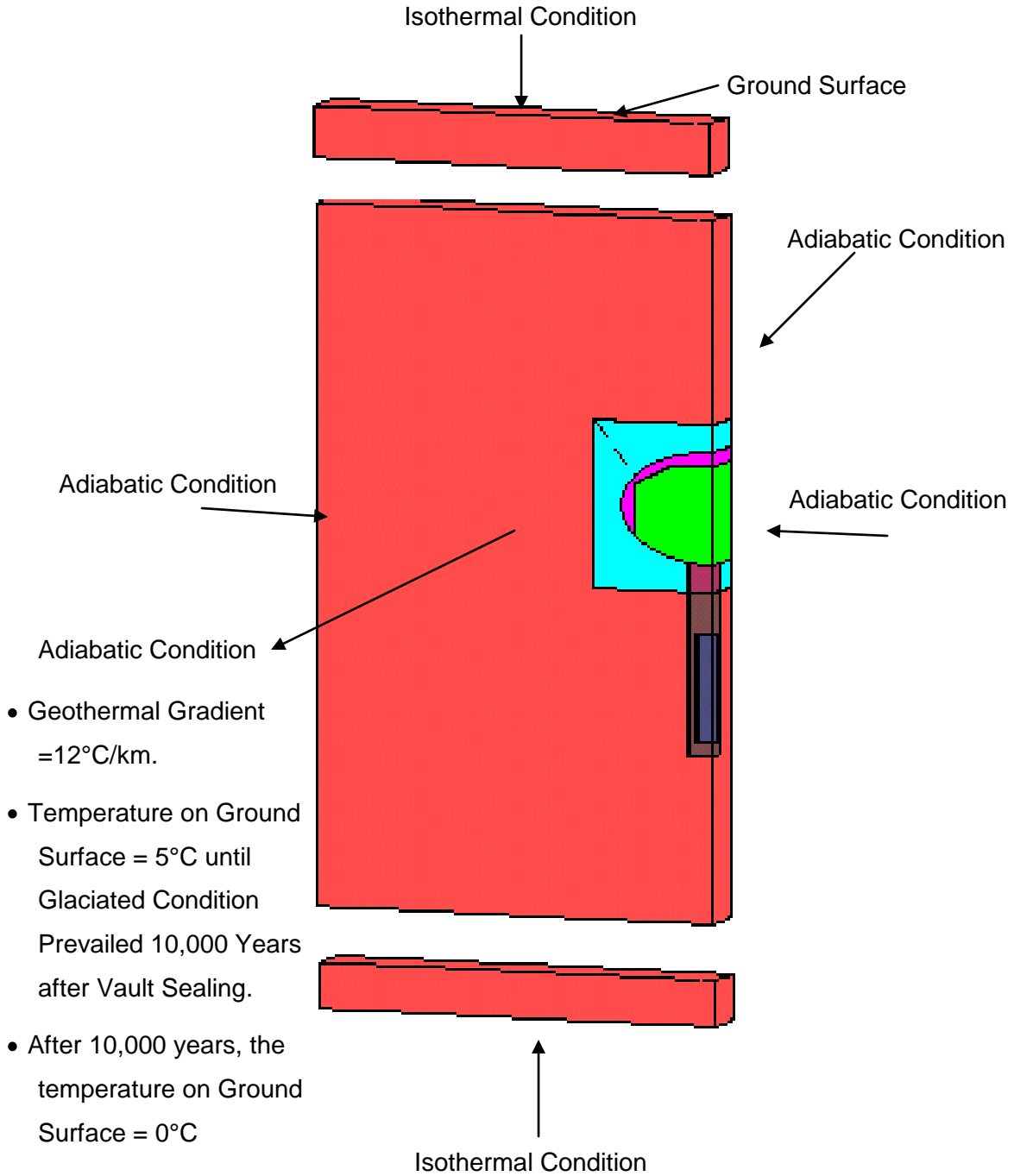


Figure 5: Thermal Boundary Conditions for Near-Field Unit Cell

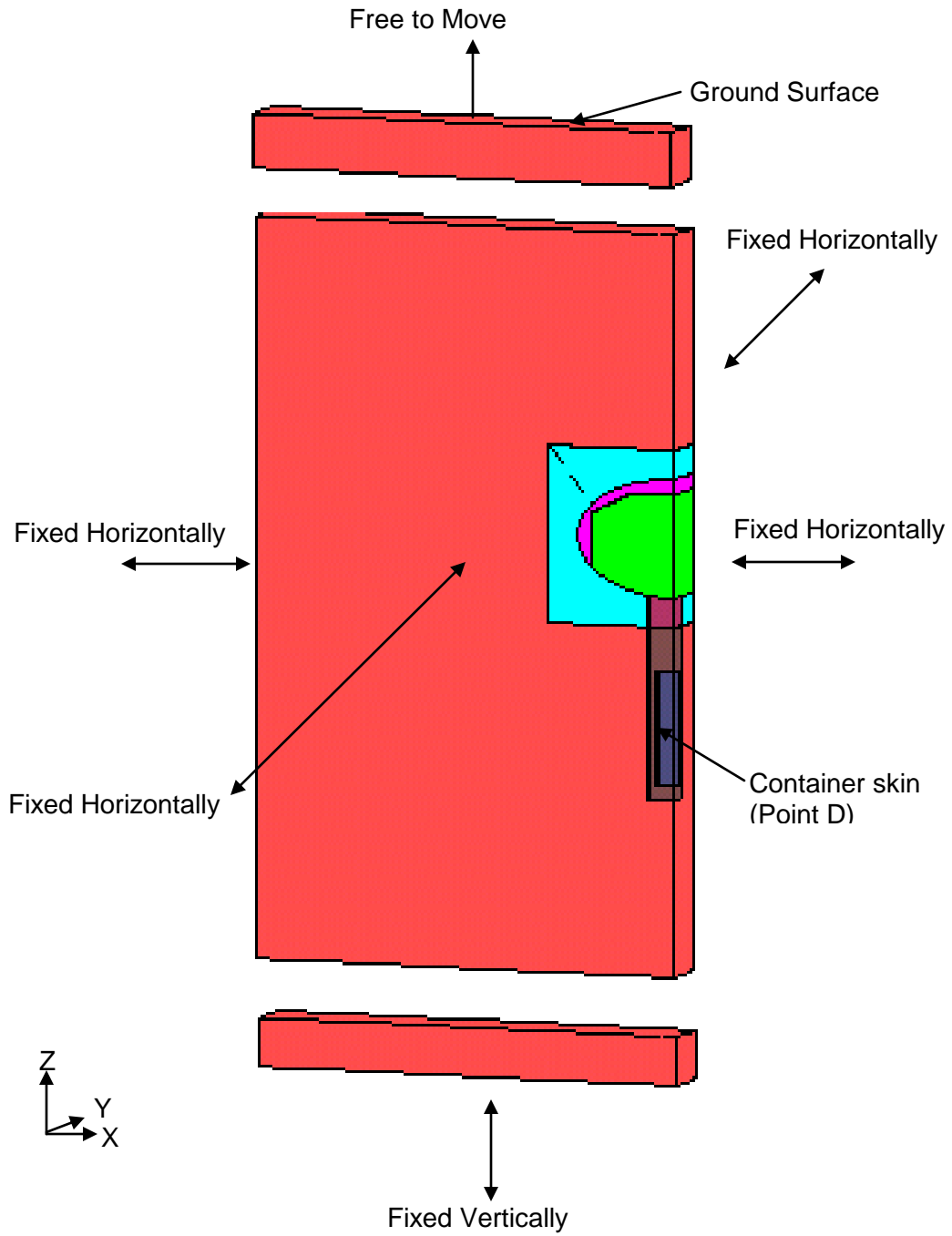


Figure 6: Mechanical Boundary Conditions for Near-Field Unit Cell

Table 3: Heat Output of Nuclear Waste per Container

Time (years)	Container heat output (W) (PTL)	0.82 x Container heat output (W) (GTL)
0	1138.6	932.5
1	1120.9	918.0
4	1067.7	874.5
10	961.4	787.4
20	821.1	672.4
40	622.4	509.7
70	440.8	361.0
105	349.0	285.8
140	289.2	236.9
190	250.5	205.2
300	215.0	176.1
420	190.9	156.3
570	169.9	139.1
770	147.6	120.9
970	125.3	102.6
1230	122.7	100.5
1500	120.2	98.5
2000	115.8	94.8
2500	111.3	91.1
3000	106.8	87.5
4200	96.0	78.6
6000	79.8	65.4
8000	61.9	50.7
10500	44.3	36.2
13000	43.1	35.3
16000	41.7	34.1
20000	39.8	32.6
25000	37.5	30.7
40000	30.5	25.0
60000	21.2	17.4
85000	9.5	7.8
100000	2.6	2.1
300000	2.2	1.8
500000	1.8	1.5
1000000	0.9	0.8
3000000	0.9	0.7
10000000	0.6	0.5

4.1.2 Model Results from the Near-Field Modelling

RWE NUKEM Limited used the heat input, which is equivalent to the load acting on a horizontal area of 15 m x 2 m with the thermal density corresponding to the GTL of a far-field model, to get the thermal response at different locations for the near field modelling using ABAQUS. The same thermal load shown in Table 3 is used to conduct the near field modelling using CODE_BRIGHT. The simulated temperatures on the skin of the container and the crown

location of the tunnel using CODE_BRIGHT match the results from the ABAQUS model as shown in Figure 7. There are two factors that must be considered when using the information in Figure 7.

- (1) The near-field modelling results presented underestimate the temperatures because RWE NUKEM (2003b) used the GTL rather than the PTL for their analyses.
- (2) The near-field model shown in Figure 4 represents a repository that is infinite in horizontal extent (i.e., in the model there is no heat losses at the edge of the repository) therefore, at longer times, the temperatures are overestimated because of the absence of heat losses at the edge of the repository².

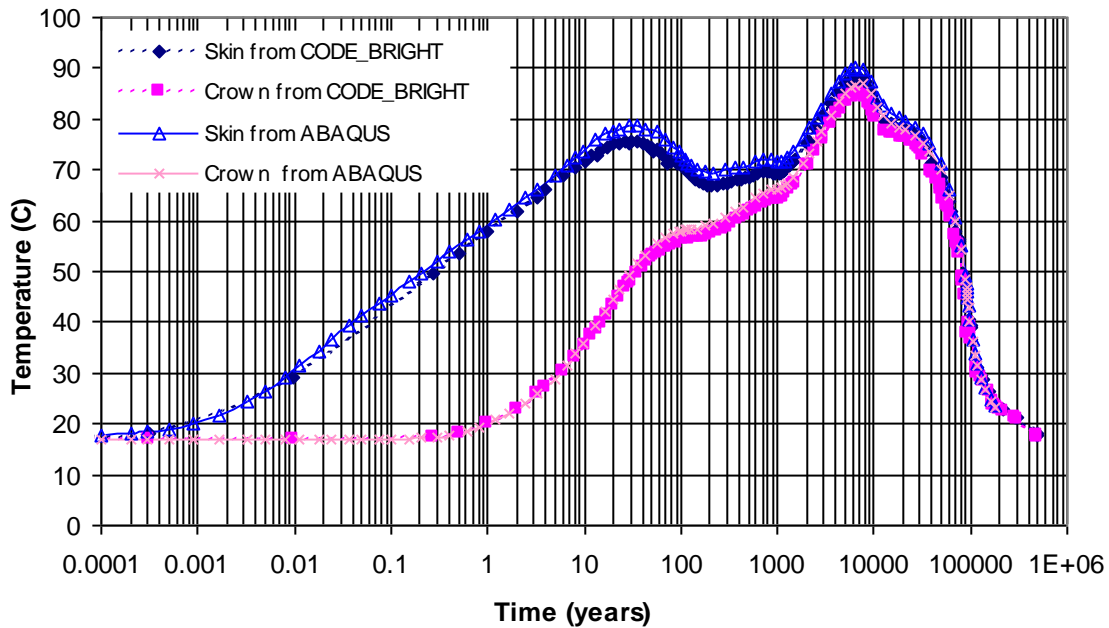


Figure 7: Comparison of Near-field Modelling Temperature Results for an Infinite DGR using a Thermal Load Corresponding to the GTL

4.2 FAR-FIELD MODELLING

4.2.1 Model Geometry, Thermal and Mechanical Boundary Conditions

Far-field analysis can provide an assessment of the thermal and stress conditions in the rock mass at some distance away from a repository having finite dimensions. It can also estimate the uplift of the rock on the ground surface to help evaluate the potential for rock fracturing due to the thermal expansion of the formations proximate to the repository.

² Unpublished thermal comparisons have been made between near-field, three-dimensional finite-element analyses assuming a near-field unit cell of a repository with adiabatic boundary conditions on the horizontal boundaries (Wai and Tsai 1995, Tsui and Tsai 1994a) and corresponding HOTROK analyses (e.g., HOTROK is an analytical solution for simple, finite-sized repository configurations (Mathers 1985)). These comparisons have shown that the near-field unit cell treats the repository as having infinite horizontal extent, which tends to over predict the container temperature and its time of occurrence.

4.2.1.1 Model Geometry

The perspective view of the far-field model of a repository using the in-room placement method is shown in Figure 8. Due to symmetry, only a quarter section of a DGR needs to be modelled. The model is bounded vertically by the ground surface on the upper side and by a plane 10,000 m from the ground surface, at the bottom. The horizontal dimensions of the model in the X and Y directions are 5,000 m x 5,000 m. These dimensions are considered to be sufficient such that the temperature and mechanical response of the rock at the boundaries remain unaffected by the presence of the DGR during the simulation time period. The DGR is represented by a plate of material providing the required heat loading, although details of the placement rooms are not included. The horizontal dimensions of a quarter of a DGR are 639 m x 642 m and it is 4.2 m thick, the same as that used in the ABAQUS modelling by RWE NUKEM Limited. The thermal load corresponds to the GTL.

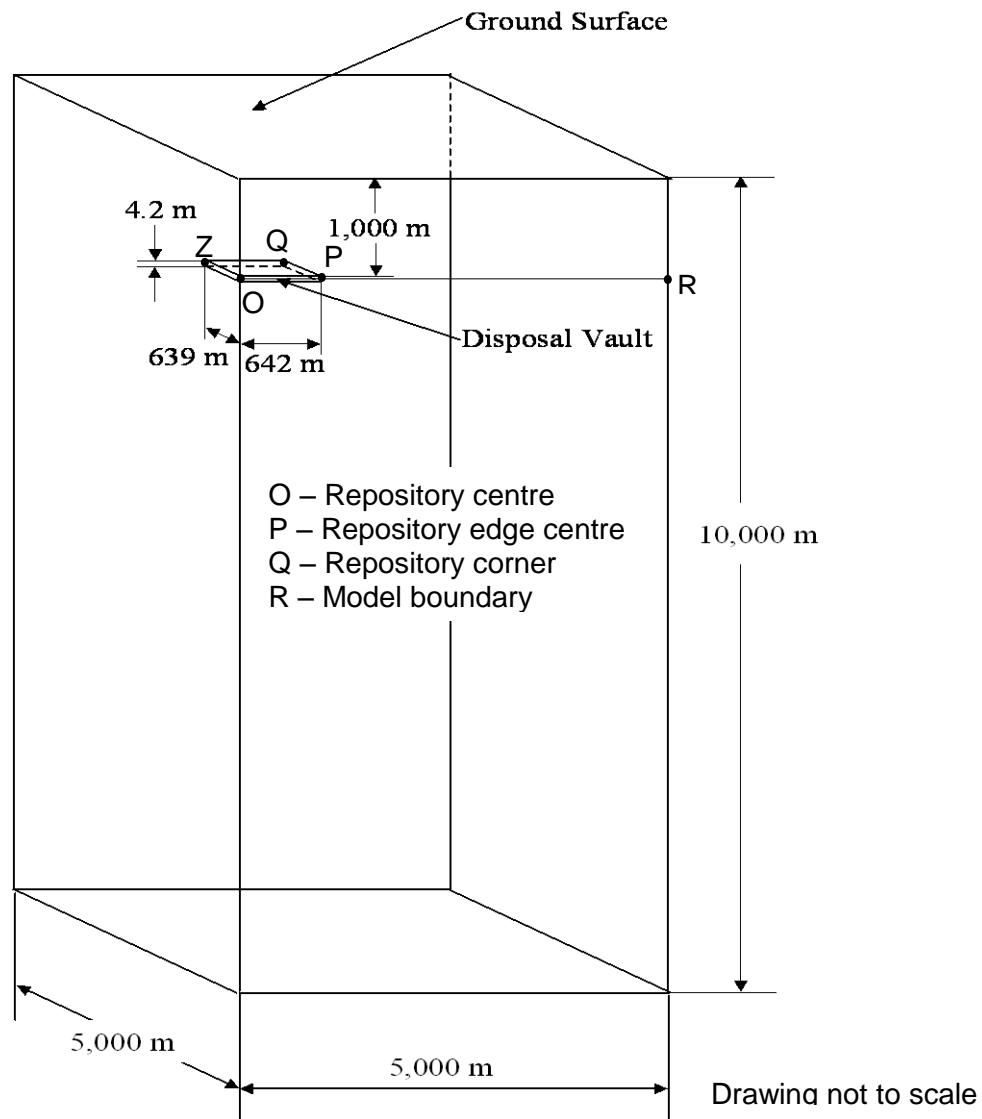


Figure 8: Perspective View of Far-Field Model of a DGR using the In-Room Placement Method

4.2.1.2 Thermal Boundary Conditions

As with the near-field model, the thermal boundary conditions are defined as follows (Figure 9).

- The upper surface boundary condition is modelled as an isothermal boundary, with a temperature of 5°C, representing the average Canadian Shield surface temperature, reducing to 0°C after 10,000 years to account for a period of glaciation.
- The lower boundary is also modelled as an isothermal boundary, such that a geothermal gradient of 0.012°C/m of depth is achieved in the absence of a repository. The bottom surface of the model is set at a constant temperature of 125°C.
- The vertical boundaries are modelled as adiabatic planes of symmetry as shown in Figure 9.
- Heat generated from individual disposal rooms throughout the one-quarter of the repository is distributed evenly over the entire volume of this rectangular plate of 639 m x 642 m x 4.2 m (4.2 m is the height of the placement rooms).

Isothermal 5°C (0°C during glaciation, beginning at 10,000 years)

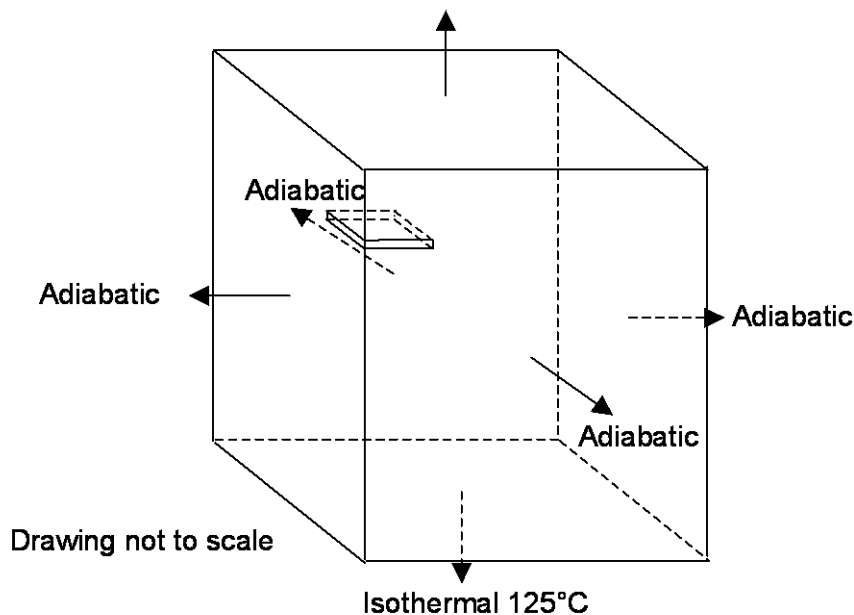


Figure 9: Thermal Boundary Conditions for Far-Field Model

4.2.1.3 Mechanical Boundary Conditions

The mechanical boundary conditions are defined as follows (Figure 10)

- The vertical planes of the model are constrained not to move in the horizontal direction.
- The bottom plane of the model is fixed in the vertical direction.
- The upper horizontal plane, the ground surface, is free to move in the vertical direction.

The model is representative of a DGR positioned in an infinite extent of granite.

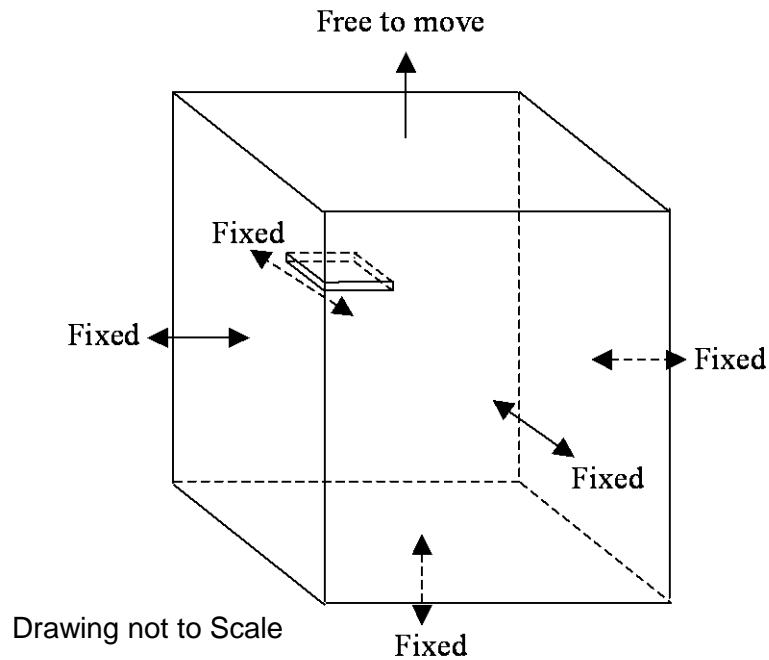


Figure 10: Mechanical Boundary Conditions for Far-Field Model

4.2.2 Finite Element Discretization

The finite element discretization of the far-field model is shown in Figure 11. The domain is discretized such that the elements are more densely distributed in the rock mass just above and beneath the repository level. Dimensions of a typical element in the repository are 42.6 m x 42.8 m x 0.62 m. The model has 22,984 nodes and 20,625 eight-noded elements.

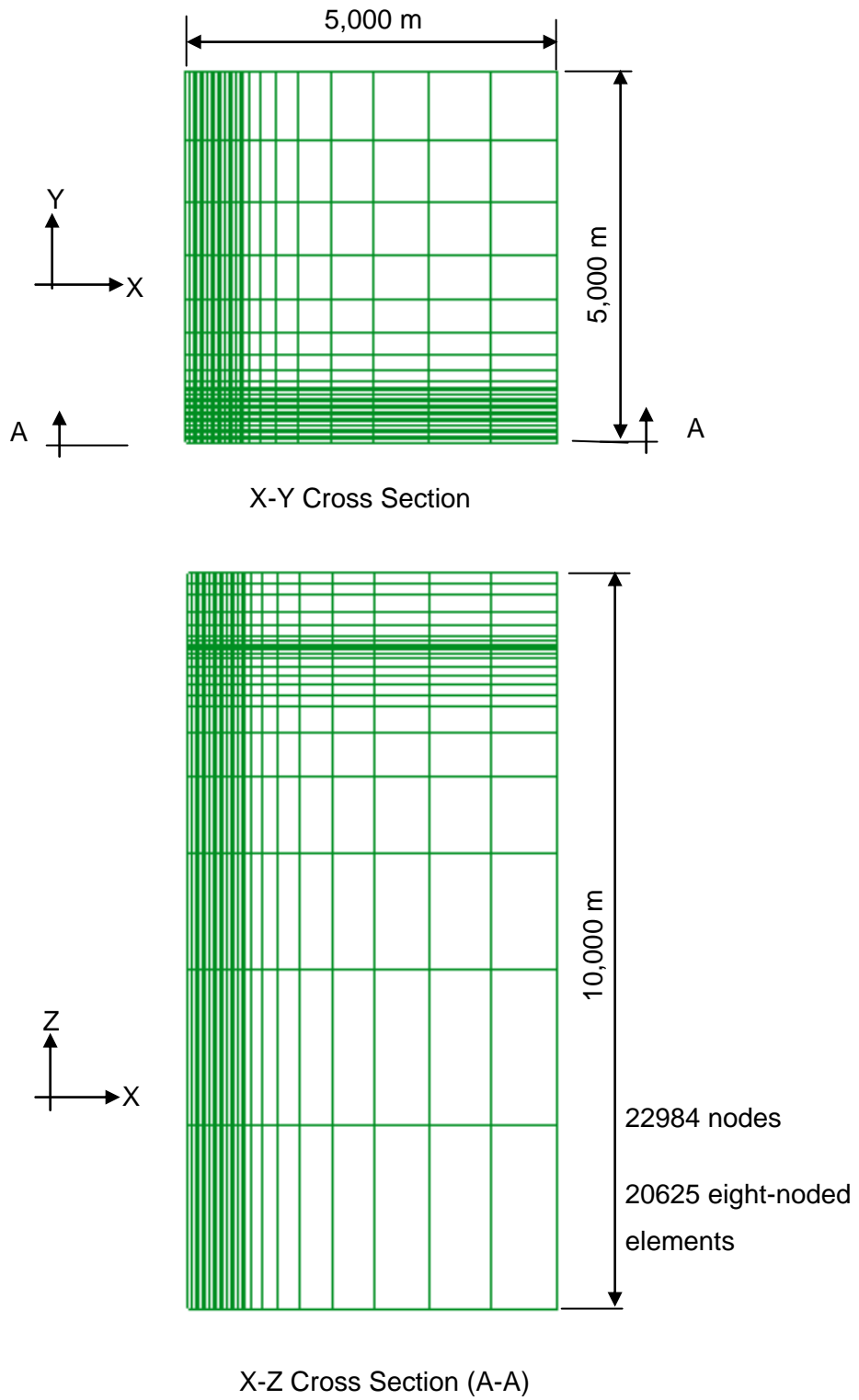


Figure 11: Mesh for the Far-Field Thermal Model

4.2.3 Numerical Results from Far-Field Modelling

RWE NUKEM Limited conducted their far-field modelling using ABAQUS using the dimensions for a DGR using the in-room placement method. Their results are compared with new analyses using CODE_BRIGHT for a DGR having the same dimensions and GTL used by RWE NUKEM. The objectives of this comparison are to develop our modelling skills using CODE_BRIGHT and to verify the numerical modelling result obtained using CODE_BRIGHT. The comparisons of the simulated temperatures at three different locations in a DGR: centre of the DGR; corner of the DGR; and the middle point of the outside edge of the DGR are shown in Figure 12. For different locations, the results from the CODE_BRIGHT model match the results from the ABAQUS model well 20 years after waste placement. During the period of 0.1 to 20 years after waste placement, the temperatures at the centre of a DGR or an edge centre of a DGR obtained using CODE_BRIGHT are much higher than the results obtained using ABAQUS. The difference may be caused by a different method of applying heat load in the CODE_BRIGHT model than in the ABAQUS model. In CODE_BRIGHT model, the heat load is applied at each node, which locates at the area of a DGR. If the heat load were applied in term of per unit of volume instead of each node, the simulated temperature using CODE_BRIGHT would be much lower and match ABAQUS results much better during the period of 0.1 to 20 years after waste placement. The peak temperature is 33°C at a corner of the DGR and 70.5°C at the centre of the DGR. This indicates that CODE_BRIGHT can be successfully used to model the thermal response of a DGR.

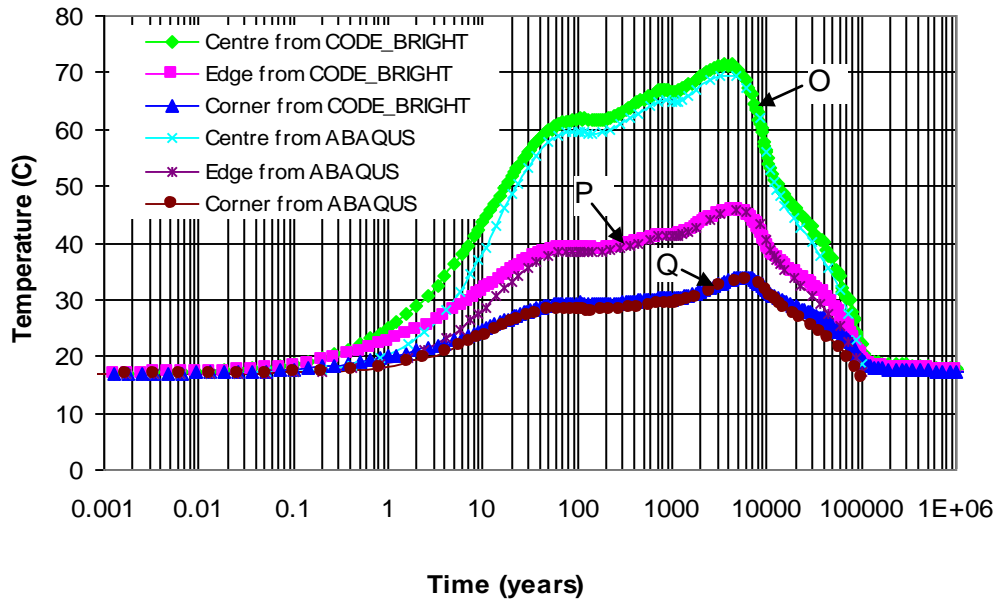


Figure 12: Comparison of Simulated Temperatures from Far-Field Analyses using ABAQUS and CODE_BRIGHT for a Finite Repository (for location see Figure 13)

5. NUMERICAL RESULTS USING CODE_BRIGHT FOR A DEEP GEOLOGICAL REPOSITORY

In Section 4, both near-field and far-field thermal numerical modelling results using CODE_BRIGHT match the results using ABAQUS reasonably well. Both near-field simulations using ABAQUS and CODE_BRIGHT assume that the horizontal dimensions of the DGR are infinite. Since the dimensions of any DGR are finite, the results from near-field modelling shown in Section 4 (Figure 7) might not be representative for a finite DGR some time after waste placement. In this Section, a method is proposed to calculate more accurate temperatures for the near-field modelling.

The infinite-repository near-field temperature results are corrected using information from finite-repository far-field analyses. This will be demonstrated in this section by discussing the far-field modelling.

5.1 FAR-FIELD MODELLING FOR A FINITE REPOSITORY

5.1.1 Far-Field Model Geometry

The perspective view of the far-field model of a repository using the in-floor placement method is shown in Figure 13. The far-field model represents the finite dimensions of a repository using the in-floor borehole placement method as developed by RWE NUKEM (2003a). The outer boundaries of this model are the same as the model shown in Figure 8, but the repository dimensions have been changed from those used by RWE NUKEM (2003b) in their far-field analyses (i.e., those of a repository using the in-room placement method) to those of the RWE NUKEM (2003a) in-floor borehole placement method. The horizontal dimensions of a repository using the in-floor borehole placement method are 1390 m x 1450 m (RWE NUKEM Limited 2003a). The horizontal dimensions of a quarter of a DGR using the in-floor placement method are 695 m x 725 m and 3.867 m thick, which is the height of a container.

5.1.2 Far-Field Modelling Boundary Conditions

5.1.2.1 Far-Field Modelling Thermal Boundary Conditions

The far-field modelling thermal boundary conditions for the in-floor placement method are the same as those presented in Section 4.2.1.2.

5.1.2.2 Far-Field Modelling Mechanical Boundary Conditions

The far-field modelling mechanical boundary conditions for the in-floor placement method are also the same as those presented in Section 4.2.1.3.

5.1.3 Initial Conditions for the Far-Field Modelling

The initial temperature of the model is that the geothermal gradient is 0.012°C/m of depth, with the ground surface temperature being 5°C and the model bottom temperature of 125°C.

The initial stresses and displacement are assumed to be zero.

5.1.4 Far-Field Model Discretization

Discretization of the far-field model for the in-floor placement method is the same as shown in Figure 11. There are 22984 nodes and 20625 eight-noded elements. Although the number of elements and nodes is the same for both far-field models (i.e., Figures 8 and 13), the dimensions of the individual elements differ because of the dimensional differences between the repositories represented by each model.

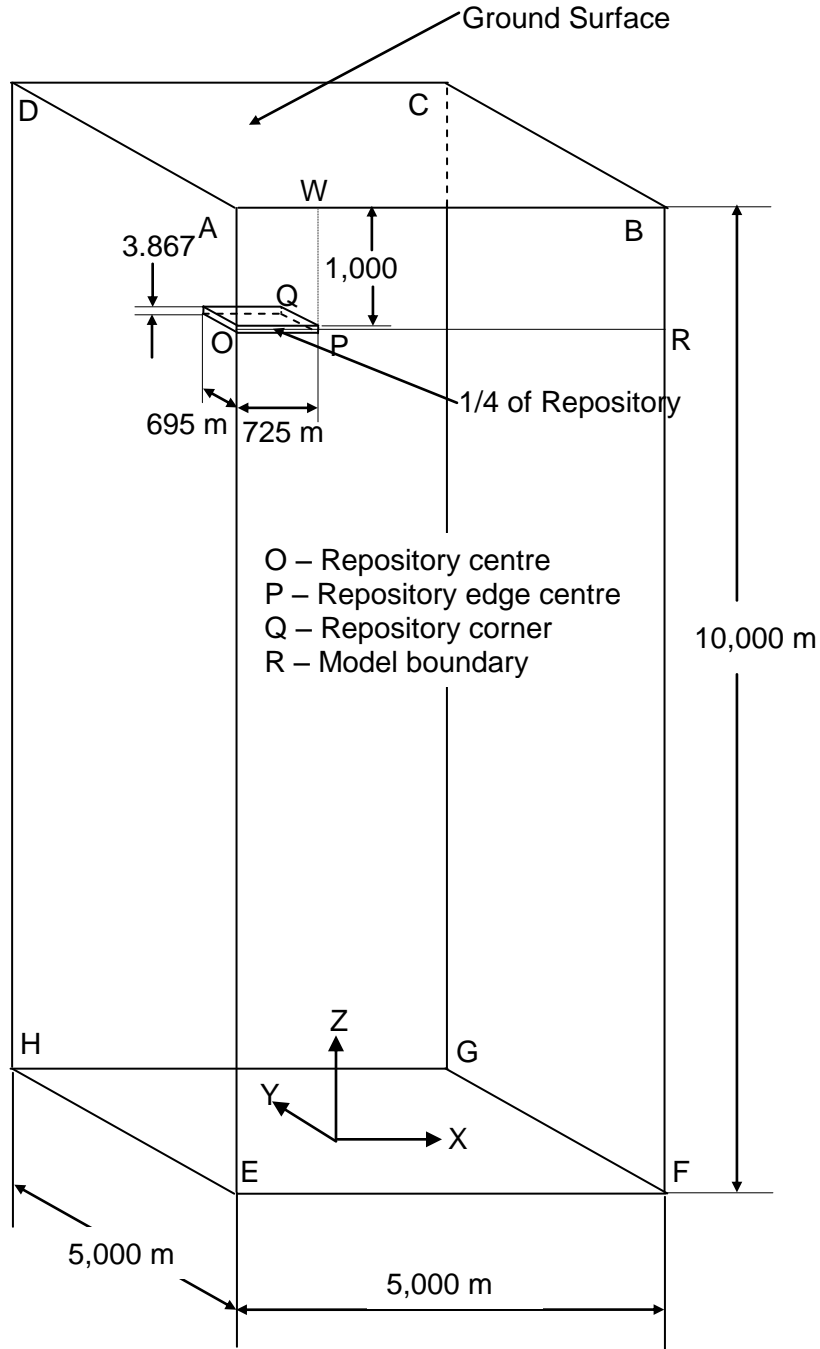


Figure 13: Geometric Model for the Far-Field Analyses of a DGR using the In-floor Borehole Placement Method

5.1.5 Far-Field Modelling Results

The results from far-field numerical simulation of a repository with finite horizontal dimensions are presented in this Section. The modelled results include temperatures, thermally induced stresses, total thermal and in-situ stresses, and thermally induced displacements at selected locations.

5.1.5.1 Thermal Results from the Far-Field Modelling

Figure 14 illustrates the temperature histories at the four different locations O, P, Q and R shown in Figure 13. The peak temperature occurs after 4200 years at the repository centre with a magnitude of 62°C. The peak temperatures at the centre of a repository edge and repository corner are 41°C and 30°C, respectively. The temperature at Point R decreases 10,000 years after waste placement because of the thermal boundary change on the ground surface to account for a period of glaciation.

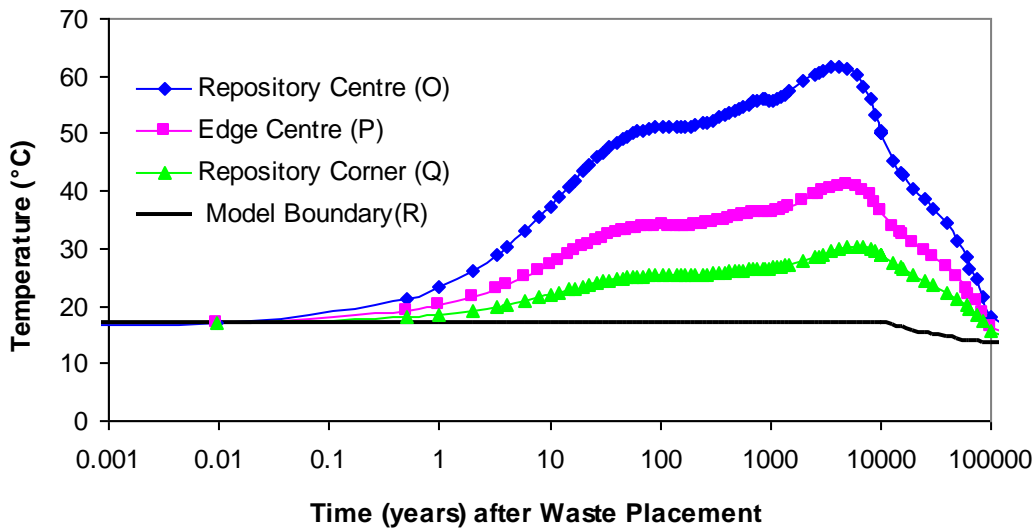


Figure 14: Far-Field Analyses Temperature Histories at Four Different Locations

Temperature profiles along horizontal symmetric line OR (refer to Figure 13 for location) at seven different times are shown in Figure 15. The thermal load caused by used nuclear fuel influences the temperature of the rock in a range of 2,500 m or less from the centre of the repository. Therefore, the horizontal dimensions of 5000 m of the model are sufficient to conduct the far-field modelling.

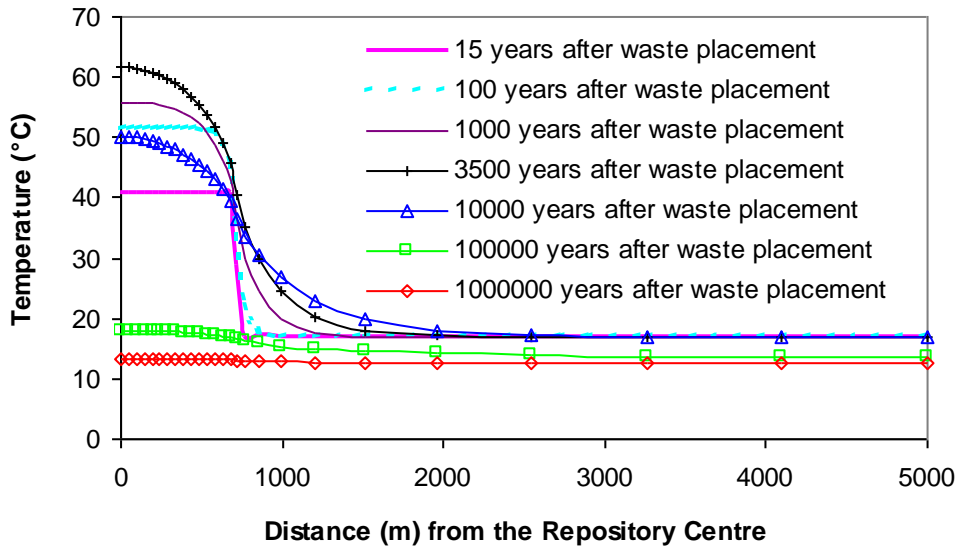


Figure 15: Far-Field Temperature Profiles at Different Times along Horizontal Symmetric Line OR (refer to Figure 13 for locations)

Temperature rise time histories at selected points along the vertical line through the repository centre are shown in Figure 16. At the centre of the repository (1,000 m below the ground surface), the net rise of the temperature is about 45°C. At a location 2,000 m below the ground surface, the temperature rise is only 7.5°C.

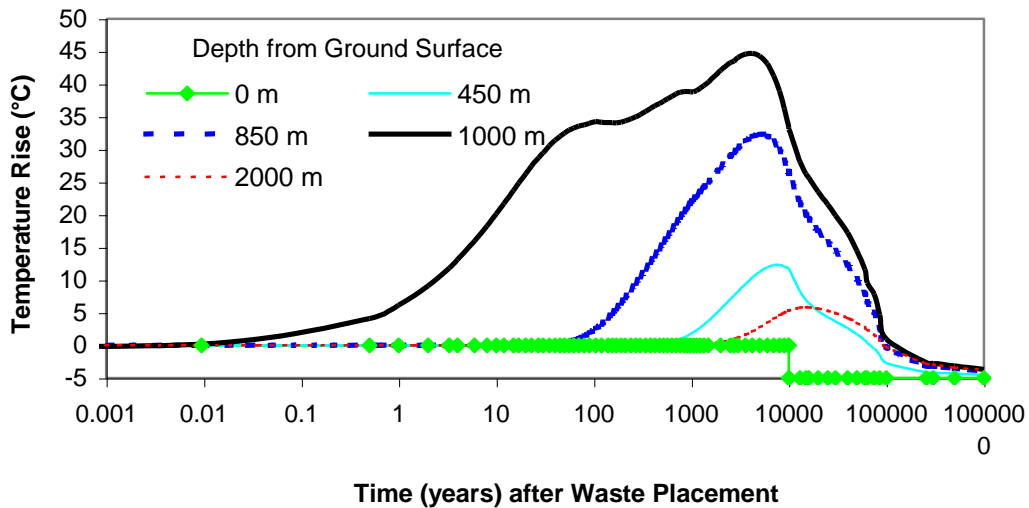


Figure 16: Far-Field Temperature Rise Time Histories at Selected Points along the Vertical Line through the Repository Centre

Temperature profiles along the vertical axis through the centre of the DGR at different times are shown in Figure 17. The thermal influence of the DGR only reaches a depth of 3,000 m at 100,000 years after placement.

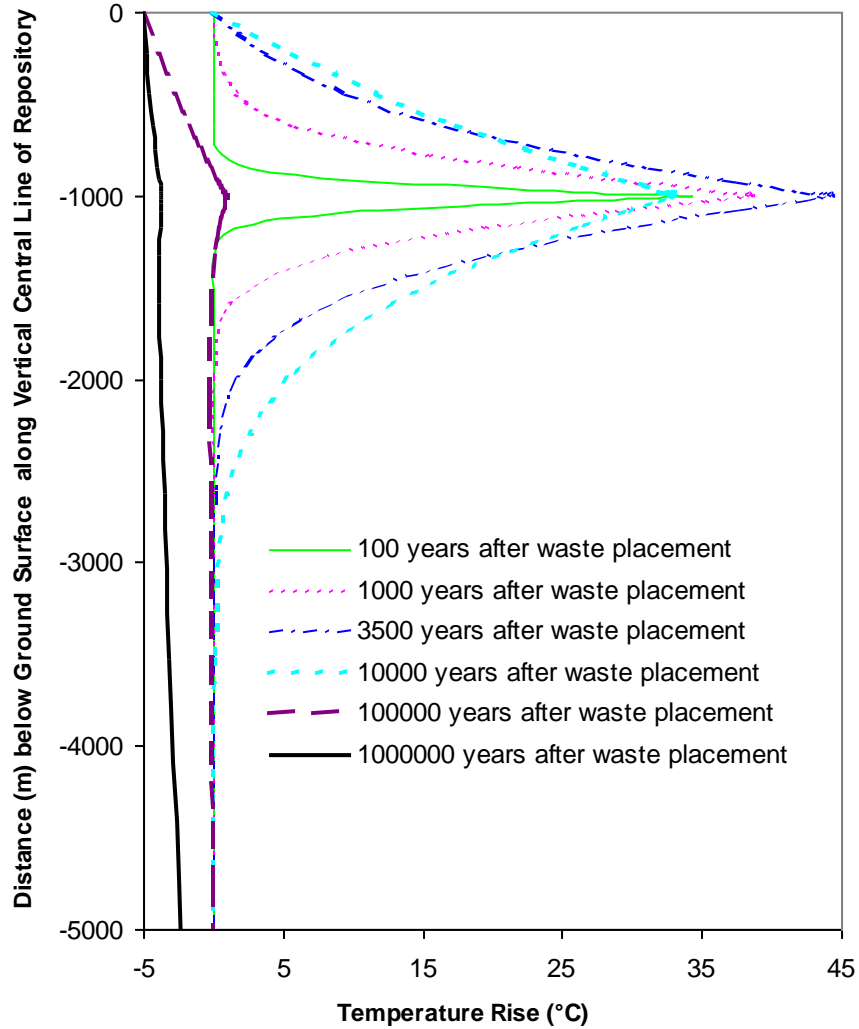
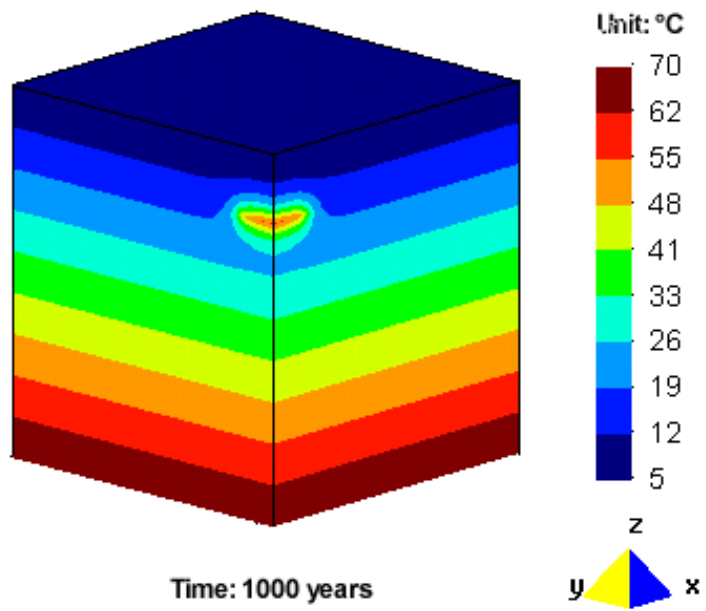
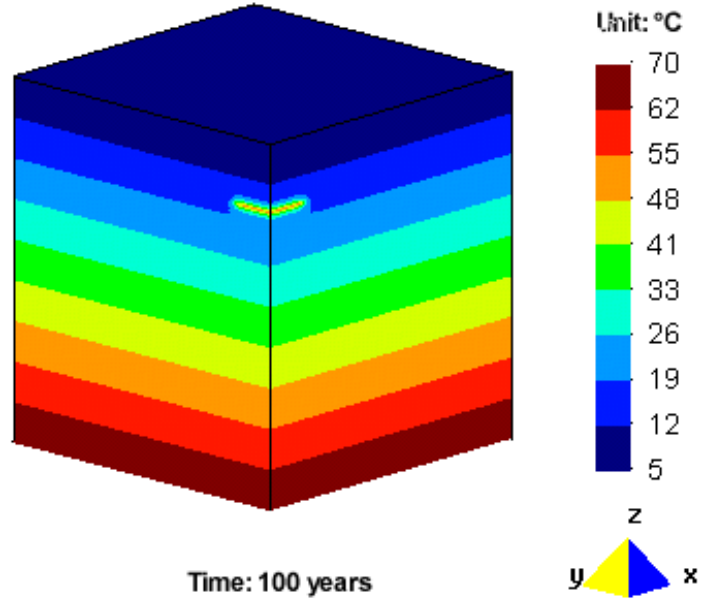
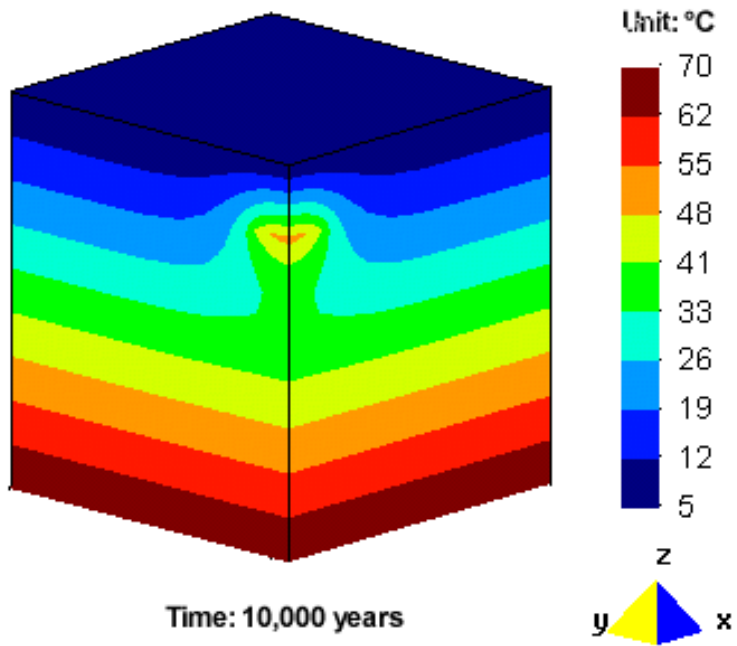
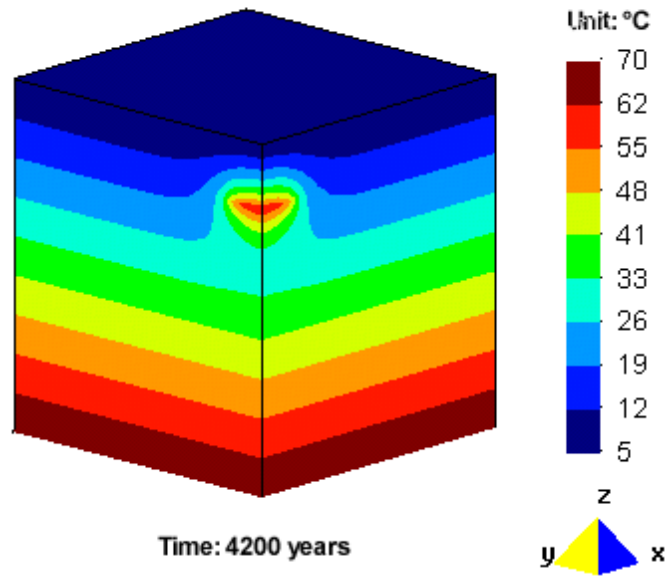


Figure 17: Temperature Distributions along the Vertical Axis of the Repository

The temperature rise occurs only near the repository area for the first 100 years as shown in Figure 18. After 100,000 years, the temperature around the repository approaches ambient temperatures.





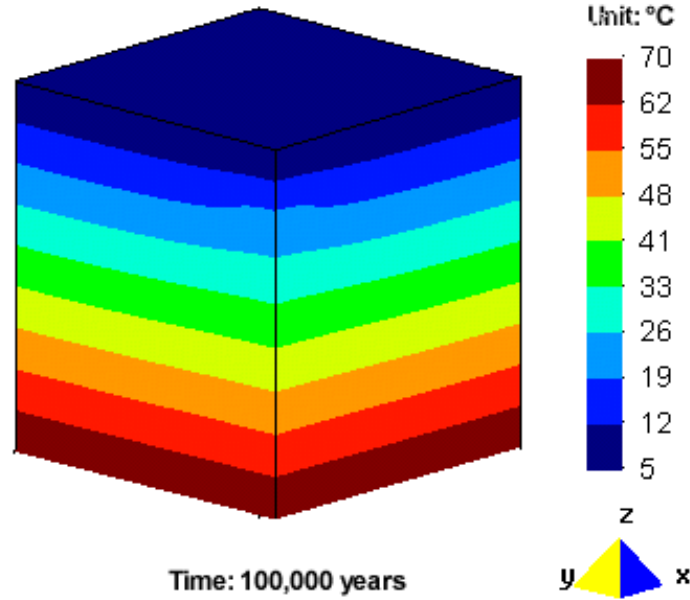


Figure 18: Temperature Profiles at Five Different Times (The bottom of the figures is 5800 m below ground surface)

5.1.5.2 Mechanical Results from the Far-Field Modelling

In accordance with Baumgartner et al. (1995), the ambient in-situ stresses used in these analyses are as follows:

$$\sigma_1 = \begin{cases} 0.1345 \text{ MPa} / m \cdot \text{depth} + 18.5 \text{ MPa} & < 300 \text{ m} \\ 0.00866 \text{ MPa} / m \cdot \text{depth} + 56.3 \text{ MPa} & \text{from } 300 \text{ m to } 1400 \text{ m} \\ 0.0403 \text{ MPa} / m \cdot \text{depth} + 12.1 \text{ MPa} & > 1400 \text{ m} \end{cases} \quad (2)$$

$$\sigma_2 = \begin{cases} 0.1112 \text{ MPa} / m \cdot \text{depth} + 9.9 \text{ MPa} & < 300 \text{ m} \\ 0.00866 \text{ MPa} / m \cdot \text{depth} + 40.7 \text{ MPa} & \text{from } 300 \text{ m to } 1660 \text{ m} \\ 0.0293 \text{ MPa} / m \cdot \text{depth} + 6.4 \text{ MPa} & > 1660 \text{ m} \end{cases} \quad (3)$$

$$\sigma_3 = \sigma_v = 0.026 \text{ MPa} / m \cdot \text{depth} \quad (4)$$

where σ_v is the vertical stress; and

σ_1, σ_2 and σ_3 are the major, intermediate and minor principal stresses, respectively.

Due to the presence of a heat-generating source, temperature changes in the rock give rise to thermal stresses, caused by thermal expansion of the rock mass. The thermally induced stresses are obtained by numerical simulation using CODE_BRIGHT. The simulated mechanical results are superimposed on the in-situ stresses as shown in Equations 2, 3 and 4

to obtain the total stresses in the rock mass. The ambient in-situ stress, σ_1 , is applied in the X direction and the stress, σ_2 , is applied in the Y direction.

Profiles of total stresses in the X direction along a horizontal line (Line OR) through the repository centre are illustrated in Figure 19. From the mechanical point of view, the influence of the repository thermal load exists only in the area less than 3,000 m horizontally from the centre of the repository. The horizontal stress in the X direction peaks at 85 MPa.

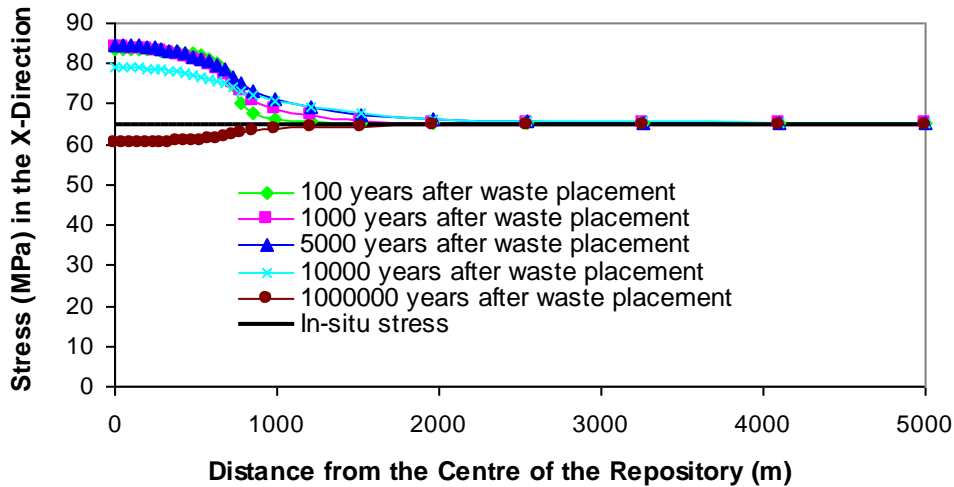


Figure 19: Profiles of Stresses in the X Direction along a Horizontal Line through the Repository Centre (Compressive stresses are positive)

The thermally induced stresses in the X direction along the horizontal line (Line OR in Figure 13) at five different times are shown in Figure 20. At a time of 1,000,000 years after waste placement, the stresses in the X direction in the area of the repository are reduced by about 4.5 MPa. The reason of the decrease of the X-directional stress in the area of the repository at a time of 1,000,000 years after waste placement is not clear at this moment. The peak thermally induced stress in the X direction is about 20 MPa.

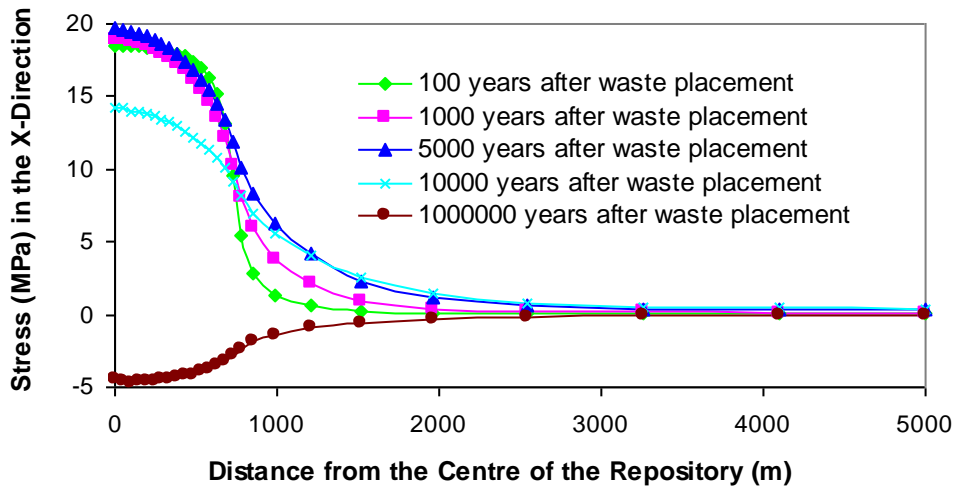


Figure 20: Thermally Induced Stresses in the X Direction along a Horizontal Line through the Repository Centre (Reduction of compressive stress is negative)

Profiles of stresses in the Y direction along the horizontal line (Line OR in Figure 13) at six different times are shown in Figure 21. The peak stress in the Y direction is 69 MPa at the centre of the repository. At a time of 1,000,000 years after waste placement, the stress in the Y direction drops to about 45 MPa at the centre of the repository.

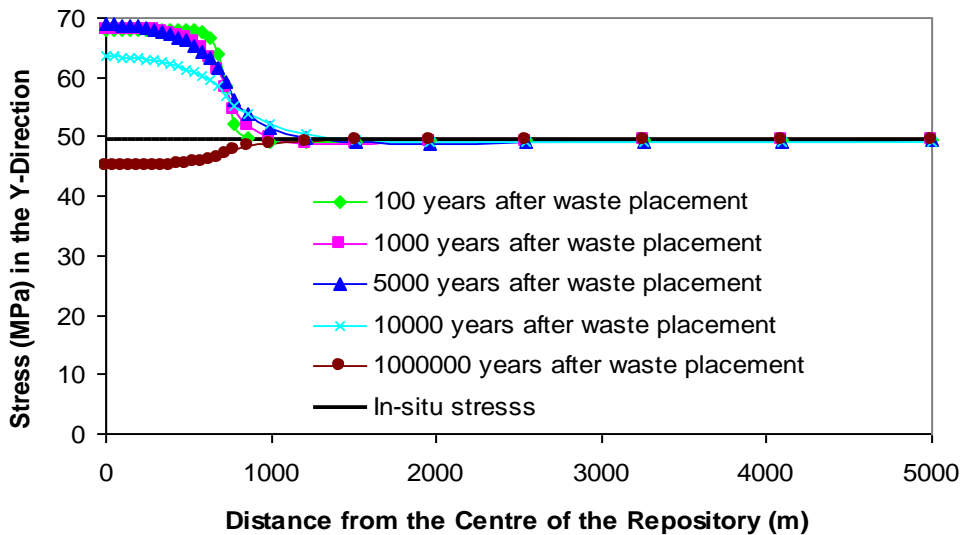


Figure 21: Profiles of Stresses in the Y Direction along a Horizontal Line through the Repository Centre

As shown in Figure 22, the peak thermally induced stress in the Y-direction along the horizontal line (Line OR (see Figure 13 for location)) is about 19.5 MPa. At a time of 1,000,000 years after waste placement, the reduction of thermally induced stresses in the Y direction in the rock at the repository is about 4.6 MPa. As expected, the thermally induced stresses in the Y direction are similar to the thermally induced stresses in the X direction.

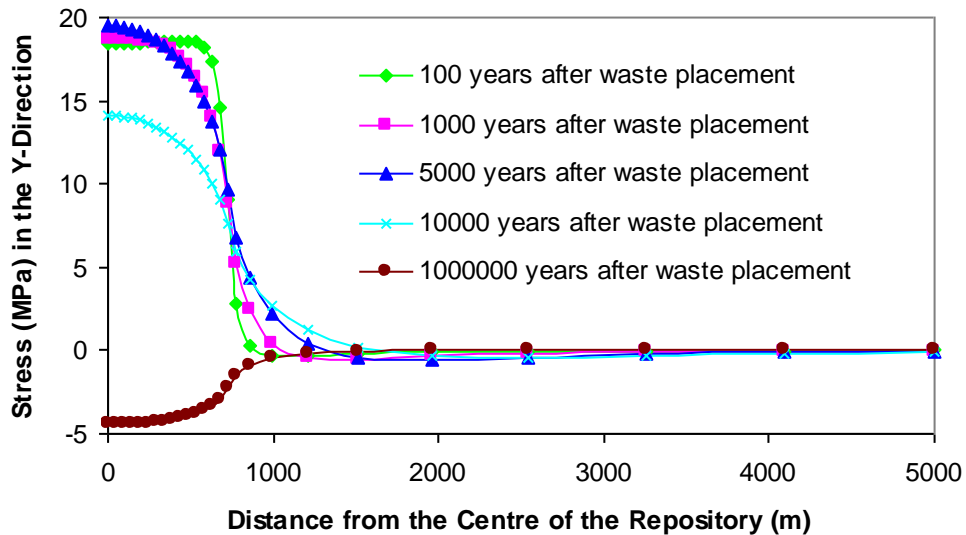


Figure 22: Thermally Induced Stresses in the Y Direction along a Horizontal Line through the Repository Centre (Reduction of compressive stress is negative)

Profiles of stresses in the Z direction along the horizontal line (Line OR in Figure 13) are shown in Figure 23. The stress in the Z direction peaks at about 34.6 MPa.

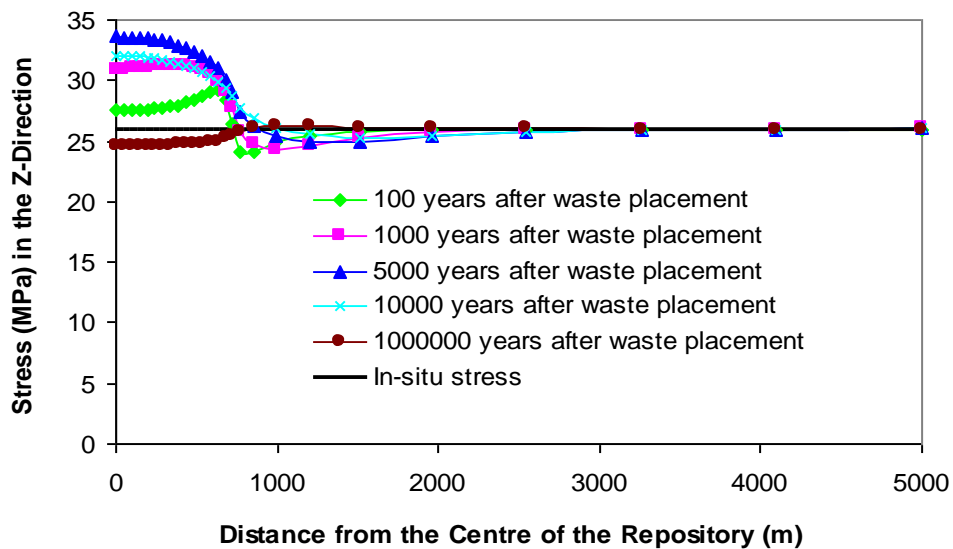


Figure 23: Profiles of Stresses in the Z Direction along a Horizontal Line through the Repository Centre

The thermally induced stresses in the Z direction along the horizontal line OR (Figure 13) can be seen in Figure 24. The peak thermally induced stress in the Z direction is about 7.5 MPa. The thermally induced peak stress reduction is about 2 MPa occurring at the location near the edge of repository.

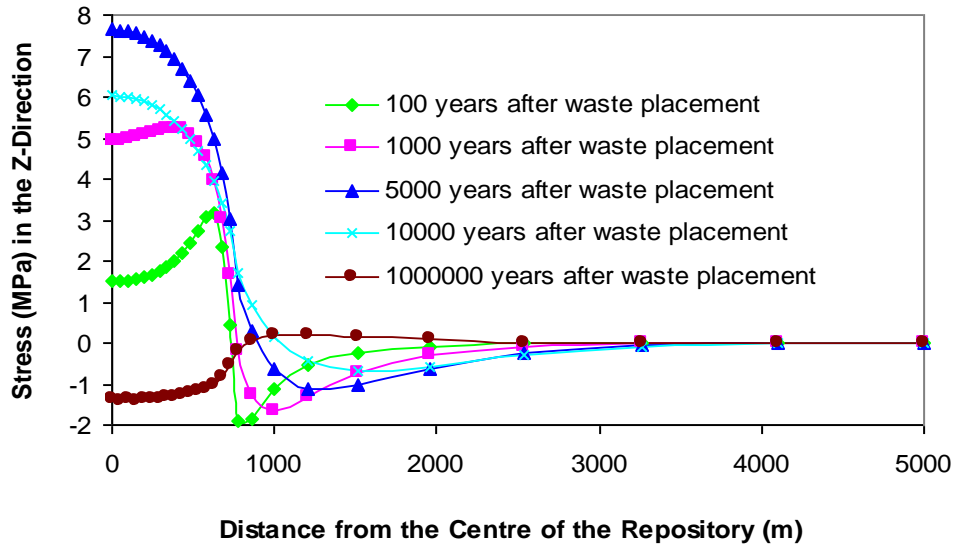


Figure 24: Thermally Induced Stresses in the Z Direction along a Horizontal Line through the Repository Centre (Reduction of compressive stress is negative)

The apparent influence of heating caused by the used nuclear fuel on the X-direction stress exists only in the depth from the ground surface to about 2,500 m, as shown in Figure 25. Figure 26 shows the thermally induced stress in the X direction along the vertical line through the repository centre. The peak thermally induced compressive stress in the X direction is 20 MPa. At the ground surface, the thermally induced stress reduction in the X direction is 5.5 MPa. At a time of 1,000,000 years after waste placement, the thermally induced stress reduction at the centre of the repository is 4.5 MPa, while on the ground surface, the thermally induced compressive stress increase is 1.2 MPa.

Profiles of total stresses and thermally induced stresses in the Y direction along the vertical line through the repository centre are shown in Figures 27 and 28, respectively. The thermally induced compressive stress increase in the Y direction peaks at 19.3 MPa 5,000 years after container placement and the stress decrease in the Y direction peaks at 4.5 MPa at the repository depth 1,000,000 years after container placement. At the ground surface, the thermally induced compressive stress increase in the Y direction peaks at 1 MPa at 1,000,000 years after container placement and the thermally induced compressive stress decrease peaks at 5.7 MPa at 5,000 years after container placement.

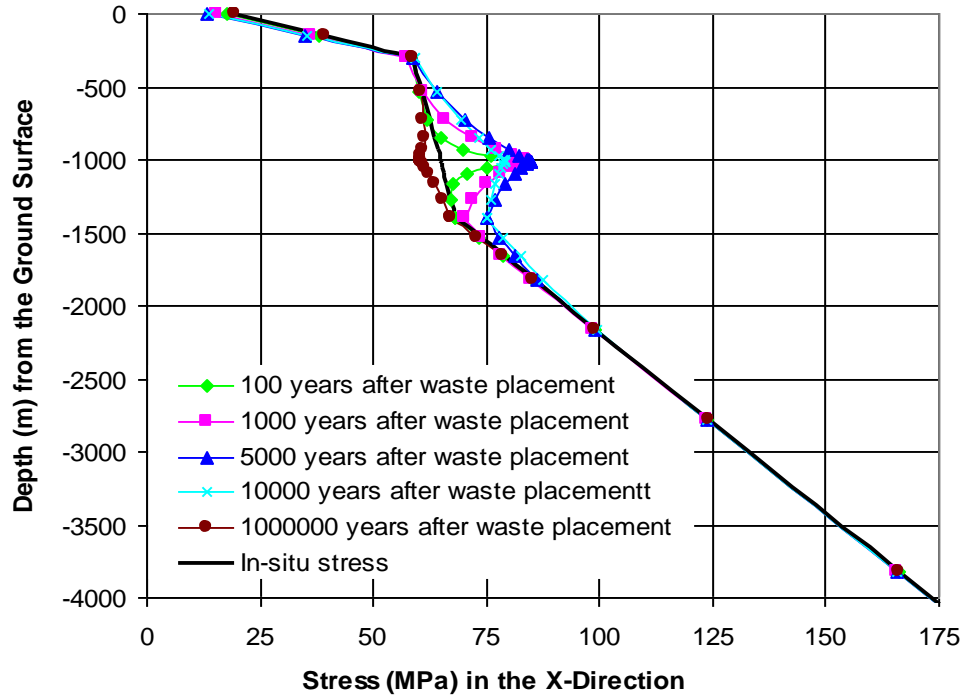


Figure 25: Profiles of Stresses in the X Direction along the Vertical Line through the Repository Centre

Profiles of stresses and thermally induced stresses in the Z direction along the vertical line through the repository centre are shown in Figures 29 and 30, respectively. The thermally induced compressive stress increase in the Z direction at the repository level peaks at 7.5 MPa 5,000 years after container placement and the thermally induced compressive stress reduction peaks at 1.6 MPa 1,000,000 years after container placement.

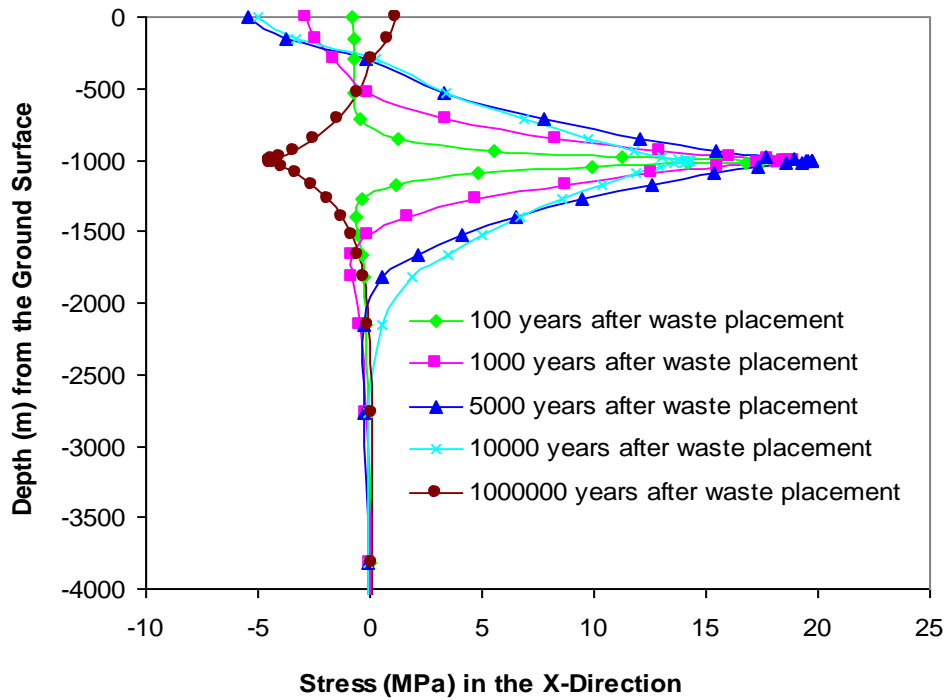


Figure 26: Thermally Induced Stresses in the X Direction along the Vertical Line through the Repository Centre (Reduction of compressive stress is negative)

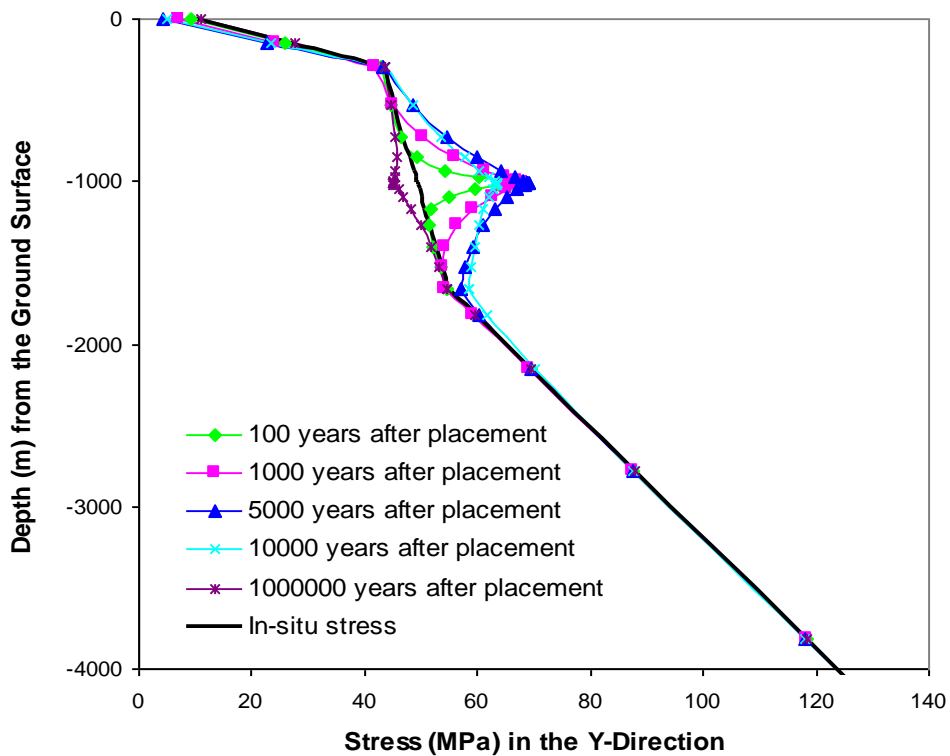


Figure 27: Profiles of Stresses in the Y Direction along the Vertical Line through the Repository Centre

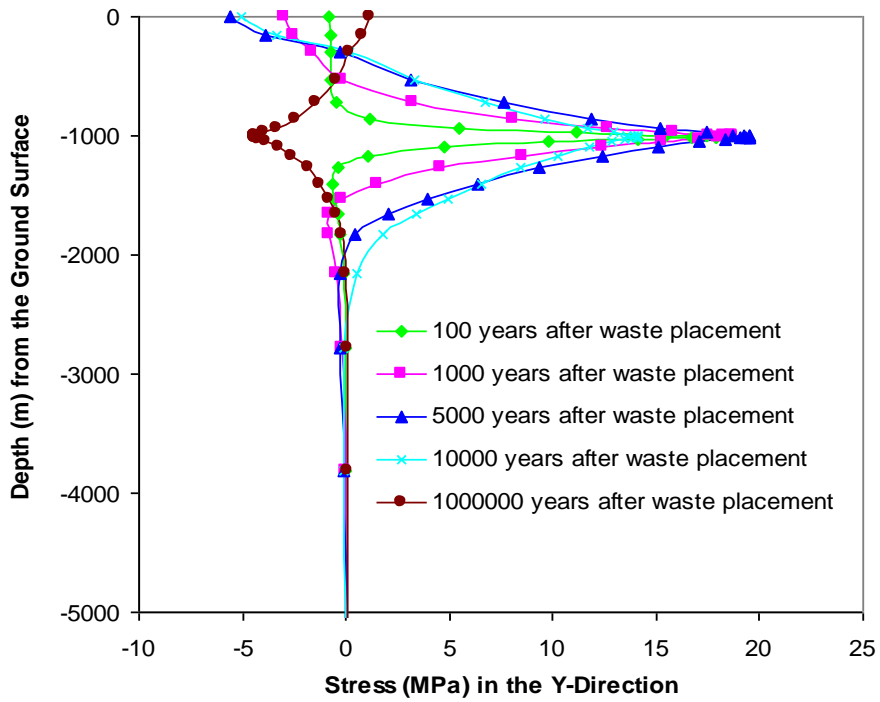


Figure 28: Thermally Induced Stresses in the Y Direction along the Vertical Line through the Repository Centre (Reduction of compressive stress is negative)

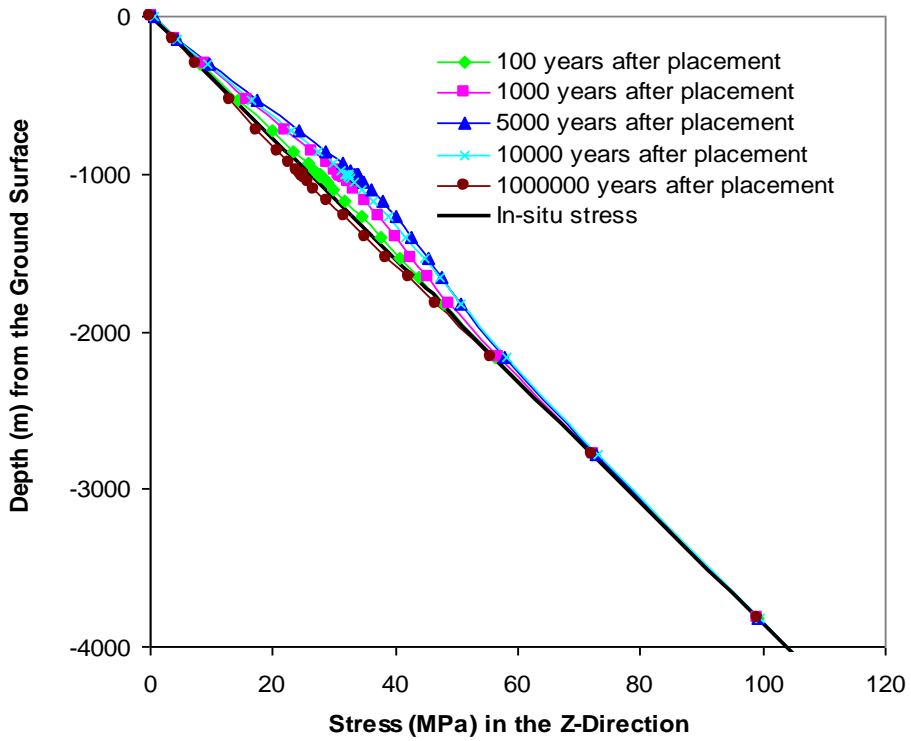


Figure 29: Profiles of Stresses in the Z Direction along the Vertical Line through the Repository Centre

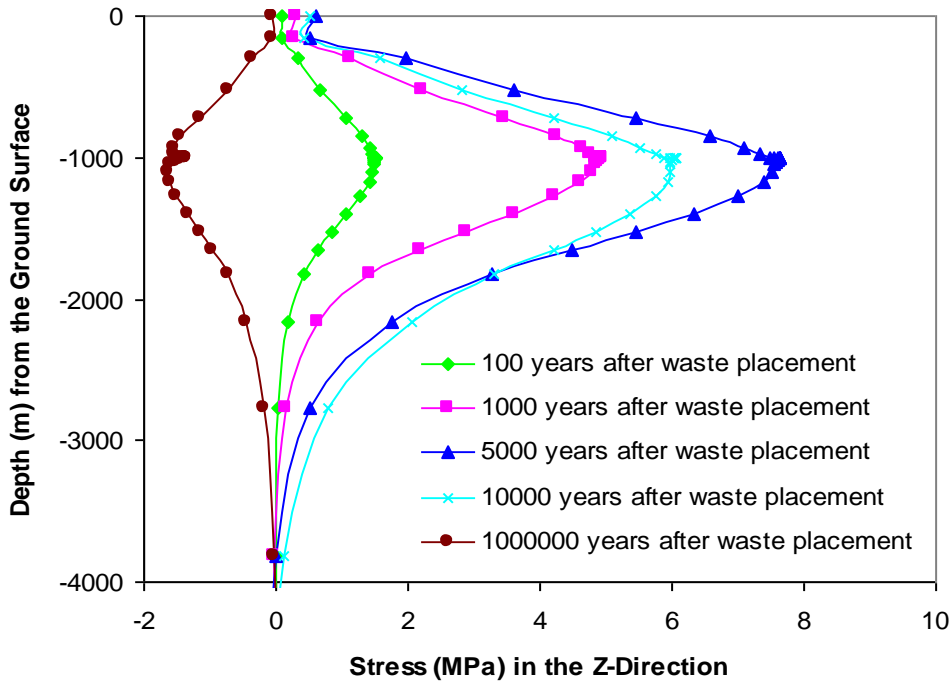


Figure 30: Thermally Induced Stresses in the Z Direction along the Vertical Line through the Repository Centre (Reduction of compressive stress is negative)

Thermally induced horizontal stresses on the ground surface above the repository centre with time are shown in Figure 31. The peak thermally induced stress reduction on the ground surface induced by thermal expansion of the rock mass near the repository is 5.7 MPa at 7,000 years after waste placement. The compressive stress increase on the ground surface induced by thermal contraction of the rock mass near the repository at 1,000,000 years is 1.2 MPa. The reason of the difference between the initial stress state and stress at 1,000,000 years after waste placement is that the surface temperature is dropped by 5°C at 10,000 years after waste placement to represent glacial cooling.

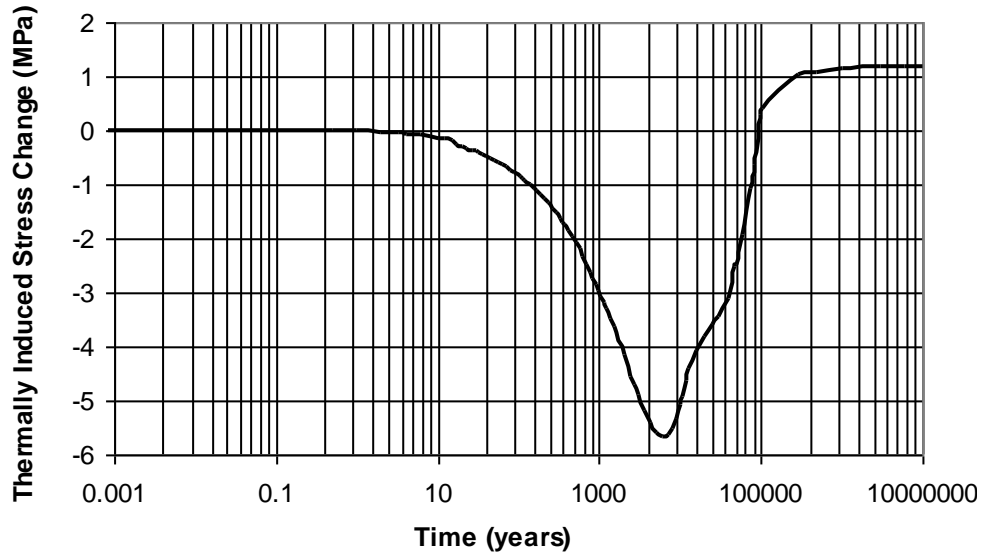


Figure 31: Thermally Induced Horizontal Stresses on the Ground Surface above the Repository Centre (Reduction of compressive stress is negative)

Stress contours in the X, Y, and Z directions on the vertical cross section (Plane ABFE, refer to Figure 13 for location) for selected times after waste placement can be seen in Figures 32, 33 and 34, respectively. These confirm the existence of stress reduction in the X and Y directions near the ground surface and in the Z direction near the edge of the repository.

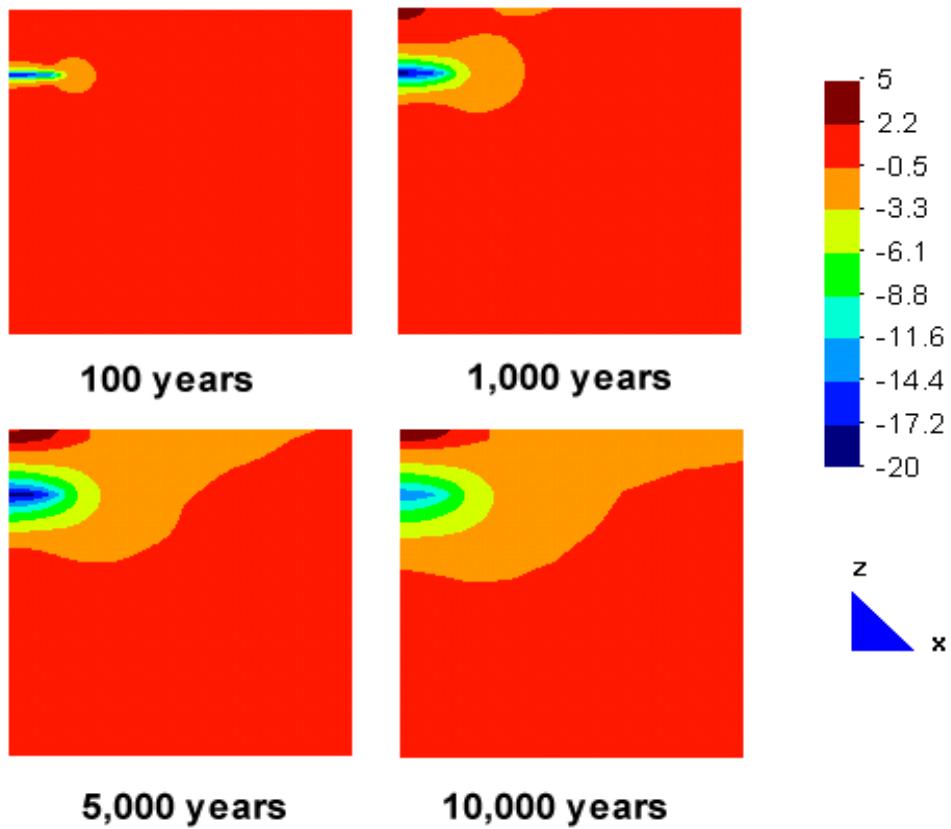


Figure 32: Contours of Stresses in the X Direction on the Vertical Cross-Section through the Centre of the Repository at Four Different Times (Increase of compressive stress is negative) (The bottom of the figures is 5,000 m below ground surface)

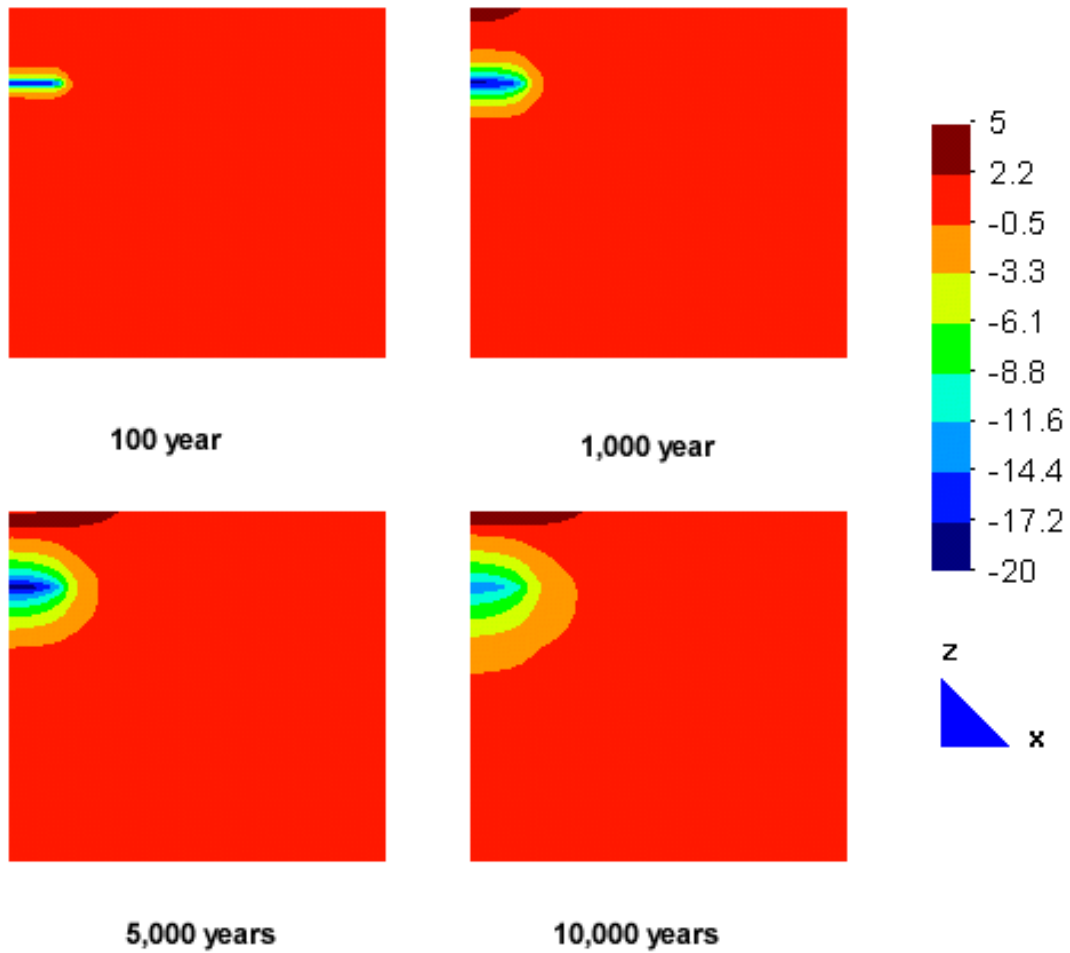


Figure 33: Contours of Stresses in the YDirection on the Vertical Cross-Section through the Centre of the Repository at Four Different Times (Increase of compressive stress is negative) (The bottom of the figures is 5,000 m below ground surface)

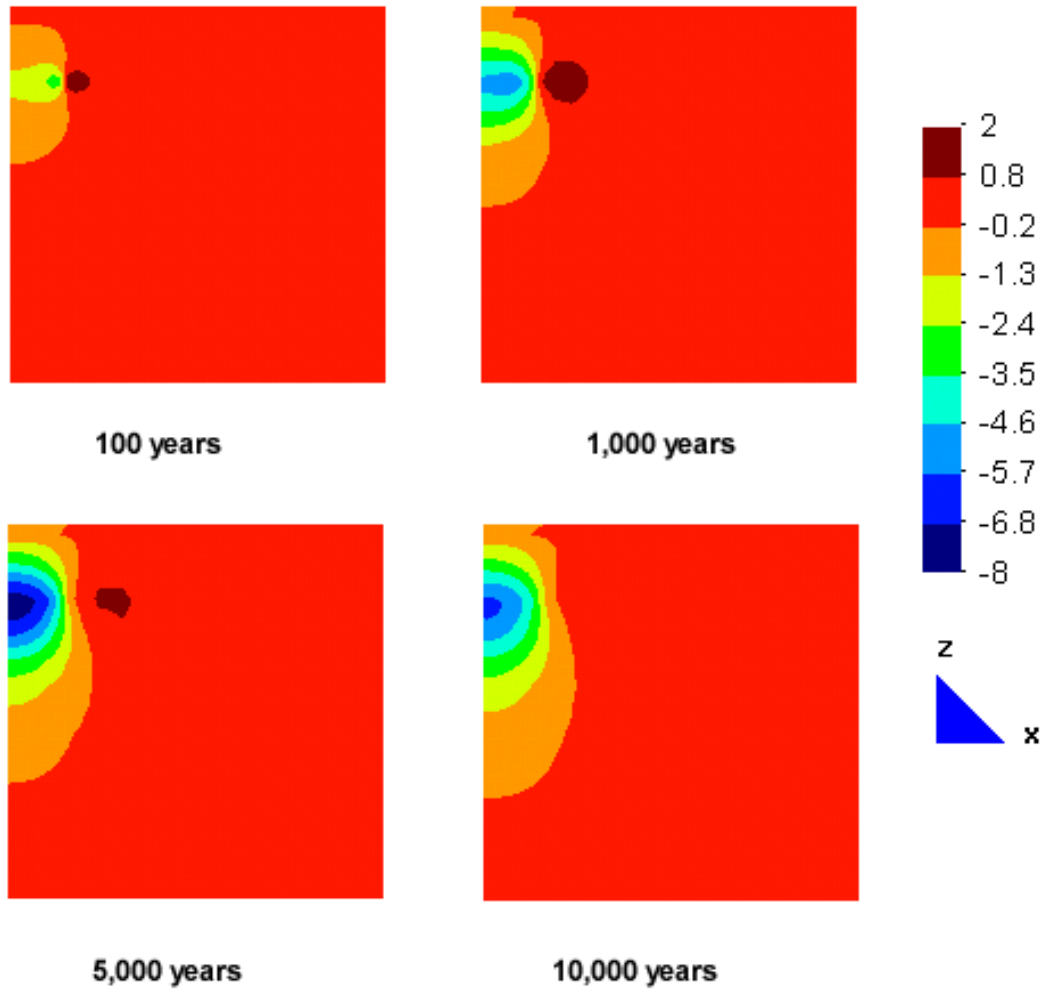


Figure 34: Contours of Stresses in the Z Direction on the Vertical Cross-Section through the Centre of the Repository at Four Different Times (Increase of compressive stress is negative) (The bottom of the figures is 5,000 m below ground surface)

The thermally induced maximum and minimum principal stresses for four different times are shown in Figures 35 and 36, respectively. These contours also show the development of stress reduction on the ground surface above the repository during the time of from 0 to 10,000 years after waste placement, and the existence of stress reduction at the repository level 10,000 years after waste placement.

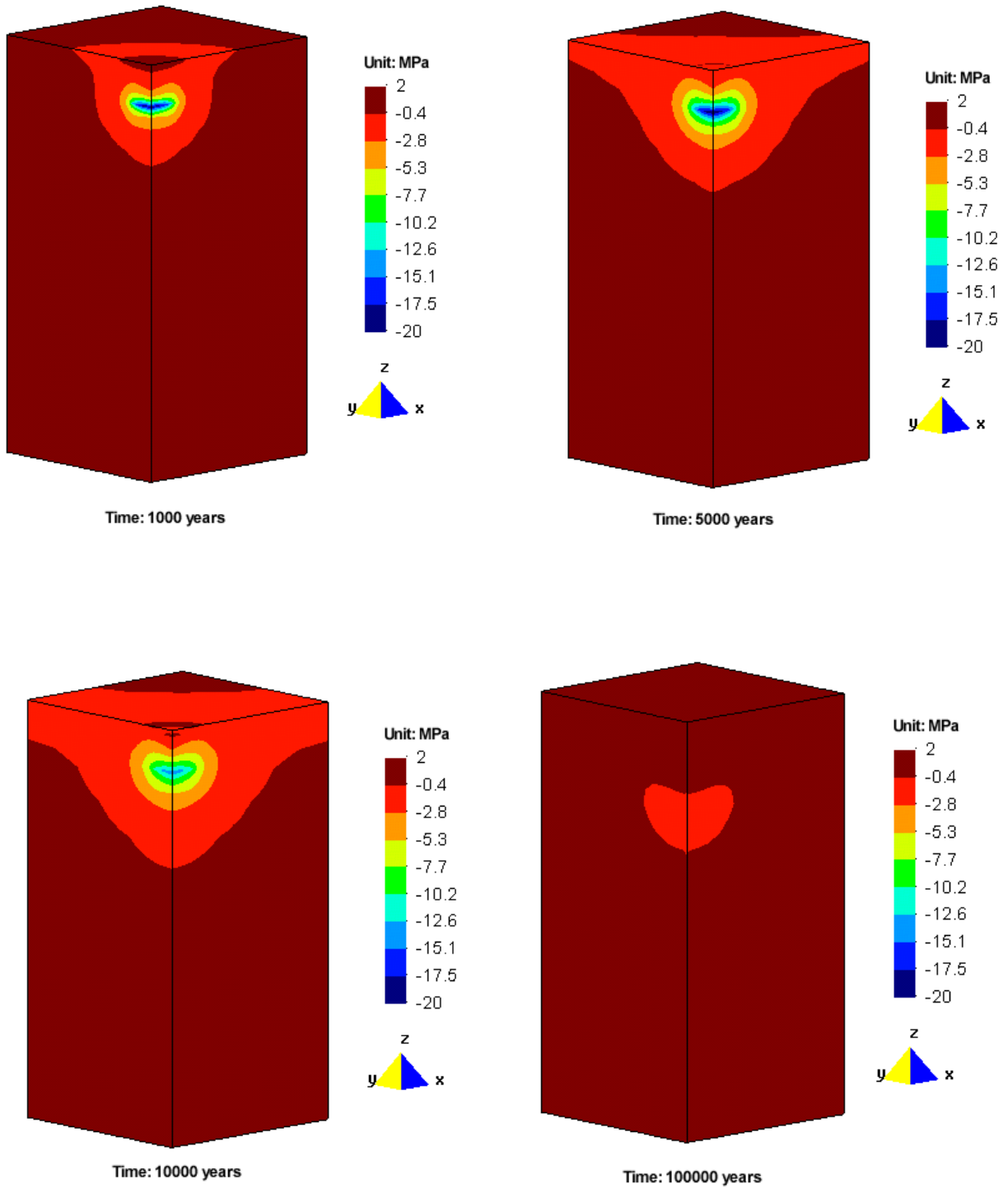


Figure 35: Thermally Induced Maximum Principal Stresses at Different Times (Increase of compressive stress is negative)

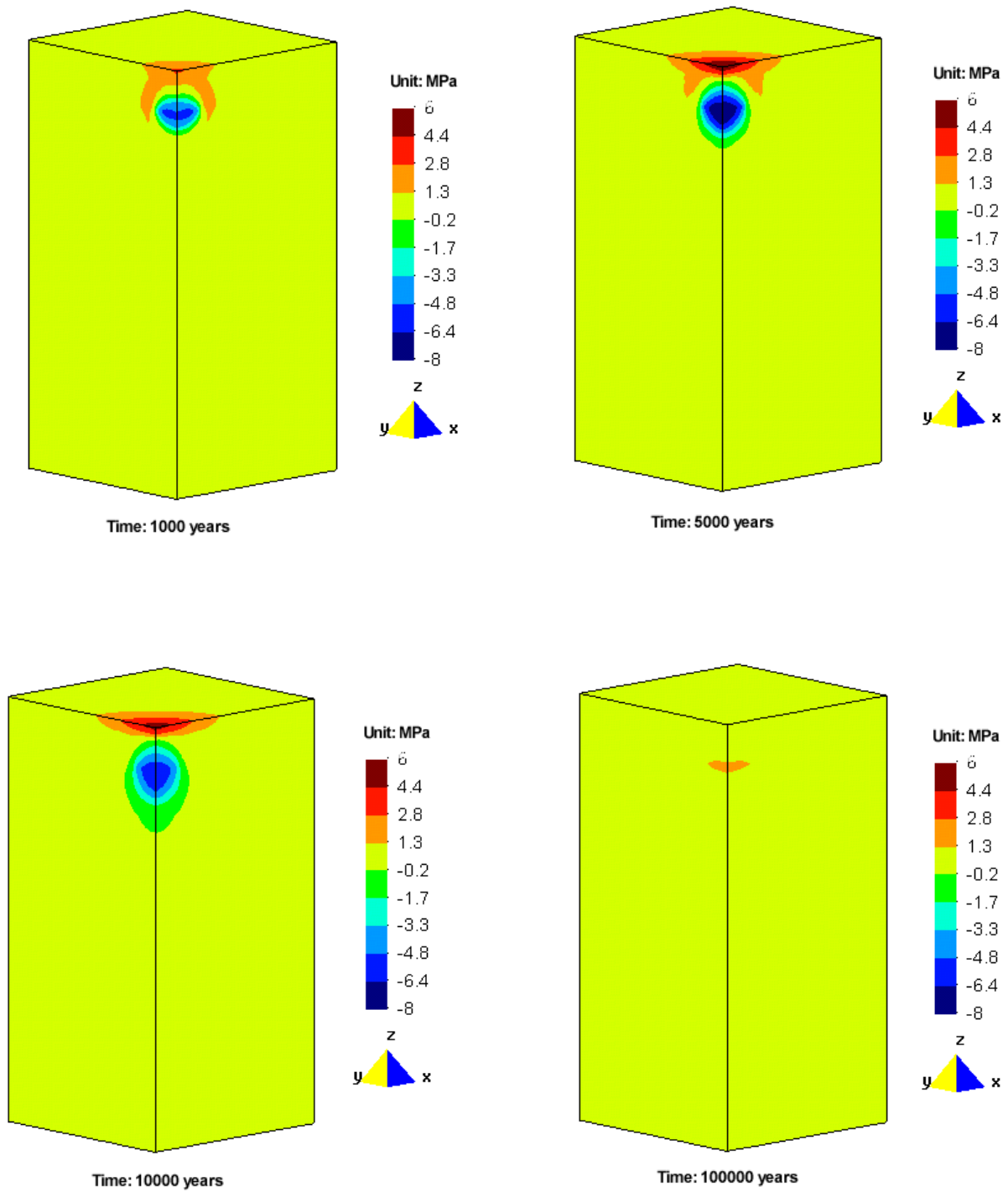


Figure 36: Thermally Induced Minimum Principal Stresses at Different Times (Increase of compressive stress is negative)

The thermally induced vertical displacements along the vertical line through the repository centre (Line AE in Figure 13) are illustrated in Figure 37. The displacement of the rock near the ground surface increases for the first 10,000 years after waste placement and then decreases. The rock underneath the repository displaces downward due to the thermal expansion of the rock near the nuclear waste. 1,000 years after waste placement, the downward displacement peaks at 26 mm, occurring at a depth of 1,400 m below ground surface. The rock above a depth of 1,000 m from the ground surface displaces in an upward direction.

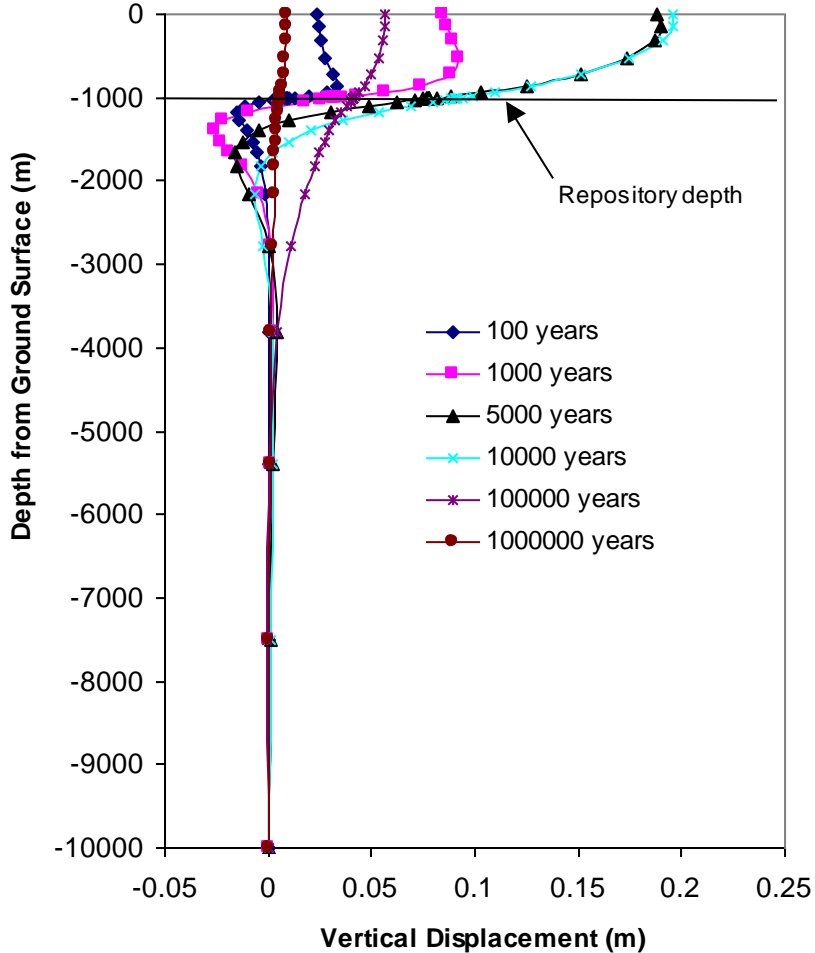


Figure 37: Thermally Induced Vertical Displacements along the Vertical Line through the Repository Centre (Positive is upward)

The vertical displacements along a horizontal line on ground surface passing over the centre of the repository (Line AB in Figure 13) are shown in Figure 38. During the first 10,000 years after waste placement, the lateral extent of thermally induced displacement on the ground surface is only about 3,500 m from the vertical line through the repository centre. At different locations on the ground surface, the vertical displacements as a function of time show the same pattern (Figure 39). That is, vertical displacements increase as a function of time until they reach a peak value and then decrease, except the time of peak displacement at each location is

different. At the ground surface above the centre of the repository, the vertical displacement peaks at 0.2 m at a time of 8,000 years after waste placement. At Point W (refer to Figure 13 for location), the peak vertical displacement is 0.15 m at 9,000 years after waste placement. At Point B, the vertical displacement peaks at 0.016 m approximately 100,000 years after waste placement.

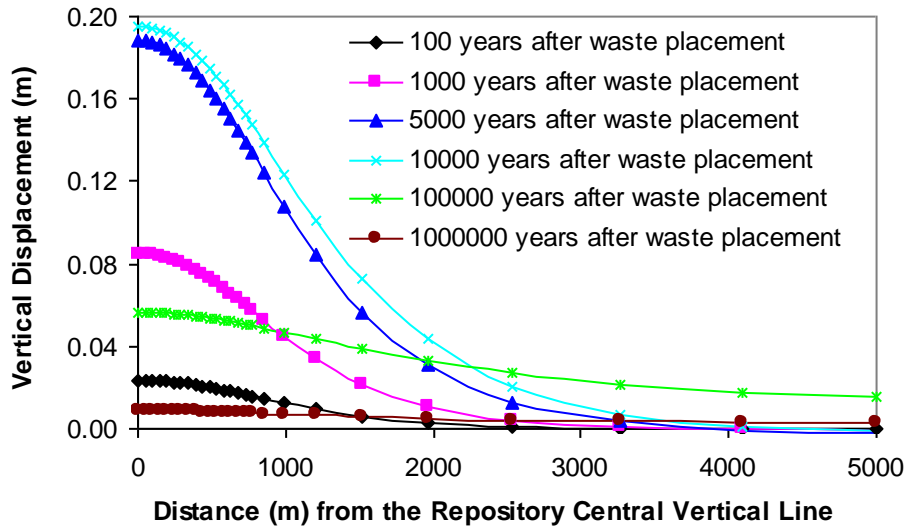


Figure 38: Vertical Displacements along the Ground Surface (Positive is upward)

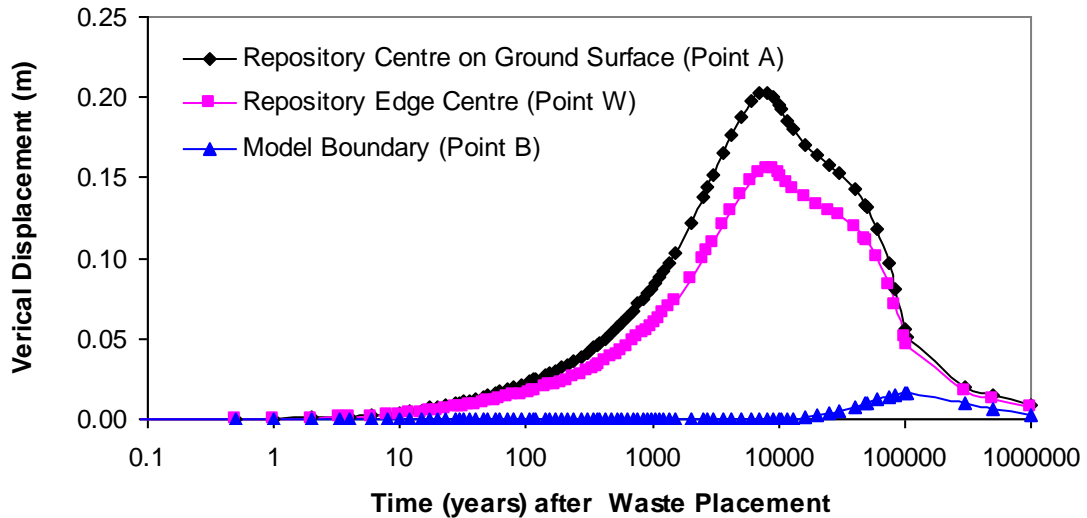


Figure 39: Thermally Induced Vertical Displacements with Time at Three Different Locations on the Ground Surface (Positive is upward)

The vertical displacements in a three-dimensional model at a time of 8,000 years after waste placement are shown in Figure 40. The rock above the repository is uplifted and the rock below the repository is displaced in a downward direction due to thermal expansion.

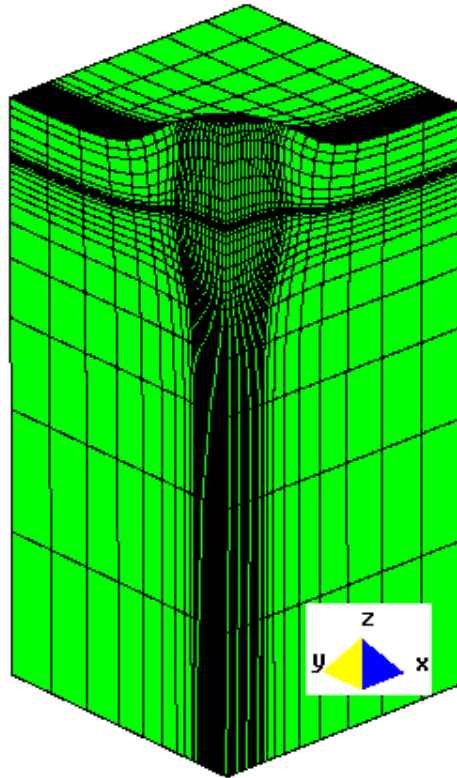


Figure 40: Thermally Induced Vertical Displacements 8000 Years after Waste Placement with a Maximum Value of 0.203 m (Note: the vertical displacement scale is exaggerated for clarity)

In summary, the thermally induced temperature rise from far-field modelling of a DGR using the in-floor borehole placement method with a uniformly distributed heat source is 62°C at the centre of the DGR and 30°C at a corner of the DGR. This is lower than that of the modelling results for a DGR using the in-room placement method because the dimensions of the in-floor borehole repository are greater than those of the in-room placement method model for the same total heat load (Section 4). The maximum thermally induced stresses in the X, Y and Z directions at the centre of the repository are 20 MPa, 19.5 MPa and 7.5 MPa, respectively, occurring at 5,000 years after waste placement. At the location on the ground surface above the centre of the repository, the thermally induced vertical displacement peaks at 0.2 m approximately 8,000 years after waste placement. The stress analyses predict a maximum horizontal stress reduction at the ground surface of 5.7 MPa after 7,000 years. Due to the minimum initial horizontal compressive stress on the ground surface being 9.9 MPa, there is no zone of tensile stress created at surface during the modelling period of 1,000,000 years.

5.2 INFLUENCE OF FINITE VERSUS INFINITE REPOSITORY MODEL ON THE CALCULATED THERMAL RESPONSE

In order to examine the influence of thermal boundary conditions on the near-field modelling, two far-field models are simulated: one is a model with a finite repository and the other is a model with an infinite repository. These analyses are done using the far-field model rather than the near-field model because it is not practical to expand the near-field unit cell to the scale of the entire repository.

Figure 41 illustrates the model geometry with a finite repository, in which the thermal load corresponds to the PTL. The PTL is used in these analyses because this heat load is appropriate for the near-field modelling and the results of these analyses will be used to propose a correction to the near-field modelling. In order to make the total thermal load the same as the load in Figure 13 (a far-field model for a DGR using the in-floor borehole placement method), the dimensions of the repository are reduced from those of the model shown in Figure 13. Therefore, the horizontal dimensions of one quarter of the repository are 600 m x 560 m. The other dimensions of the model are the same as those shown in Figure 13. The horizontal dimensions of the model are 5,000 m and the vertical dimension was 10,000 m.

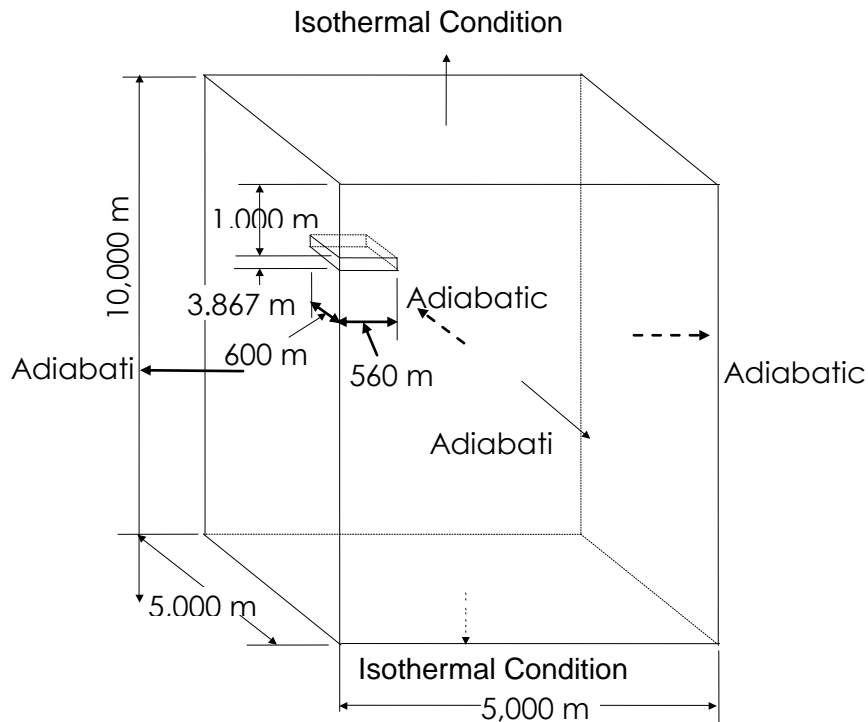


Figure 41: Model Geometry for a Finite Repository with the Same Total Thermal Load without Considering the Auxiliary Unheated Spaces

The upper surface boundary condition is modelled as an isothermal boundary, with a temperature of 5°C, representing the average Canadian Shield surface temperature. The lower

boundary is also modelled as an isothermal boundary with a temperature of 125°C, such that a geothermal gradient of 0.012°C/m of depth is achieved in the absence of a repository. The vertical boundaries are modelled as adiabatic planes of symmetry.

Figure 42 shows the model geometry with a horizontally infinite repository, in which the thermal load corresponds to the PTL. The horizontal dimensions of the repository are 5,000 m x 5,000 m and the thermal boundary conditions are the same as those for the model shown in Figure 41.

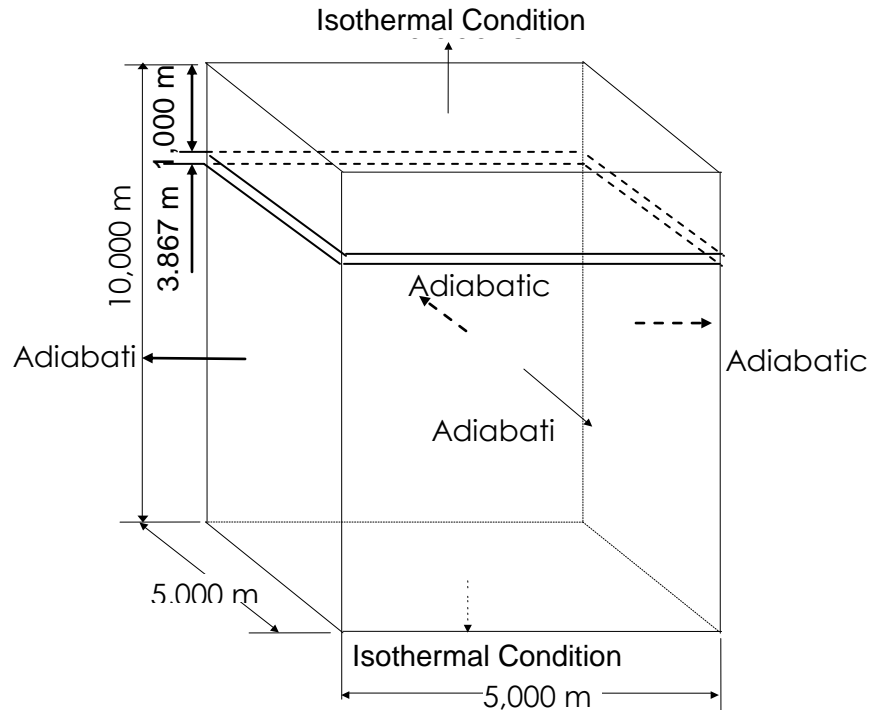


Figure 42: Model Geometry for a Repository with Infinite Horizontal Dimensions and the Same Density of Thermal Load as a Repository with Finite Horizontal Dimensions

A comparison of the central temperature for a finite repository and an infinite repository is shown in Figure 43. For the first 1,000 years, there is no obvious difference between the two models. After 1,000 years, the difference between the two models increases until 30,000 years after waste placement, at which time the difference peaks at 42°C. After 30,000 years, the difference decreases as the temperatures from both models converge to the ambient temperature.

Temperatures along the vertical line through the centre of the finite repository model are shown in Figure 44. The depth of the rock influenced by repository heating is 3,500 m or less from the ground surface.

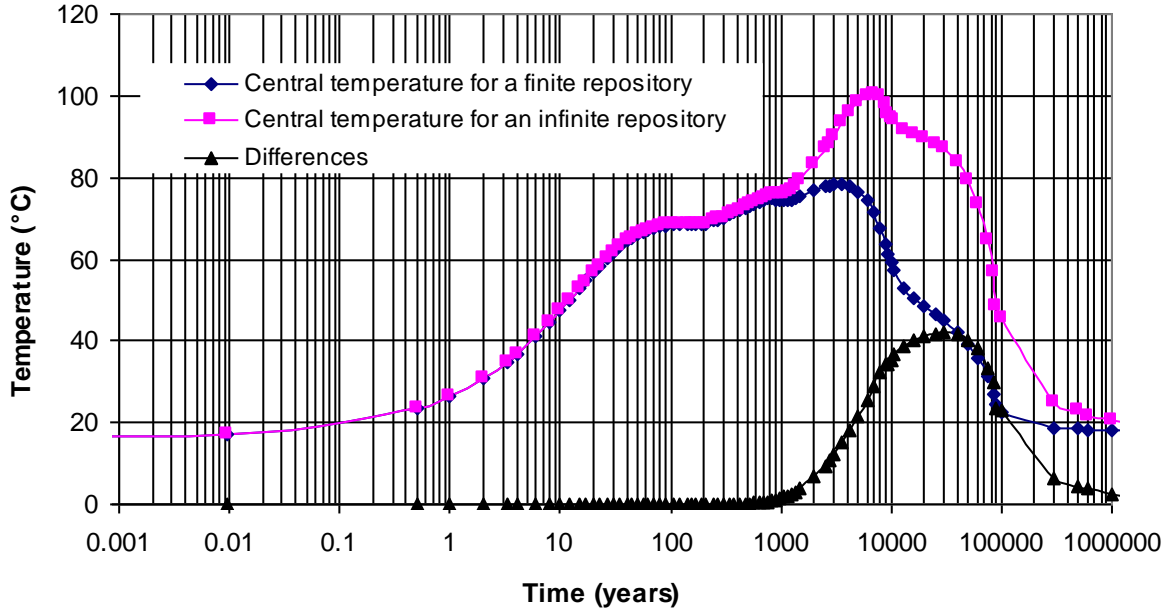


Figure 43: Comparison of the Central Temperature between a Finite Repository and an Infinite Repository and their Differences

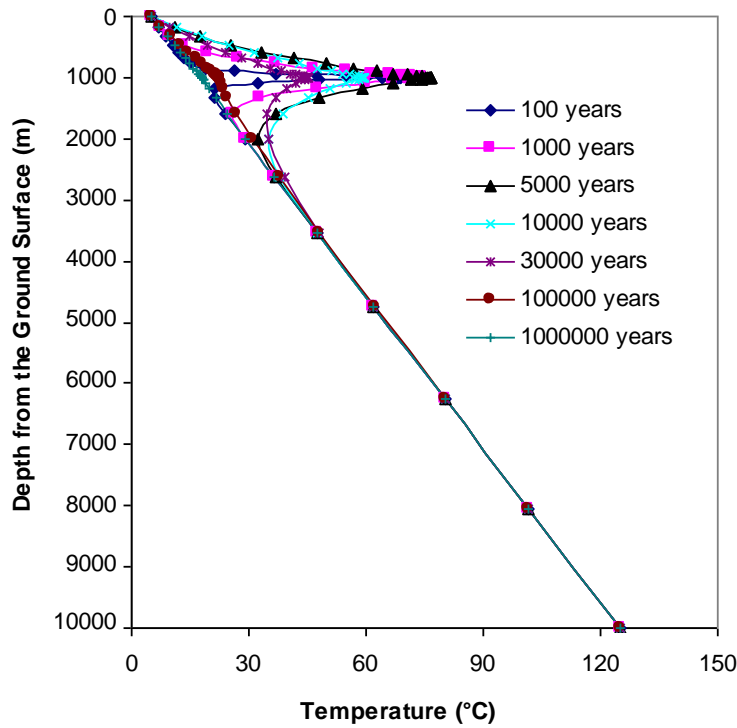


Figure 44: Temperatures along Central Vertical Line for a Finite Repository

Profiles of temperatures along the vertical line through the centre of the infinite repository model are shown in Figure 45. At 10,000 years, the temperature of the rock is affected to a depth of 10,000 m below the ground surface (i.e., to the base of the model, which is a constant temperature boundary).

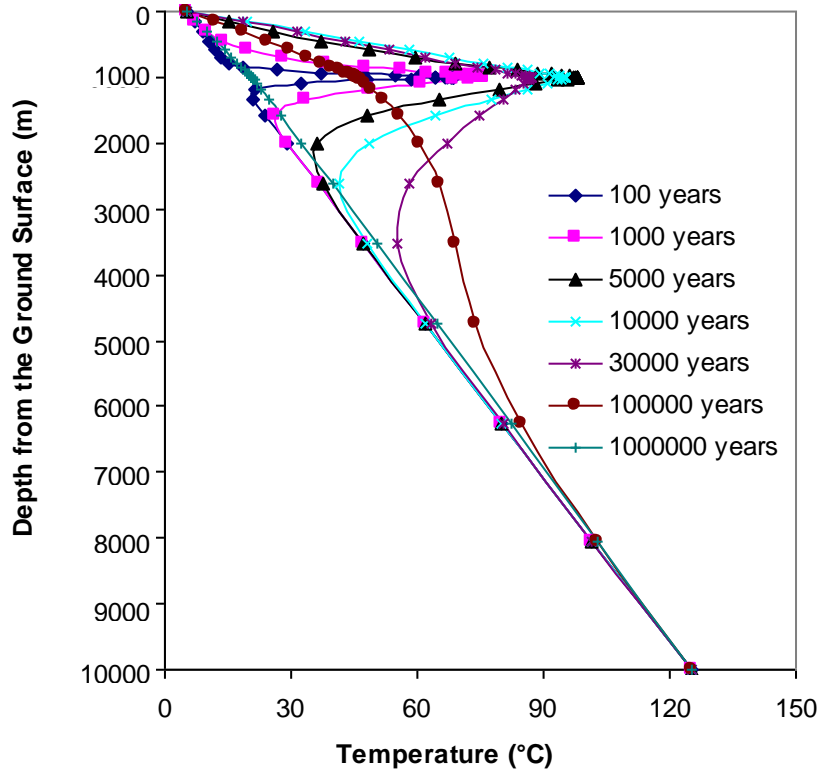


Figure 45: Temperatures along Vertical Axis for an Infinite Repository

Temperature differences between an infinite repository model and a finite repository model are shown in Figure 46. Using the boundary conditions for an infinite repository model as the boundary conditions for a finite repository model not only influences the peak temperatures in the rock around the repository but also influences the temperature of the rock at depth.

The temperature difference between the infinite and finite repository models at the repository centre was less than 0.7°C during the first 800 years after waste placement (Figure 43). The greatest difference of the temperature at the centre of the repository for the two models is 42°C at approximately 30,000 years after waste placement. These two observations form the basis for correcting the results from the near-field model so that they are representative of a finite repository.

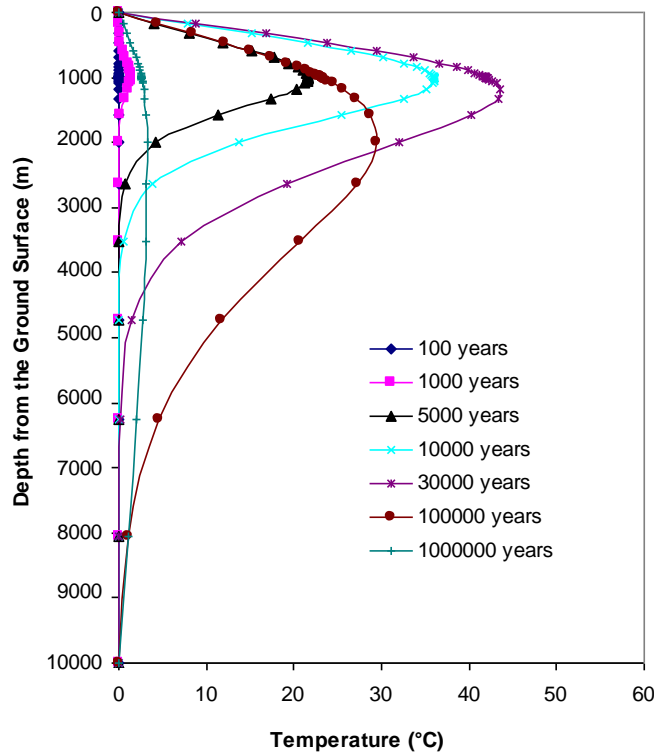


Figure 46: Temperature Differences between an Infinite Repository Model and a Finite Repository Model

5.3 NEAR-FIELD MODELLING

Three simulations are presented in this section. The first simulation is a thermal near-field model using a thermal load corresponds to the PTL. The second simulation is a coupled thermal-mechanical model with initial stresses of zero and a thermal load corresponding to the PTL. The third model is designed to calculate stresses in the rock induced by excavation of the placement room and the in-floor borehole with the initial stresses equal to representative in situ stresses. The first simulation includes the application of a temperature correction to account for the finite horizontal extent of a repository, based on the analyses described in Section 5.2.

5.3.1 Thermal Near-Field Modelling

5.3.1.1 Model Geometry, Boundary Conditions and Initial Conditions

The model geometry for the thermal near-field modelling is the same as shown in Figure 4. The thermal boundary conditions are shown in Figure 5. The thermal load uses one quarter of a container heat output, which corresponds to the PTL as shown in Table 3. The initial temperature in the rock is 5°C on the upper surface with a geothermal gradient of 0.0012°C/m of depth.

Some selected locations and lines near the placement room and in-floor borehole are marked in Figure 47. The numerical results for these selected locations are given in this section.

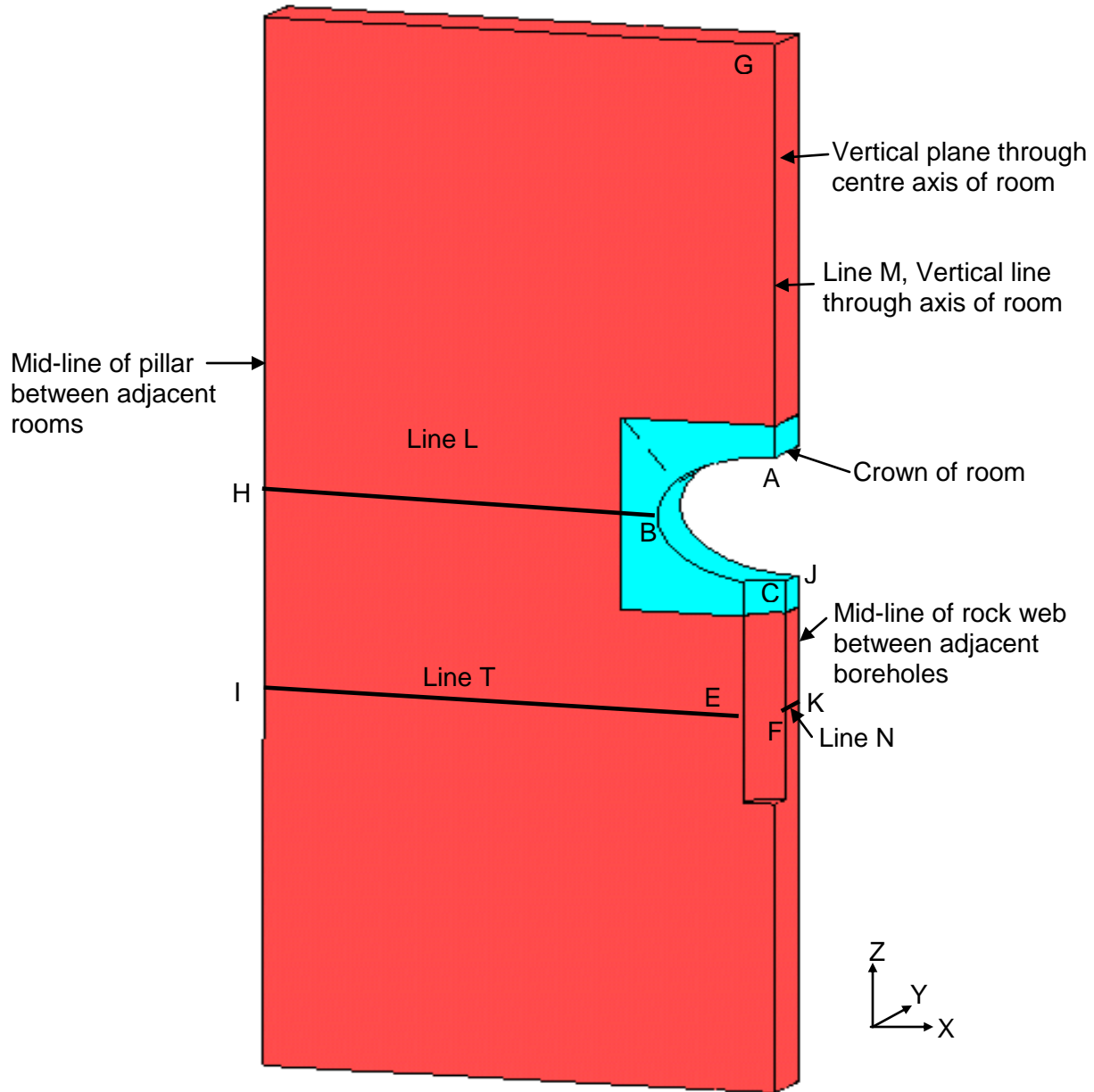


Figure 47: Locations for Presentation of Near-Field Modelling Results

5.3.1.2 Thermal Near-Field Modelling Results

Temperatures versus time at the tunnel crown (Point A) and container skin for an infinite DGR are shown in Figure 48. There are two peaks in temperature at the container skin. The first peak occurs 30 years after waste placement with a value of 88°C. The second peak occurs 7,200 years after waste placement with a value of about 105°C. The temperature of the rock at the tunnel crown also reaches 101°C approximately 7,200 years after waste placement.

As discussed previously, these results represent the thermal response for a DGR with infinite horizontal dimensions and do not represent the thermal response for a DGR with finite horizontal dimension. The difference between the temperature at the tunnel crown and the temperature on container skin is small after 1,000 years (less than 4°C, with time the difference gets smaller and smaller), indicating that the temperature at the level of repository is very uniform.

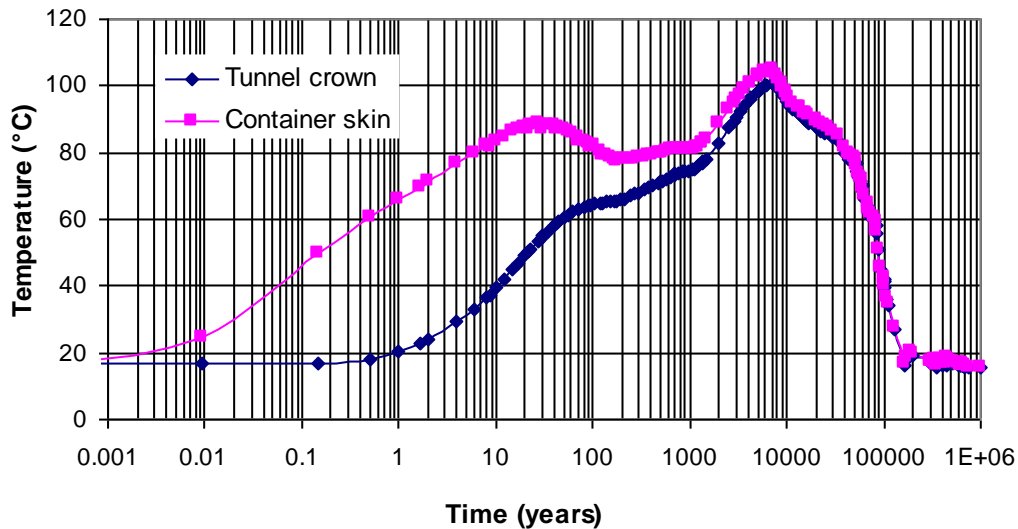


Figure 48: Near-field Modelling Results for an Infinite DGR (using load corresponding to the PTL)

Section 5.2 describes modelling that is performed to determine the difference in temperature between a finite repository and an infinite repository. The temperature difference at the centre of the repository is shown in Figure 43 and is presented again in Figure 49. Since the temperature at all locations at the repository depth are within a few degrees of each other 1,000 years after waste placement, and since these temperatures are close to the temperature at the centre of an infinite repository, then the same temperature can be subtracted from the temperatures at all locations. Subtracting the temperature difference shown in Figure 49 from temperatures at all locations will result in all these temperatures being representative of the temperature in a finite repository with a thermal load equal to the PTL. For times before 1,000 years, the temperature difference in Figure 49 is near zero. Although this may not be very

rigorously correct approach for modelling the near field in a finite repository, it will provide reasonable temperature predictions at the repository depth.

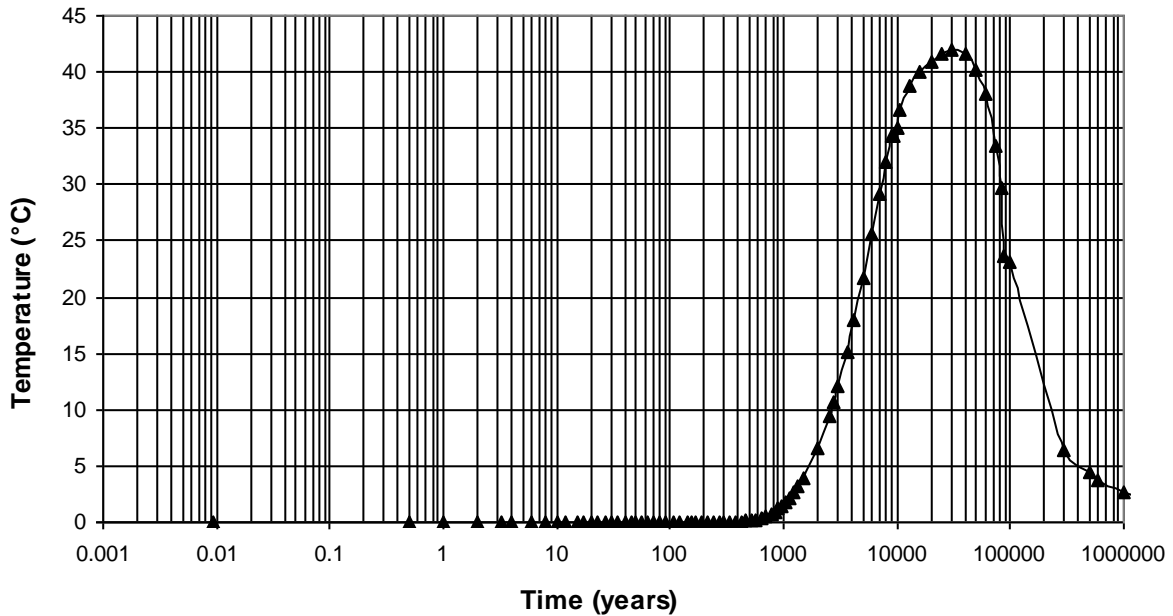


Figure 49: Differences of Temperature at the Centre of Repository between Infinite – Dimension Model and Finite Dimension Model

The modified results at different locations for a finite repository using a thermal load corresponding to the PTL are illustrated in Figure 50 (refer to Figure 47 for locations of Points A, B, C and E; refer to Figure 6 for location of Point D). The results are obtained by subtracting the differences shown in Figure 49 from the results of near-field modelling based on the assumption that the temperature is uniform 1,000 years after waste placement (Figure 48 shows that the temperature at different locations approaches uniform). The modified temperature of the container skin is 88°C at 35 years after waste placement, and 84°C at 3,500 years after waste placement. The modified temperature at Point E (the wall of in-floor borehole) has the first peak value of 78°C occurring 55 years after waste placement and the second peak value of 82°C occurring approximately 3,600 years after waste placement.

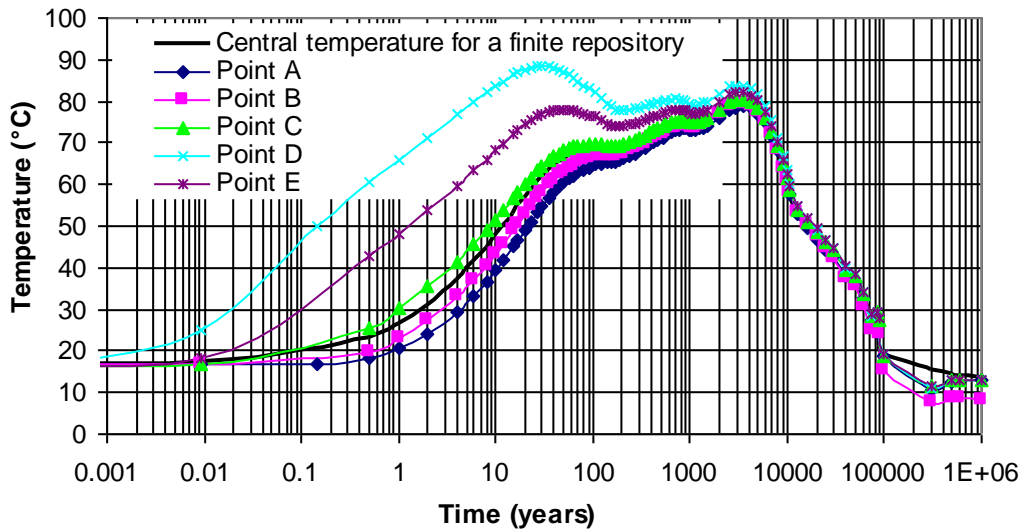


Figure 50: Modified Results at Different Locations for a Finite Repository using a Thermal Load Corresponding to the PTL

Figure 51 shows the modified near-field temperatures on the container skin and at the tunnel crown, compare to the original temperatures at the same locations. It also shows the central temperature from far-field modelling for a finite repository. During the first 1,000 years after waste placement, the modified temperatures are the same as the original temperature from the near-field modelling. The modified temperatures have a significant difference from the original temperatures 1,000 years after waste placement, but they are very similar to the central temperature from far-field modelling for a finite repository.

Figure 52 shows the modified temperatures along Line T (at mid-height of the container) from the container skin (Point D) to the model boundary (Point I) (refer to Figure 47 for locations) at eight different times. The temperatures are 65°C on the container skin and gradually drop to 19°C at the model boundary (Point I) 1 year after waste placement. The temperatures are 88°C on the container skin and gradually drop to 58°C at the model boundary 35 years after waste placement. With time, the temperature distribution becomes more uniform. For example, the temperatures are 63°C on the container skin and 61.2 °C at the location of model boundary 10,000 years after waste placement.

The modified temperatures along the vertical line through the repository centre at different times are shown in Figure 53. At times less than 1,000 years after waste placement, the temperatures along the vertical line were not uniform. However, the temperatures become more uniform after 1,000 years. Finally, they approach the ambient temperature 1,000,000 years after waste placement.

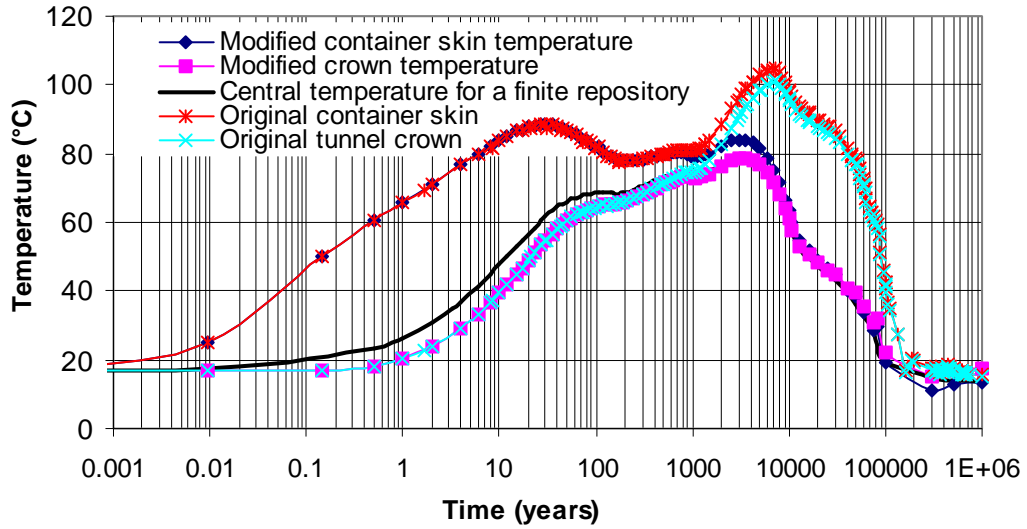


Figure 51: Comparison of Original and Modified Near-field Temperatures at the Container Skin and Tunnel Crown for a Finite Repository using a Thermal Load Corresponding to the PTL

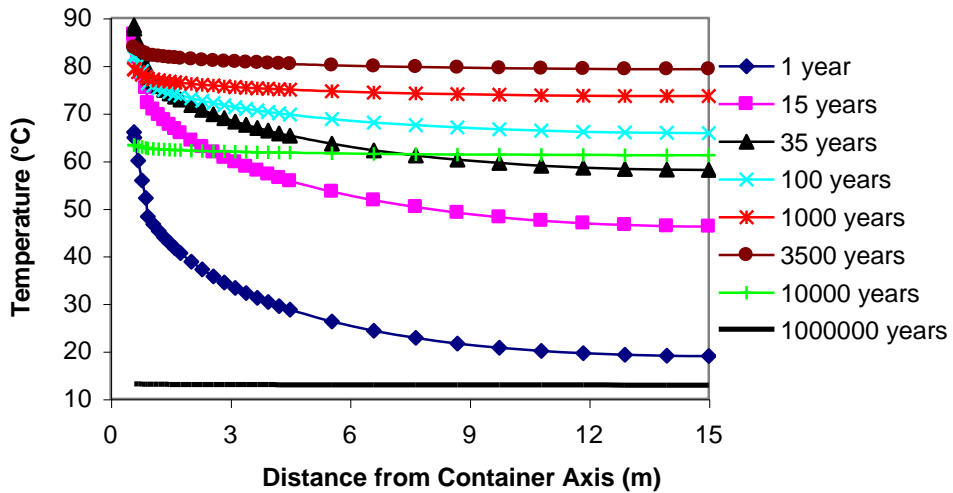


Figure 52: Modified Temperature Profiles along Line T at Different Times (see Figure 47 for locations)

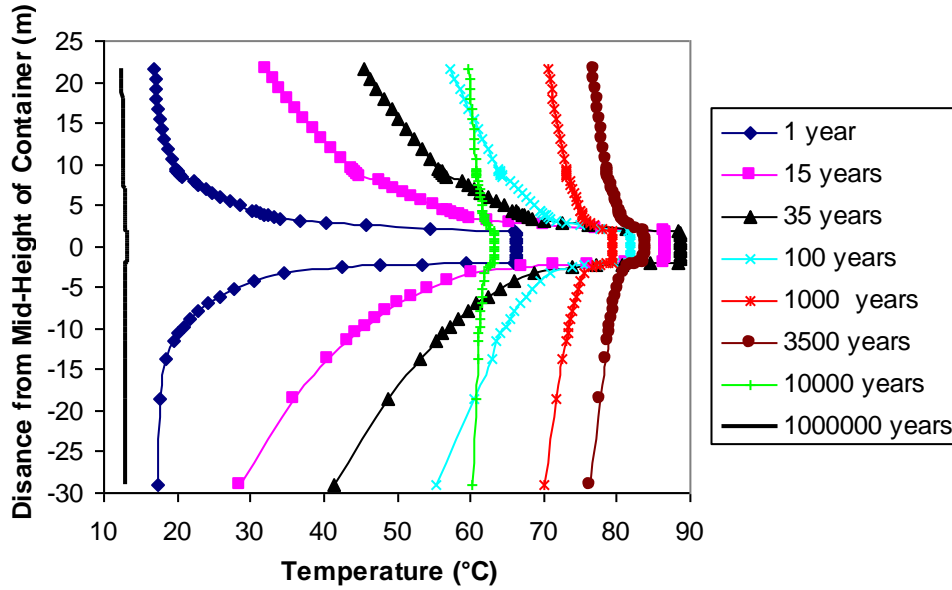


Figure 53: Modified Temperature Profiles along Vertical Line through the Container Centre at Different Times

Although the buffer and backfill materials are incorporated in the near-field thermal modelling, their temperatures are not of our interest. The temperature contours in the rock around a container and tunnel for four different times are shown in Figure 54. The plot again shows that the temperature in the rock becomes more uniform with time.

The temperature difference shown in Figure 49 is developed for use in estimating the temperatures only at the repository level. For other locations a few 10's of meters above or below a finite repository, a temperature difference like Figure 49 for that depth should be developed using the method shown in Section 5.2.

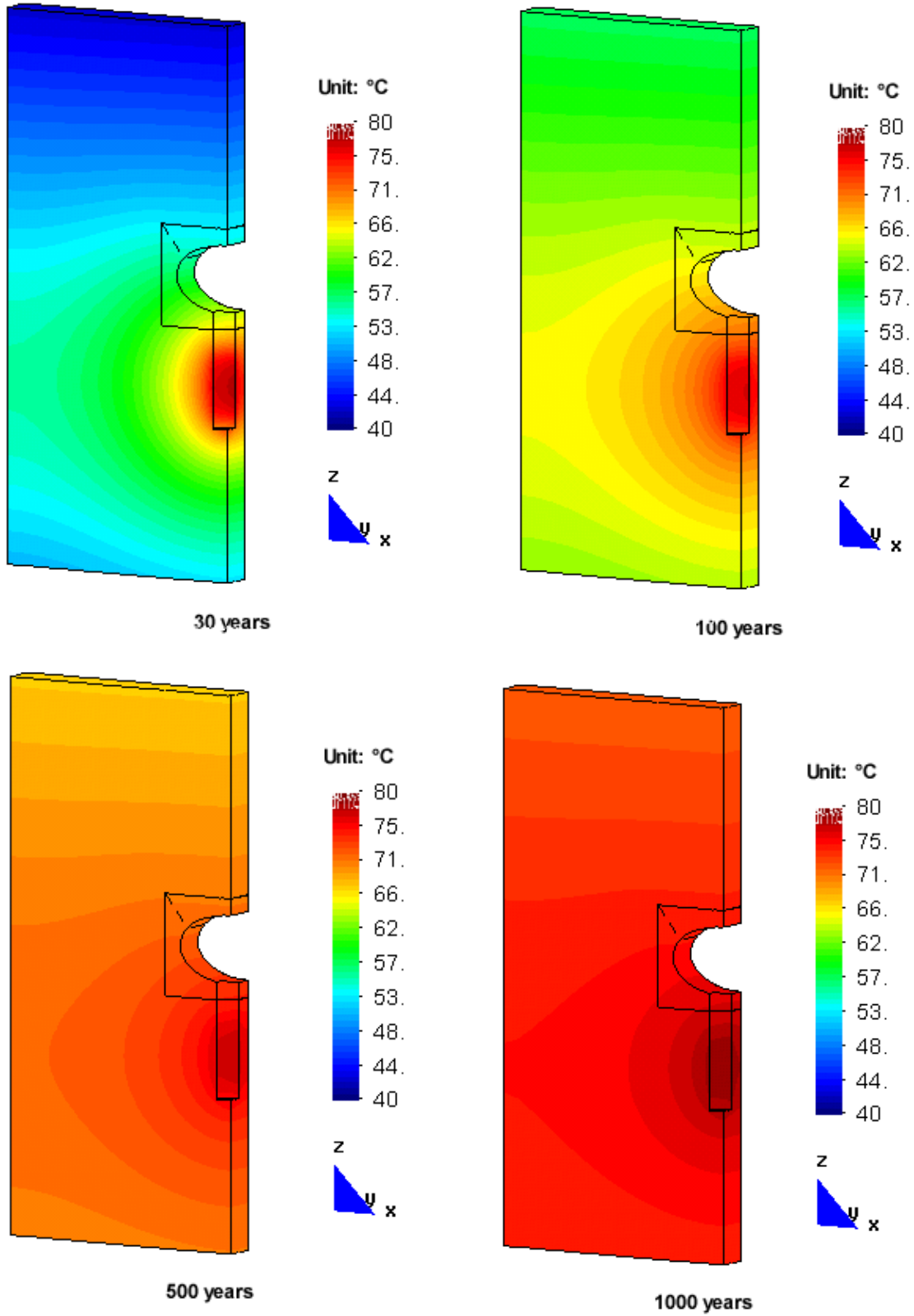


Figure 54: Temperature Contours in the Rock around a Container and the Tunnel at Four Different Times

5.3.2 Thermal-Mechanical Near-field Modelling

Based on the in-situ stresses as shown in Equations 2, 3 and 4, at the repository horizon of 1,000 m below ground surface, the three principal in-situ stress components are as follows:

$$\left. \begin{array}{l} \sigma_1 = 65.0 \text{ MPa} \\ \sigma_2 = 49.4 \text{ MPa} \\ \sigma_3 = 26.0 \text{ MPa} \end{array} \right\} \quad (5)$$

Prior to excavation, the rock mass is in a state of equilibrium under the in-situ stresses. Upon excavation of placement room and in-floor borehole, the stresses re-adjust to a new state of equilibrium. Therefore, stress concentration occurs in the rock around the placement room and the in-floor borehole.

In order to assess the stability of the rock mass around the placement room and the in-floor borehole, the total stresses induced by excavation and thermal expansion are needed. The total stresses are obtained by superimposing the thermally induced stresses on the stresses induced by excavation. Therefore, in this section, a coupled thermal-mechanical near-field model is constructed with initial stresses of zero and an excavation model is constructed based on the initial stresses shown in Equation 5.

5.3.2.1 Thermal-Mechanical Near-Field Model

Excavation Model:

Model geometry is shown in Figure 4(a). The only material in this model is rock, and the thermal boundary conditions are all isothermal. The side surfaces are fixed in their horizontal directions as shown in Figure 6. The bottom of the model is fixed in the vertical direction. On the top of the model, a vertical stress of 26.0 MPa is applied to represent the vertical in-situ stress at 1,000 m depth. The walls of the placement room and the in-floor borehole are free to move. The initial stresses in the rock are as shown in Equation 5.

Thermal-Mechanical Model:

The model geometry is the same as that shown in Figure 4. Thermal model boundary conditions are the same as those described in Section 5.3.1.1. Mechanical model boundary conditions are shown in Figure 6. Initial stresses are assumed to be zero.

Due to the near-field model only representing a model with an infinite repository, the modelling results are not representative of the results for a model with a finite repository after 1,000 years. In this section, the results for the first 100 years after waste placement are given, which are not only representative of the results for an infinite repository but also for a finite repository, since temperatures are the same for both in time period presented.

5.3.2.2 Thermal Results from the Coupled Thermal-Mechanical Modelling

Thermal response is the same as described in Section 5.3.1.

5.3.2.3 Near-Field Stresses

The thermally induced stresses along a vertical line through the tunnel crown (see Figure 47 for locations) are shown in Figures 55, 56 and 57. The peak thermally induced stress in the X direction is 43 MPa at Point A (tunnel crown) and 27 MPa at Point G (38.75 m above the tunnel crown) 100 years after waste placement. The thermally induced stress in the X direction gradually decreases with distance from the tunnel crown. Although the pattern of the stresses in the Y direction is different from that of the stresses in the X direction, the peak thermally induced stress in the Y direction also occurs at the tunnel crown with a magnitude of 35 MPa. Due to the small value of Young's modulus of light backfill, the thermally induced stress in the Z direction at the tunnel crown approaches zero.

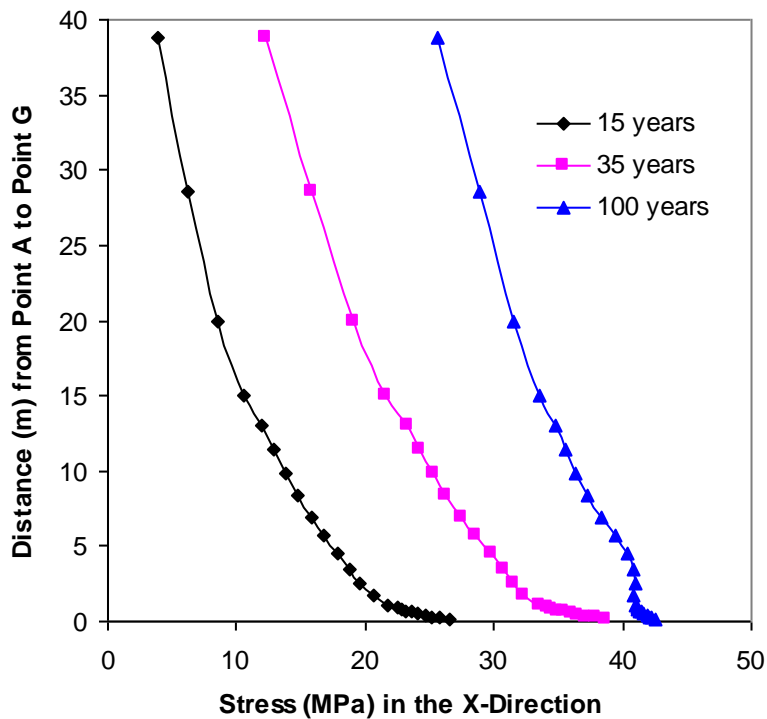


Figure 55: Thermally Induced Stresses in the X Direction along Line M (see Figure 47 for locations)

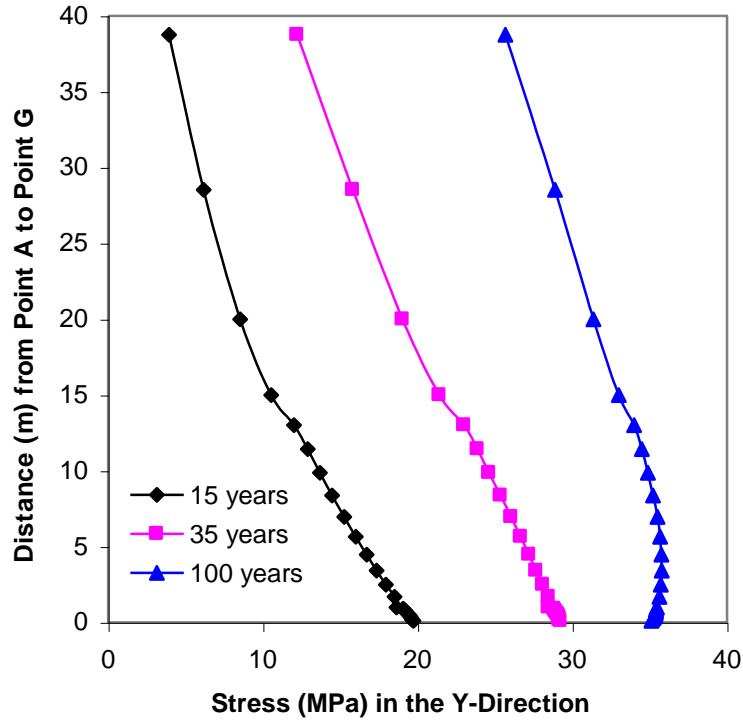


Figure 56: Thermally Induced Stresses in the Y Direction along Line M (see Figure 47 for locations)

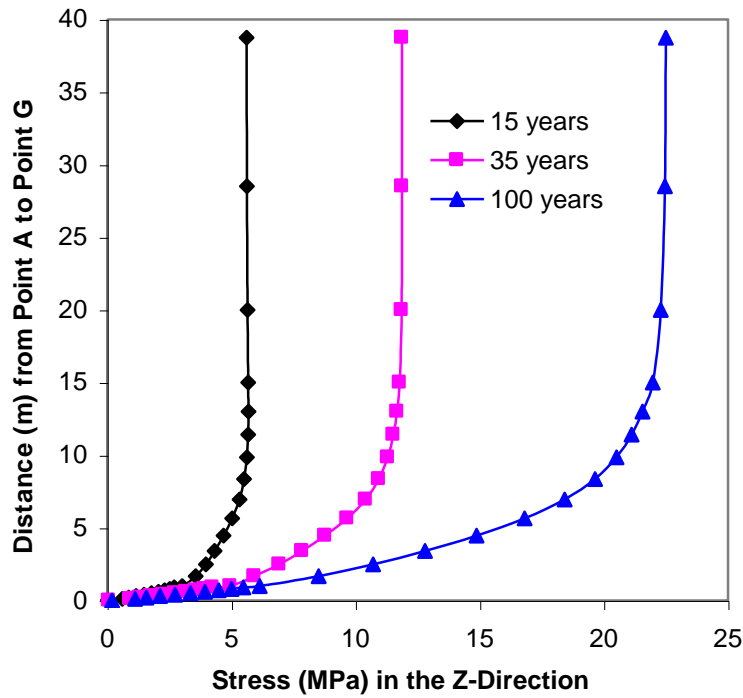


Figure 57: Thermally Induced Stresses in the Z Direction along Line M (see Figure 47 for locations)

The thermally induced stresses in the X, Y, and Z directions along the horizontal Line L extending from the tunnel mid-height to the pillar centre line (refer to Figure 47 for location) at three different times are shown in Figures 58, 59 and 60. The stresses in the X direction at different times are almost zero at Point B (the tunnel wall) because the stiffness of the light backfill is very small compared to the rock. At Point H, the thermally induced stress in the X direction increases from zero before waste placement to 33 MPa at 100 years after waste placement. The thermally induced stress in the Y direction along Line L does not change much with distance from the tunnel wall, but it does increase with time. The thermally induced stress in the Y direction increases from zero before waste placement to 37 MPa approximately 100 years after waste placement. The thermally induced stress in the Z direction is 50 MPa at Point B (the tunnel wall) and drops to 26 MPa at Point H 100 years after waste placement.

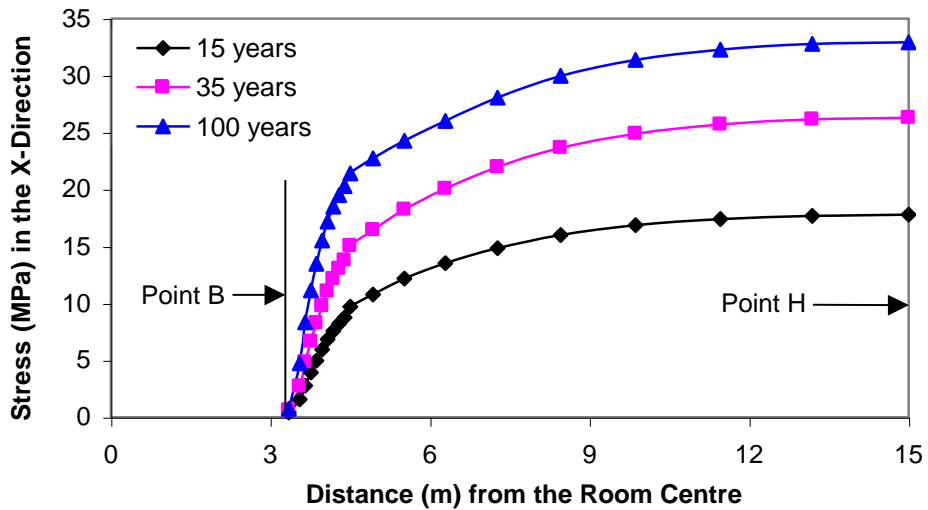


Figure 58: Thermally Induced Stresses in the X Direction along Line L (see Figure 47 for locations)

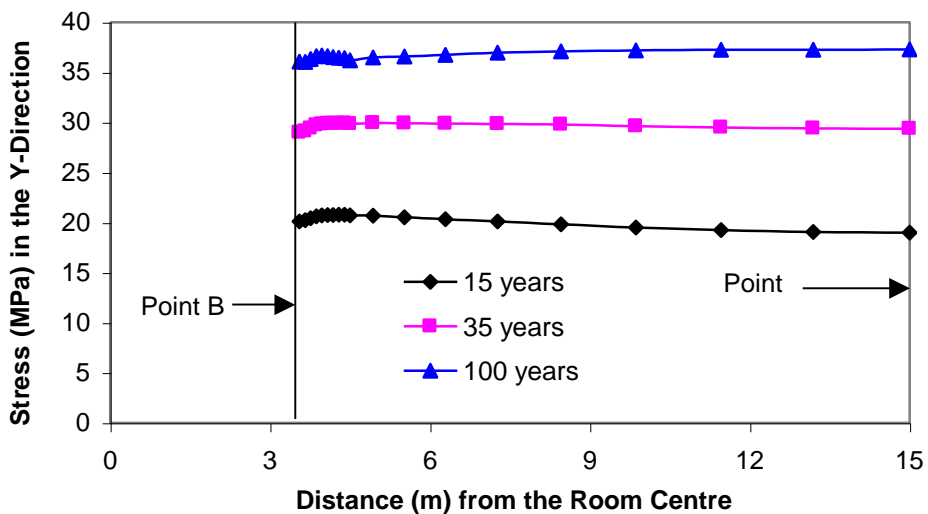


Figure 59: Thermally Induced Stresses in the Y Direction along Line L (see Figure 47 for locations)

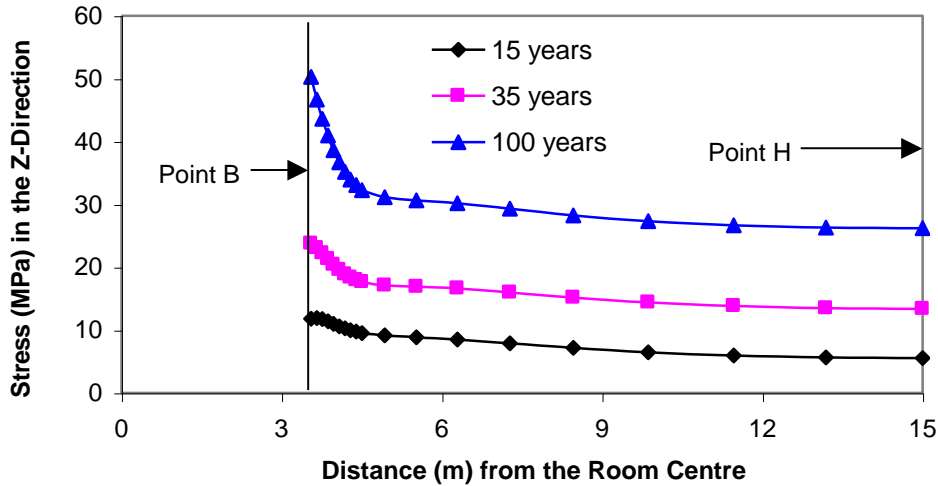


Figure 60: Thermally Induced Stresses in the Z Direction along Line L (see Figure 47 for locations)

The thermally induced stresses in the X, Y, and Z directions along a horizontal Line T extending from the mid-height of the container to the pillar centre line (refer to Figure 47 for location) at three different times are illustrated in Figures 61, 62 and 63. The stresses in the X direction at different times are about 3 MPa at Point E (the borehole wall) because the stiffness of the buffer is very small compared to the stiffness of the rock. At Point I, the thermally induced stress in the X direction increases from zero before waste placement to 34 MPa at 100 years after waste placement. The thermally induced stress in the Y direction along Line T is 54 MPa at Point E and 38 MPa at Point I 100 years after waste placement. The thermally induced stress in the Z direction is 11.5 MPa at Point E and drops to 4.3 MPa at Point I 15 years after waste placement and 16 MPa increasing to 25 MPa at Point I approximately 100 years after waste placement. The trend of decreasing the thermally induced stress in the Z direction with distance 15 years after waste placement is different from the trend of increasing stress with distance of 100 years after waste placement.

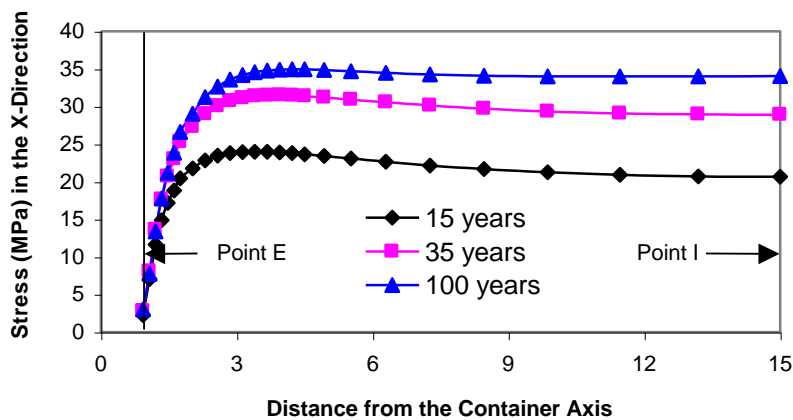


Figure 61: Thermally Induced Stresses in the X Direction along Line T (see Figure 47 for locations)

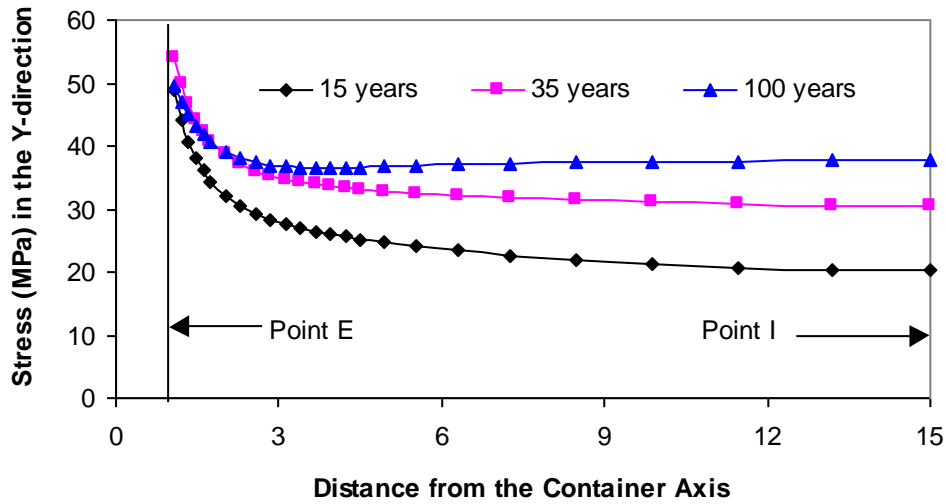


Figure 62: Thermally Induced Stresses in the Y Direction along Line T (see Figure 47 for locations)

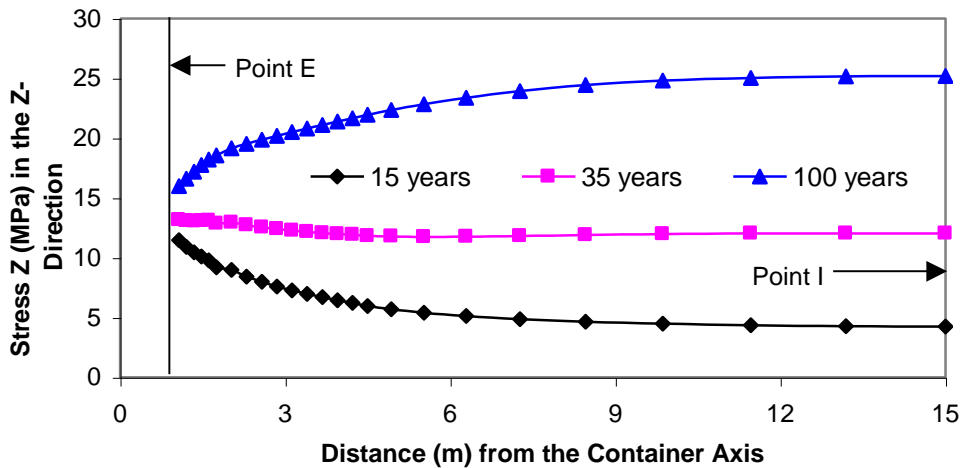


Figure 63: Thermally Induced Stresses in the Z Direction along Line T (see Figure 47 for locations)

The thermally induced stresses in the X, Y, and Z directions along Line N, a horizontal line at the container mid-height extending from the borehole wall to the mid line of the web between adjacent boreholes (refer to Figure 47 for location) at three different times are given in Figures 64, 65 and 66. The stresses in the X direction are about 74 MPa at Point F and 57 MPa at Point K 100 years after waste placement. The peak thermally induced stress along Line T is 77 MPa at 100 years after waste placement occurring at location 0.178 m from Point F (the borehole wall). The thermally induced stress in the Y direction along Line N is about 3 MPa at Point F and 24 MPa at Point K 100 years after waste placement. The thermally induced stress

in the Z direction is 13 MPa at Point F, increases to a peak values of 19.5 MPa and then drops to 19 MPa at Point K 100 years after waste placement.

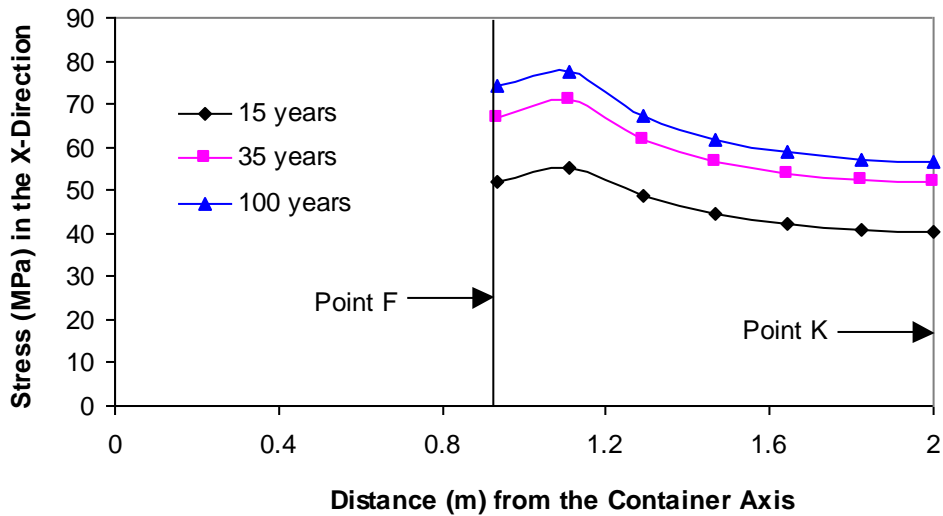


Figure 64: Thermally Induced Stresses in the X Direction along Line N (see Figure 47 for locations)

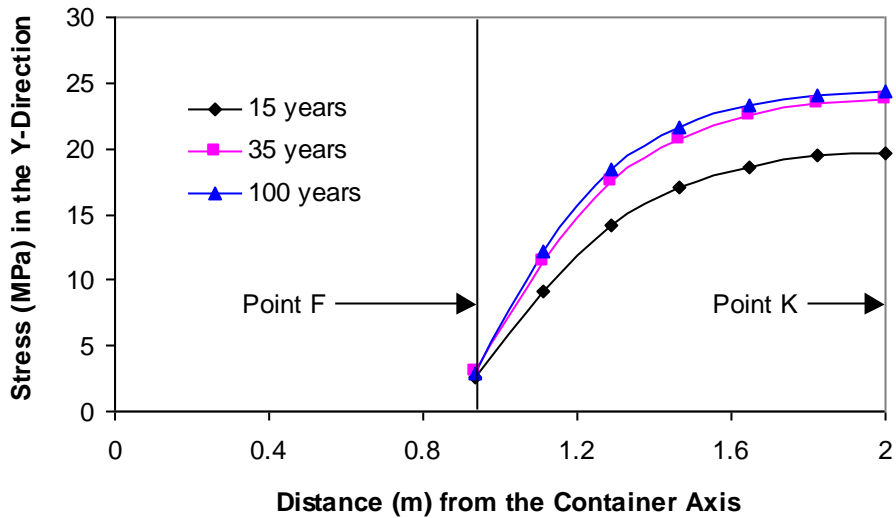


Figure 65: Thermally Induced Stresses in the Y Direction along Line N (see Figure 47 for locations)

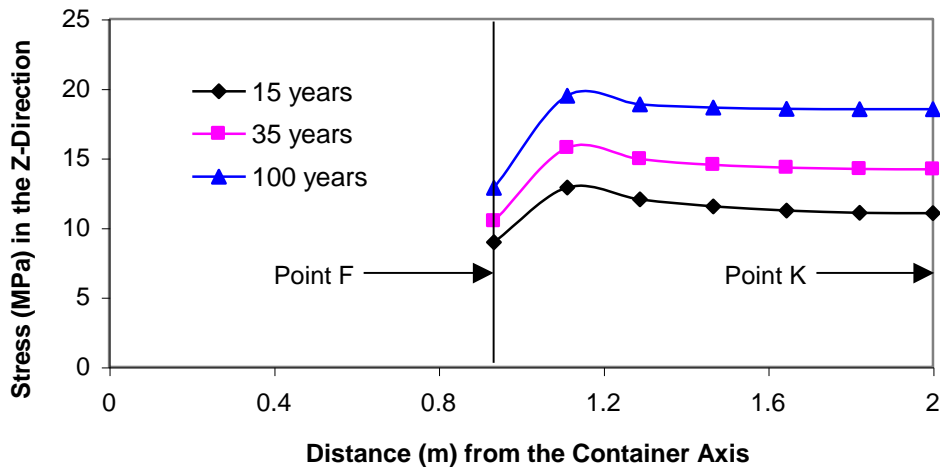


Figure 66: Thermally Induced Stresses in the Z Direction along Line N (see Figure 47 for locations)

The thermally induced stresses in the X and Y directions along Line CJ, a horizontal line from the borehole wall to the mid line of the web between adjacent boreholes along the floor of the tunnel (see Figure 47 for locations), are shown in Figures 67 and 68, respectively. The thermally induced stress in the X direction at Point C (adjacent to the borehole) is 67 MPa at 15 years after waste placement and increases to 113 MPa at 100 years after waste placement. The thermally induced stress in the Y direction at Point J is 52 MPa at 15 years after waste placement and increases to 86 MPa at 100 years after waste placement. The thermally induced stress in the Y direction ranges from about 0.5 MPa at Point C to 5.5 MPa at Point J approximately 100 years after waste placement. Thermally induced stress in the Z direction is approximately zero at all times due to the low stiffness of the backfill relative to the rock stiffness and is not presented.

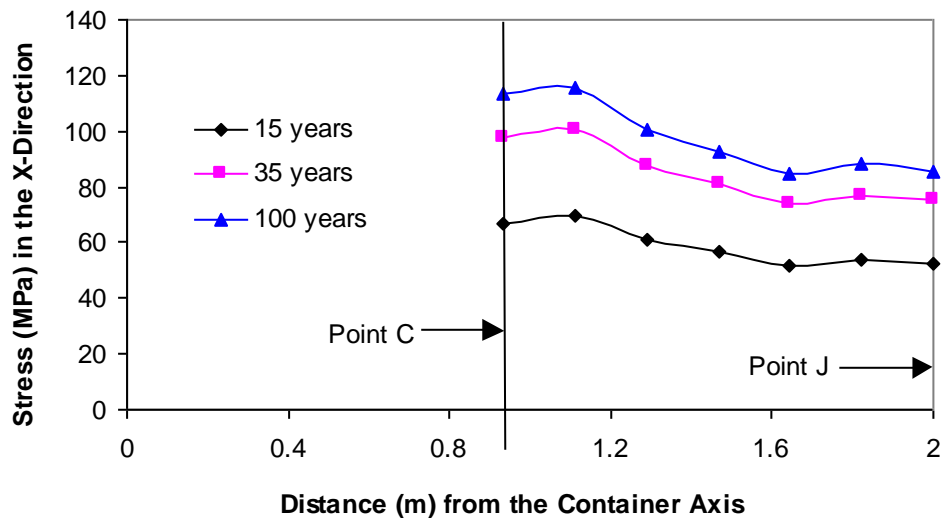


Figure 67: Thermally Induced Stresses in the X Direction along Line CJ (see Figure 47 for locations)

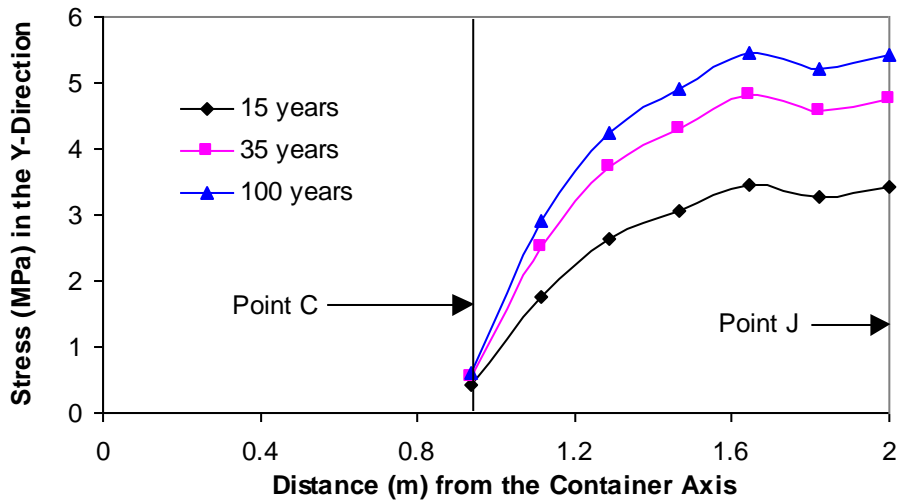


Figure 68: Thermally Induced Stresses in the Y Direction along Line CJ (see Figure 47 for locations)

It is not the thermally induced stress that controls the stability of the rock along the wall of the in-floor borehole and tunnel. It is the total stress. Therefore, it is necessary to know the total stress at selected locations. As described earlier, the total stresses are the excavation-induced stresses superimposed with the thermally induced stresses. In the following, stress after excavation refers to stresses that exist after both tunnel excavation and placement borehole drilling.

The total stresses in the X, Y, and Z directions along Line M, vertical line through the container axis and the tunnel crown (see Figure 47 for locations), at four different times are shown in Figures 69, 70 and 71. The stress in the X direction is 63 MPa at the tunnel crown (Point A) and drops to 49 MPa at Point G immediately after excavation. The peak total stress in the X direction at Point A increases to 103 MPa at 100 years after waste placement. The total stress in the X direction at Point G is 75 MPa at 100 years after waste placement. The stress in the Y direction ranges from 63.5 MPa to 65 MPa from the tunnel crown to Point G immediately after excavation. The total stress in the Y direction is 99 MPa at the tunnel crown and 91 MPa at Point G at 100 years after waste placement. The stress in the Z direction is always zero at the tunnel crown. The Z-direction stress increases from 26 MPa at Point G immediately after excavation to 49 MPa at 100 years after waste placement.

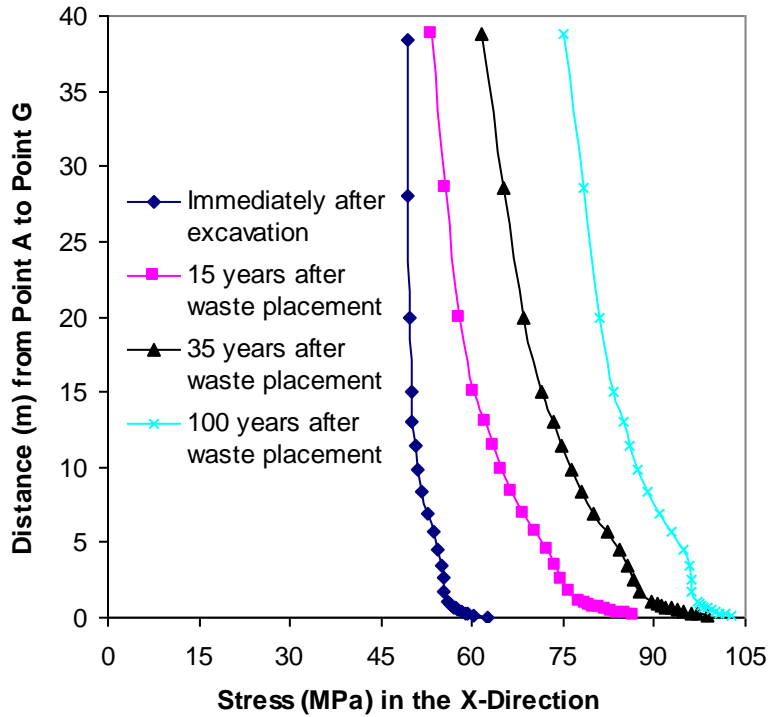


Figure 69: Profiles of Total Stresses in the X Direction along Line M (see Figure 47 for locations)

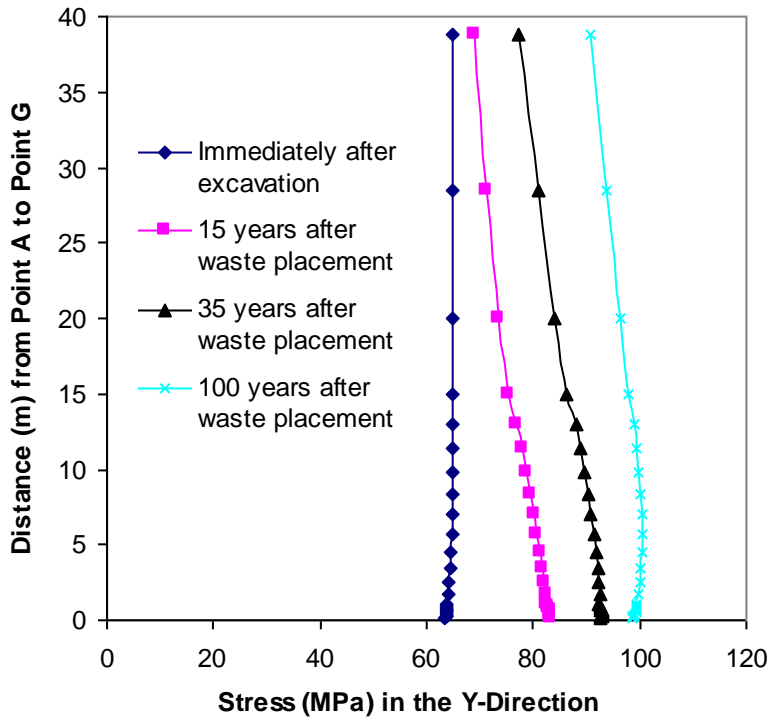


Figure 70: Profiles of Total Stresses in the Y Direction along Line M (see Figure 47 for locations)

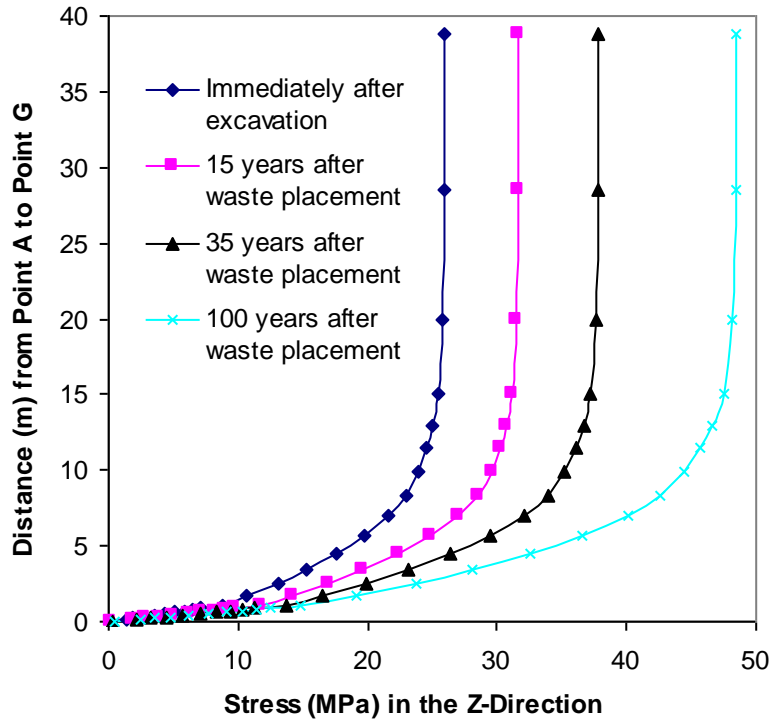


Figure 71: Profiles of Total Stresses in the Z Direction along Line M (see Figure 47 for locations)

Total stresses in the X, Y, and Z directions along Line L, a horizontal line from the placement room wall to the centre line of the pillar between adjacent rooms at placement room mid-height, at different times are shown in Figures 72, 73 and 74, respectively. The stress in the X direction is zero at Point B and increases to 43.6 MPa at Point H (model boundary) immediately after excavation. The total stress in the X direction is about 0.8 MPa at Point B (the tunnel wall) and increases to 76 MPa at Point H 100 years after waste placement. The stress in the Y direction is 63 MPa at Point B and increases to 65 MPa at Point H immediately after excavation. The total stress in the Y direction is 99 MPa at Point B and increases to 102 MPa at Point H 100 years after waste placement. The stress in the Z direction is 56 MPa at Point B and drops to 30 MPa at Point H immediately after excavation. The total stress in the Y direction is 106 MPa at Point B and drops to 56 MPa at Point H 100 years after waste placement.

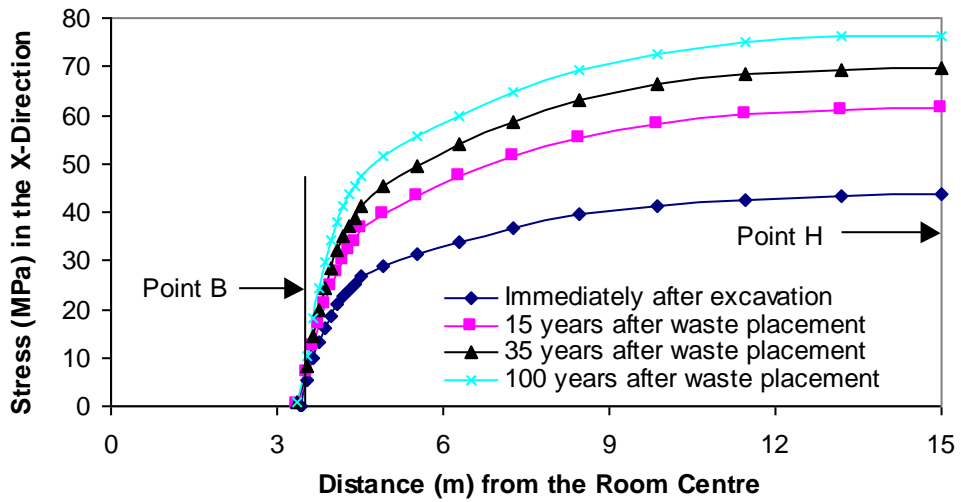


Figure 72: Profiles of Total Stresses in the X Direction along Line L (see Figure 47 for locations)

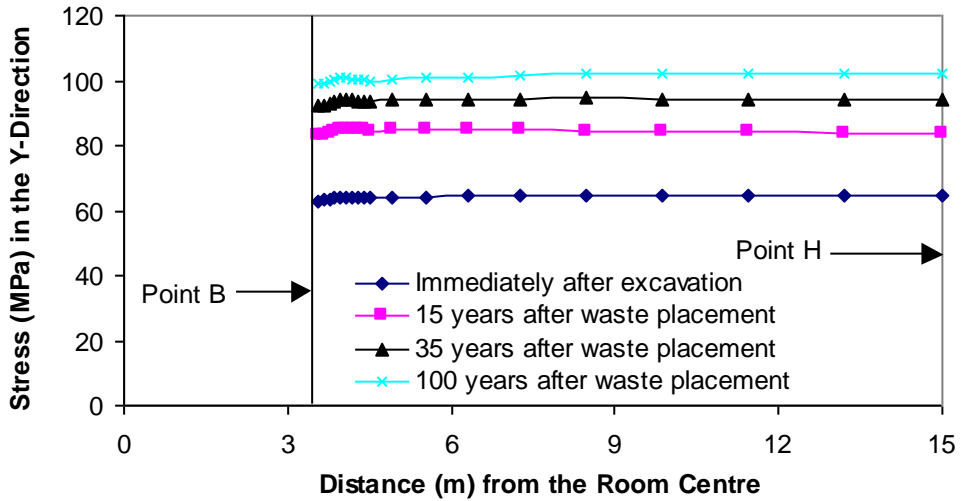


Figure 73: Profiles of Total Stresses in the Y Direction along Line L (see Figure 47 for locations)

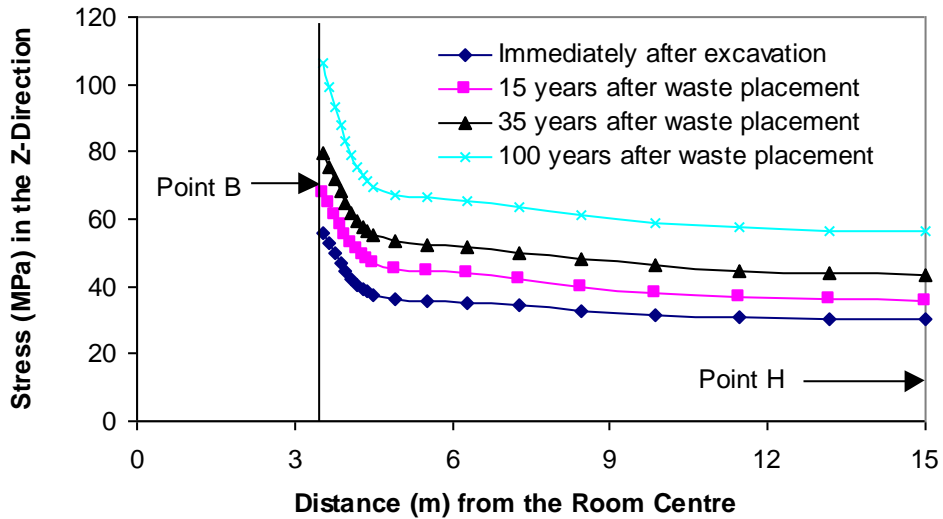


Figure 74: Profiles of Total Stresses in the Z Direction along Line L (see Figure 47 for locations)

Total stresses in the X, Y, and Z directions along Line T, a horizontal line between the centre line of the container and the centre line of the pillar between adjacent rooms at the container mid-height at four different times are shown in Figures 75, 76 and 77, respectively. The stress in the X direction is zero at Point E (in-floor borehole wall) and increases to 47.5 MPa at a distance of 4.5 m from the in-floor borehole axis, and then slowly drops to 45 MPa at Point I (model boundary) immediately after excavation. The total stress in the X direction is 3 MPa at Point E and increases to 82.5 MPa at a distance of 4.0 m from the in-floor borehole axis, and then slowly drops to 79 MPa at Point I 100 years after waste placement.

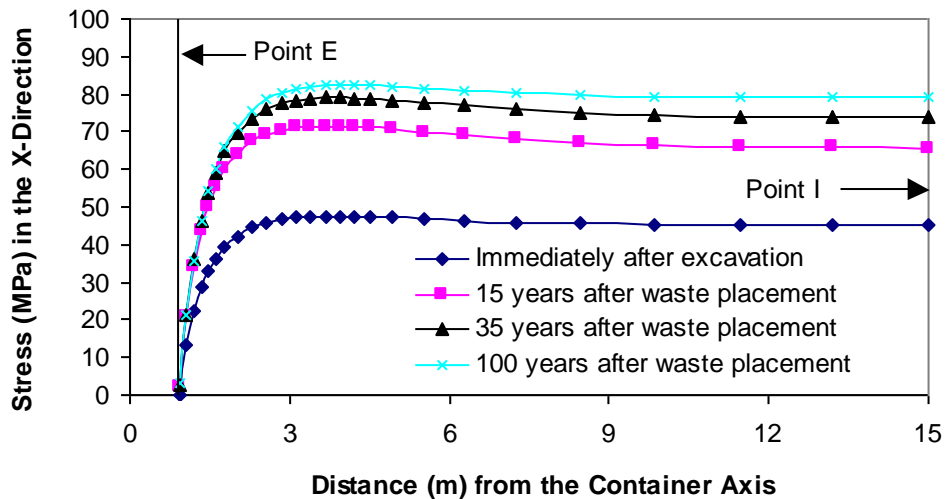


Figure 75: Profiles of Total Stresses in the X Direction along Line T (see Figure 47 for locations)

The stress in the Y direction is 108 MPa at Point E and drops to 65 MPa at Point I immediately after excavation. The total stress in the Y direction is 159 MPa at Point E and drops to 102 MPa at Point I 100 years after waste placement. The peak total stress in the Y direction is 164 MPa at Point E 35 years after waste placement. The stress in the Z direction is 22.5 MPa at Point E and increases to 28.6 MPa at Point I immediately after excavation. The total stress in the Z direction is 37.0 MPa at Point E and increases to 54 MPa at Point I 100 years after waste placement.

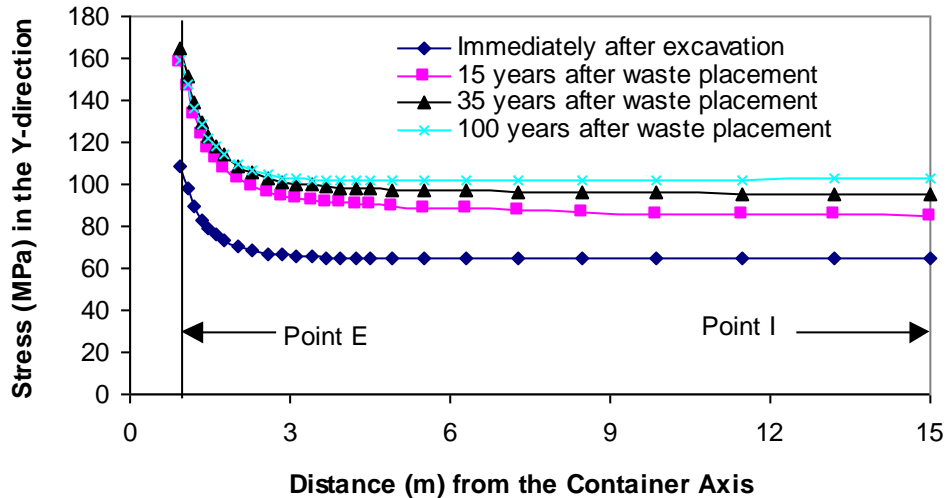


Figure 76: Profiles of Total Stresses in the Y Direction along Line T (see Figure 47 for locations)

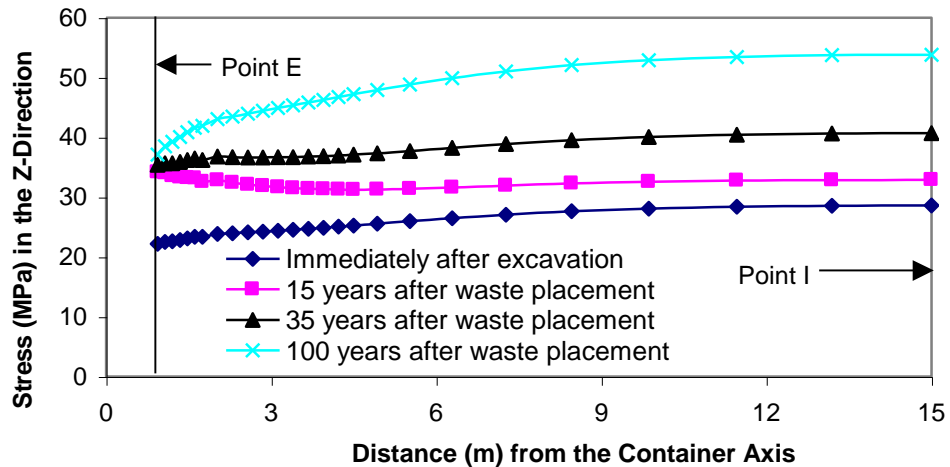


Figure 77: Profiles of Total Stresses in the Z Direction along Line T (see Figure 47 for locations)

Profiles of total stresses in the X, Y, and Z directions along Line N, a horizontal line between the container axis and the mid-line of the web between adjacent boreholes at the container mid-height at four different times are shown in Figures 78, 79 and 80, respectively. The stress in the X direction is 121 MPa at Point F (the borehole wall) and drops to 80 MPa at Point K immediately after excavation. The total stress in the X direction is 195 MPa at Point F and 136 MPa at Point K 100 years after waste placement. The stress in the Y direction is zero at Point F and increases to 37 MPa at Point K after excavation. The total stress in the Y direction is 3 MPa at Point F and 62 MPa at Point K 100 years after waste placement. The stress in the Z direction is 20 MPa at Point F and increases to 24 MPa at a distance of 0.178 m from Point F, and then drops to 23.7 MPa at Point K after excavation. The total stress in the Z direction is 33 MPa at Point F and increases to 43.5 MPa at a distance of 0.178 m from Point F, and then drops to 42 MPa at Point K 100 years after waste placement.

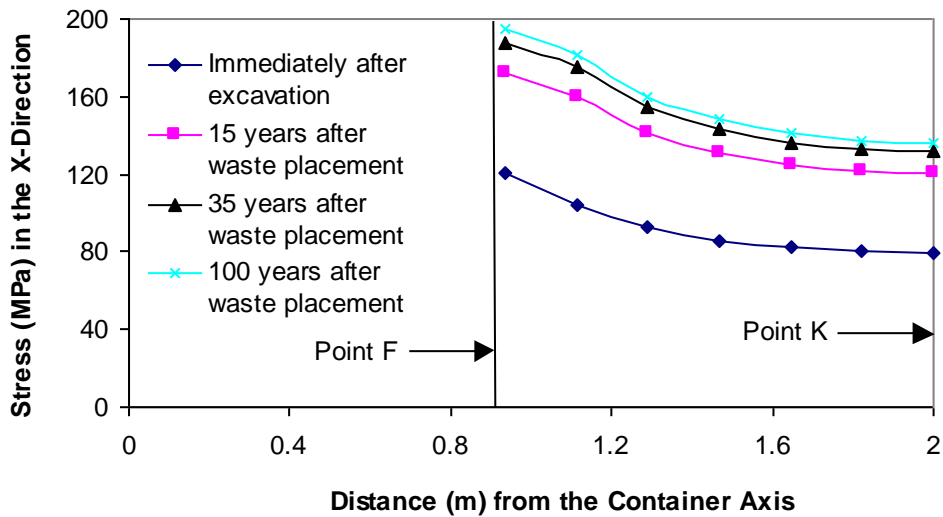


Figure 78: Profiles of Total Stresses in the X Direction along Line N (see Figure 47 for locations)

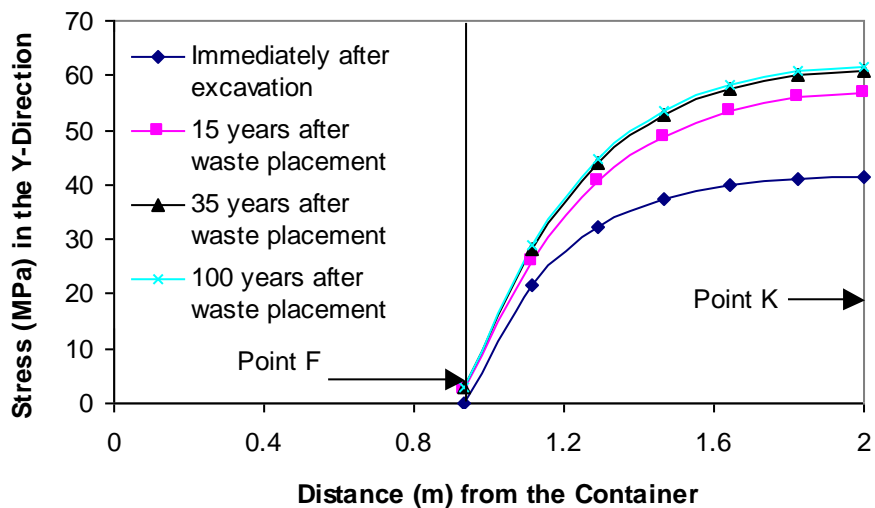


Figure 79: Profiles of Total Stresses in the Y Direction along Line N (see Figure 47 for locations)

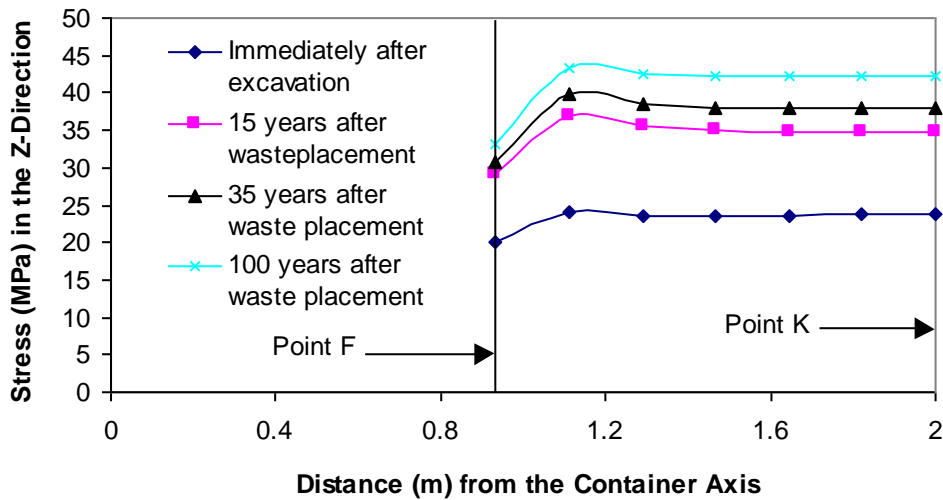


Figure 80: Profiles of Total Stresses in the Z Direction along Line N (see Figure 47 for locations)

Profiles of total stresses in the X and Y directions along Line CJ, a horizontal line between the container axis and the mid-line of the web between adjacent boreholes along the tunnel floor are illustrated in Figures 81 and 82. The stress in the X direction along Line CJ ranges from 189 MPa at Point C (the borehole wall) to 120 MPa at Point J immediately after excavation. The total stress in the X direction along Line CJ ranges from 302 MPa at Point C to 206 MPa at Point J 100 years after waste placement. The stress in the Y direction along Line CJ ranges from zero at Point C to 45 MPa at Point J immediately after excavation. The total stress in the Y direction along Line CJ ranges from 0.5 MPa at Point C to 50 MPa at Point J 100 years after waste placement

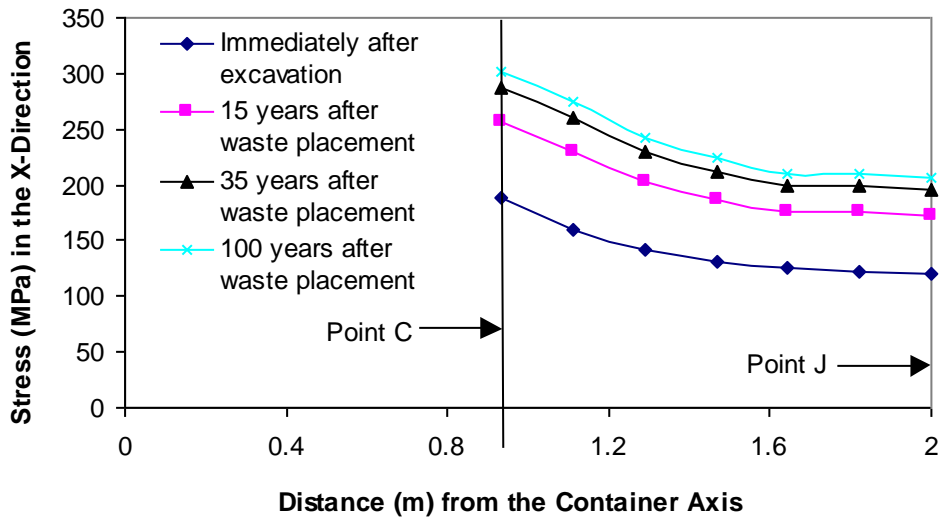


Figure 81: Profiles of Total Stresses in the X Direction along Line CJ (see Figure 47 for locations)

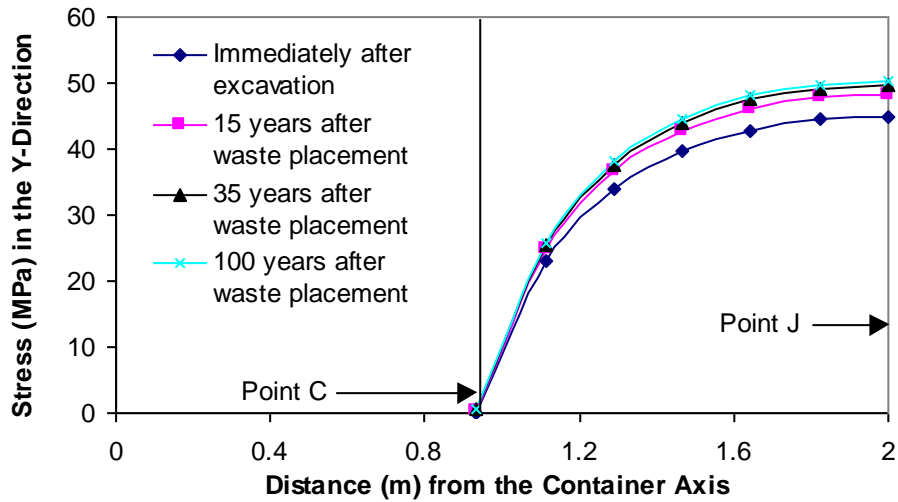


Figure 82: Profiles of Total Stresses in the Y Direction along Line CJ (see Figure 47 for locations)

5.3.2.4 Near-Field Displacements

The thermally induced displacements in the Z direction along Line M are shown in Figure 83. The rock at the tunnel crown moves upwards during the first 15 years after waste placement, and then moves downward by approximately 2 mm. At Point G, the rock moves up during the first 35 years and then moves down.

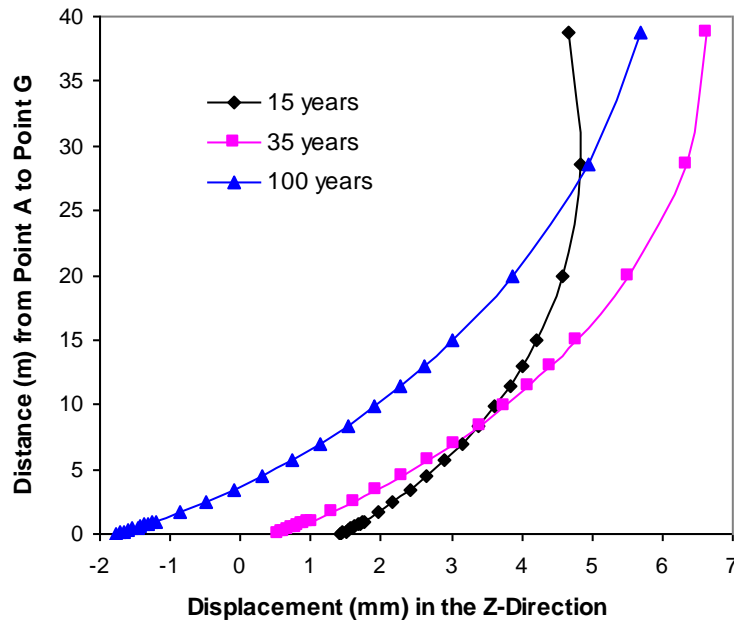


Figure 83: Thermally Induced Displacements in the Z Direction along Line M (see Figure 47 for locations)

Thermally induced displacements in the X direction along Line L are shown in Figure 84. The rock at Point B (the tunnel wall) moves inwards towards the tunnel centre by 1 mm at 15 years after waste placement, 1.5 mm at 35 years after waste placement and 1.7 mm at 100 years after waste placement. The displacement value gradually drops with distance away from the tunnel until the displacement is zero at Point H (as required by the model boundary conditions).

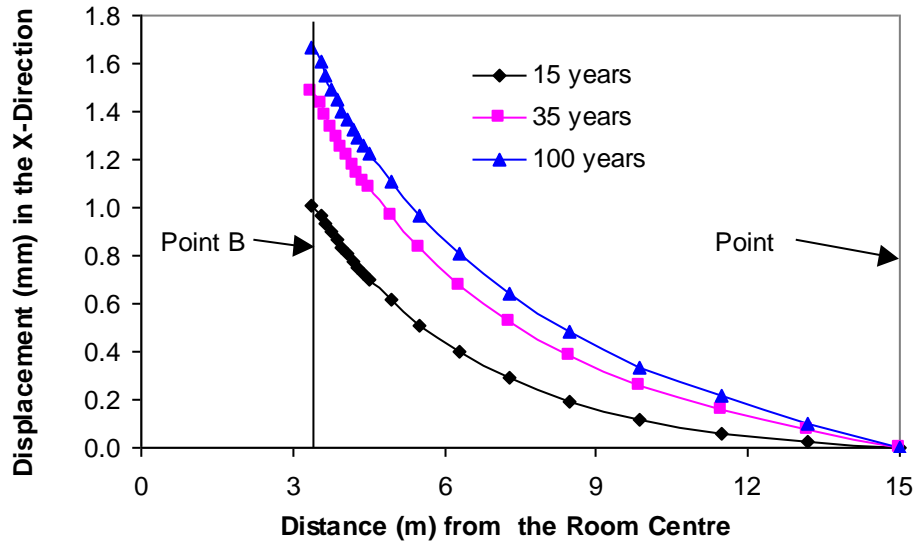


Figure 84: Thermally Induced Displacements in the X Direction along Line L (see Figure 47 for locations)

Thermally induced horizontal displacements along Line T are shown in Figure 85. The thermally induced horizontal displacement at the borehole wall (Point E) is inwards towards the borehole and is less than 1 mm at 15 years after waste placement, 0.78 mm at 35 years after waste placement and about 1 mm at 100 years after waste placement.

Thermally induced horizontal displacements along Line N, a line between the container axis and the mid-line of the web between the adjacent boreholes at the container mid-height, are shown in Figure 86. At Point F (the borehole wall), the thermally induced horizontal displacement is about 0.45 mm at 100 years after waste placement towards the in-floor borehole.

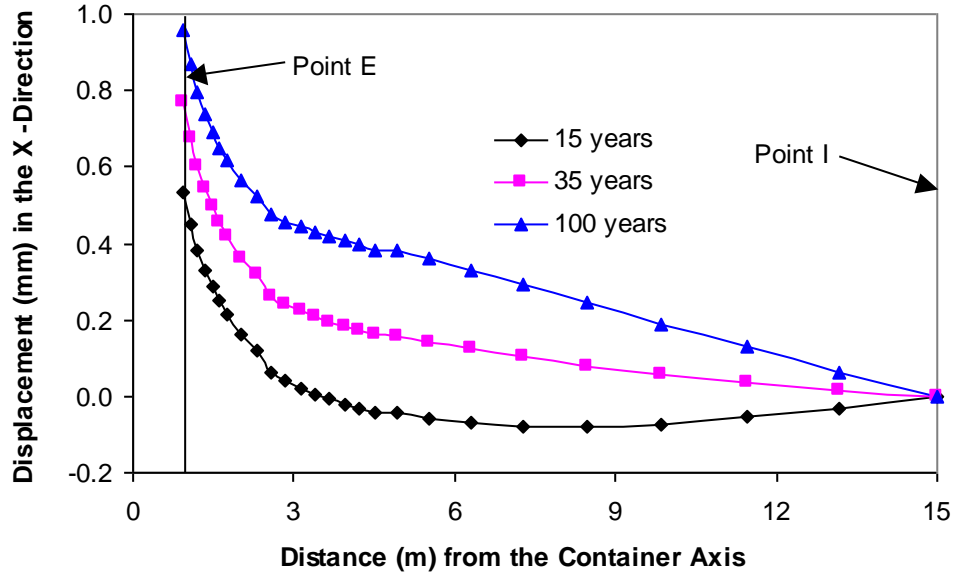


Figure 85: Thermally Induced Displacements in the X Direction along Line T (see Figure 47 for locations)

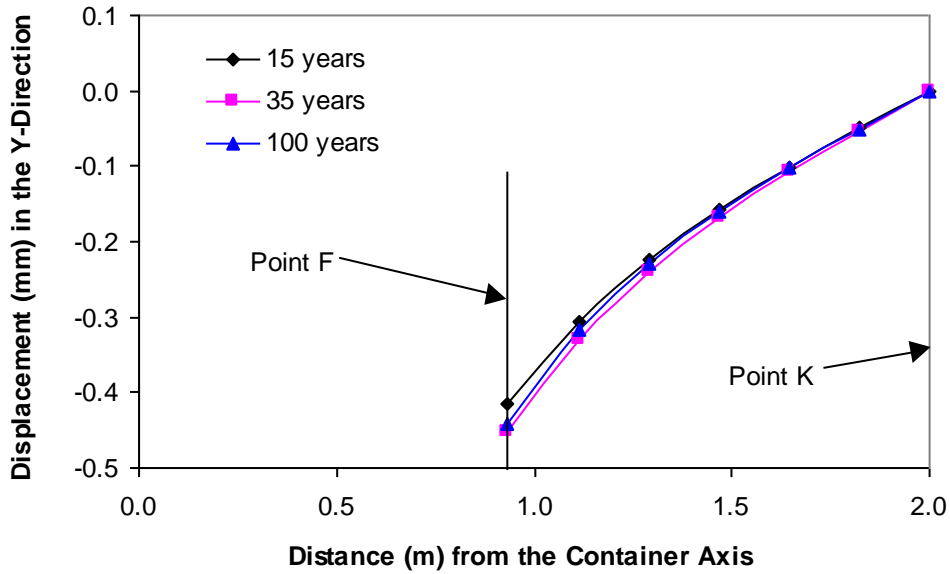


Figure 86: Thermally Induced Displacements in the Y Direction along Line N (see Figure 47 for locations)

5.4 NEAR-FIELD STABILITY ANALYSES

A safety factor is used to evaluate the rock mass stability. The procedure to calculate the safety factor is described as follows.

- First, the major and minor principal stresses are calculated as shown in Section 5.3.2.3 (The X, Y and Z directions are assumed to be the directions of three principal stresses).
- Second, the strength (σ_{1f}) is determined using Equation 1.
- Third, safety factor (SR) is calculated using the following equation: $SR = \sigma_{1f} / \sigma_1$, where σ_1 is the major principal stress.

The lowest safety factor at the tunnel crown is 1.7 immediately after excavation as shown in Figure 87. Heating makes the rock along Line M above the tunnel become more stable. The increase in safety factor can be attributed to increased confinement caused by thermal expansion of the rock. Higher safety factors are also caused by using higher “strength” values during heating of the rock for location where the rock has not exceeded a lower “strength” value during excavation, as described in Section 3.

Safety factors along Line L at four different times are shown in Figure 88. The lowest safety factor is 1.6 on the wall of the tunnel immediately after excavation. At 15 years after waste placement, the safety factor is greater than 2.5 at all locations along this line.

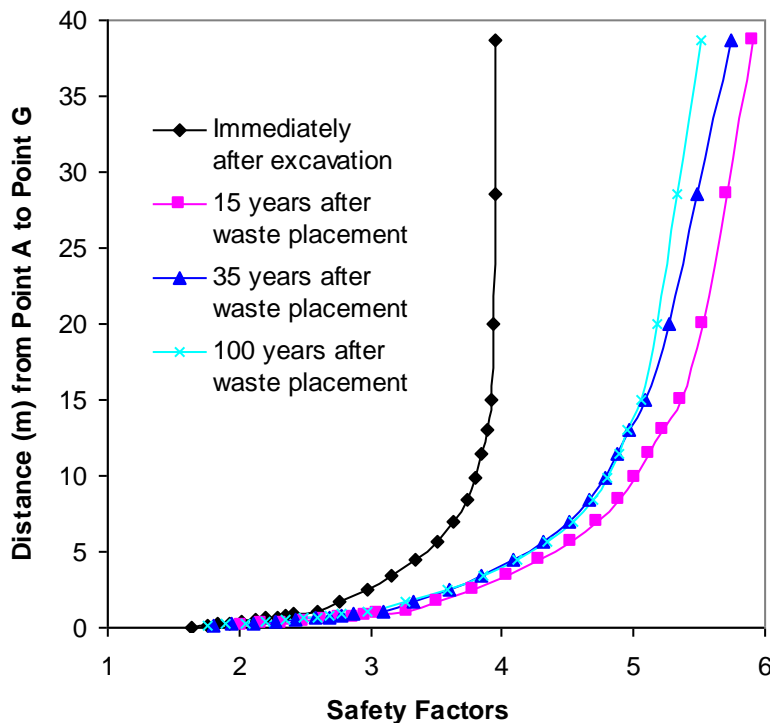


Figure 87: Safety Factors along Line M at Four Different Times (see Figure 47 for locations)

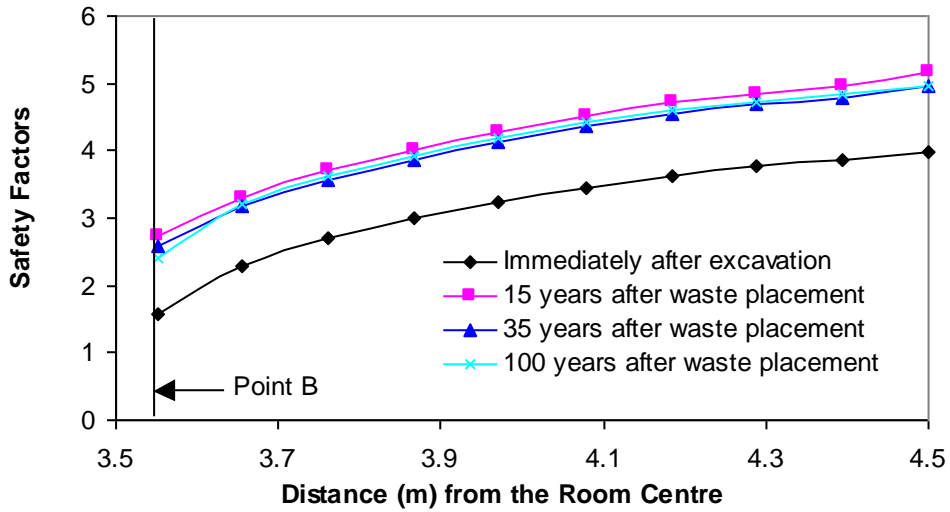


Figure 88: Safety Factors along Line L at Four Different Times (see Figure 47 for locations)

Safety factors along Line T at four different times are illustrated in Figure 89. The safety factor is 0.92 near the in-floor borehole wall immediately after excavation. There is about a 12-mm-thick layer of rock near the borehole with a safety factor of less than 1.0. This means that the in-floor borehole excavation would cause damage in the rock near the borehole wall. This damage would result in decreased strength available during heating. Since the safety factor after waste placement is also less than one near the borehole wall. It is likely that rock instability would result. The stress acting on the rock near the borehole wall would be transferred to the rock further from the borehole wall possibly causing progressive failure.

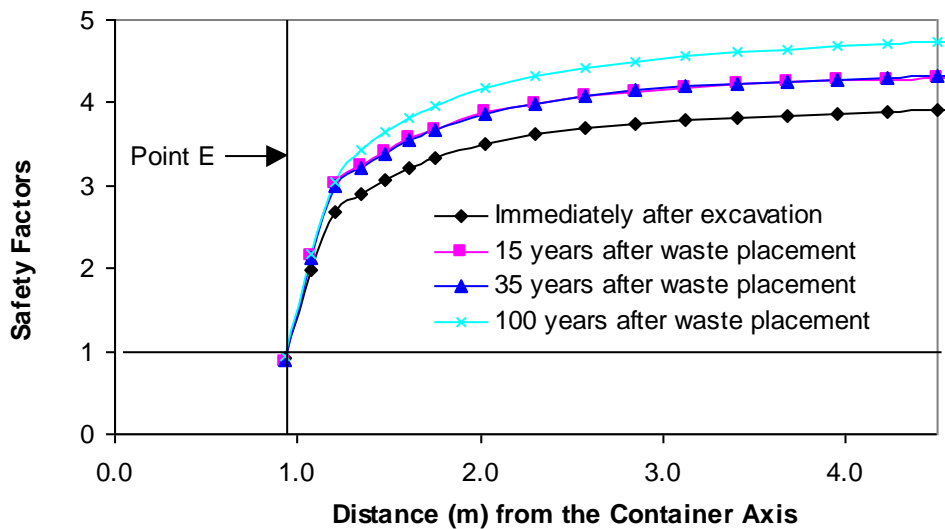


Figure 89: Safety Factors along Line T at Four Different Times (see Figure 47 for locations)

Safety factors along Line N at four different times are shown in Figure 90. The safety factor at the borehole wall is also less than one both after excavation and after waste placement. This damage implies that there is a certain thickness (about 0.04 m) of rock that is not stable. Instability of the rock during heating would result in stress redistribution and progressive failure of the rock further from the borehole wall.

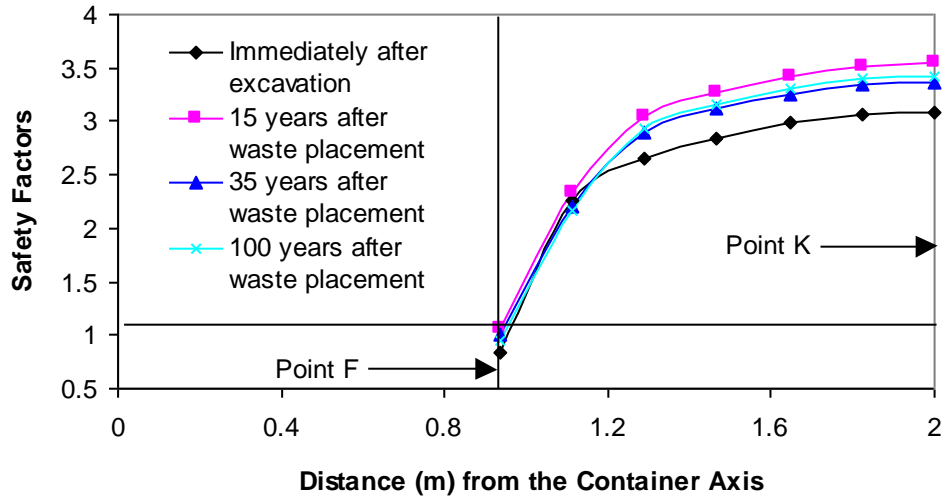


Figure 90: Safety Factors along Line N at Four Different Times (see Figure 47 for locations)

Safety factors along Line CJ at four different times are shown in Figure 91. The safety factors at different times and different locations along Line CJ are everywhere less than 0.9. At the intersection between the in-floor borehole and the tunnel floor, the safety factor is as low as 0.5. This implies that there is a certain thickness of rock, which is not stable, and that the greatest potential for rock failure is where the in-floor borehole meets the tunnel. Due to symmetry, stresses below the tunnel before borehole drilling would be similar to stresses above the tunnel. From Figure 87, it can be observed that the rock at the bottom of the tunnel is not overstressed before excavation of the in-floor boreholes. Excavation of the in-floor borehole would cause the rock on the bottom between two in-floor boreholes to be unstable, which would cause progressive failure in the rock along the tunnel bottom. The analysis suggests that, for the stress and strength parameters and placement geometry used, a connected zone of damaged and fractured rock would exist along the length of the tunnel floor between the adjacent in-floor boreholes.

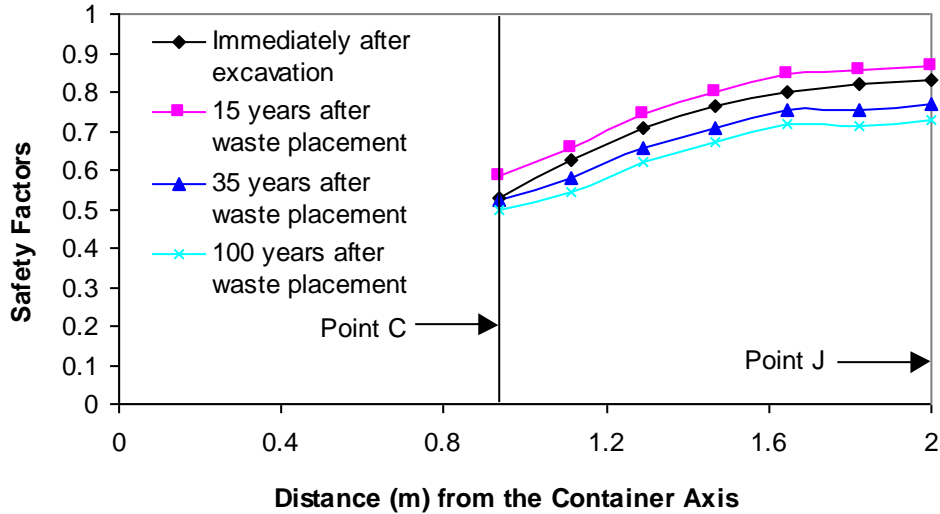


Figure 91: Safety Factors along Line CJ at Four Different Times (see Figure 47 for locations)

6. SUMMARY AND CONCLUSIONS

A series of three-dimensional finite element thermal transient and thermal-mechanical stress analyses is performed to gain a better understanding of the behaviour of the rock mass in the near-field and far-field of a disposal vault using an in-floor borehole placement method.

In order to compare the numerical modelling results using CODE_BRIGTH with results obtained by RWE NUKEM Limited using ABAQUS, a three-dimensional near-field model is established using the thermal load corresponding to the gross thermal load and a far-field model is established using the same repository dimensions used by RWE NUKEM Limited. The results of the modelling using CODE_BRIGTH match the results of the modelling using ABAQUS reasonably well for both the near-field and the far-field.

A coupled thermal-mechanical far-field three-dimensional model using the dimensions (horizontal dimensions for one quarter of a DGR are 695 m x 725 m) for an in-floor borehole placement method is established. Based on this modelling, the following conclusions can be drawn.

- Given an initial temperature of 17°C for a DGR at 1,000 m depth, the calculated peak temperature is 62°C at the centre of a repository, 41°C at the centre of an edge, and 30°C at the corner of a repository. The time to reach the peak temperature is 4,200 years after waste placement.
- The maximum thermally induced uplift at the ground surface above the centre of the repository is 0.2 m. The time to reach the peak uplift is 8,000 years after waste placement.

A thermal far-field model of a smaller repository with horizontal dimensions of 560 m x 600 m (for one quarter of a DGR), having the same total thermal load as the larger DGR in the previous analysis, is established. In this model, the thermal load density is equivalent to the

panel thermal load, while the load in the previous analysis is equivalent to the gross thermal load. The smaller DGR represents the dimensions of the larger DGR with the non-heat-generating area removed. A third thermal far-field model with the same thermal load density as the smaller DGR (i.e., the panel thermal load) is established to represent a horizontally infinite repository. The thermal results are compared between the two far-field models. The peak difference of the temperatures between the two models is 42°C approximately 30,000 years after waste placement. At the centre of the repository, the results derived from two models are the same for the first 1,000 years after waste placement, indicating that the results from near-field modelling using the boundary conditions that represents a repository with infinite horizontal extent can be used to determine the temperature results for a finite repository for times less than 1,000 years.

A near-field model (i.e., a model for a repository of infinite horizontal extent) is used to simulate the temperatures for 1,000,000 years following waste placement. The thermal results for the volume very near the container from this near-field modelling are modified to represent the results for a finite repository by subtracting the differences between the results from the far-field models for a finite repository and for an infinite repository. The modified results show that the container skin has a peak temperature of 89°C at 26 years after waste placement and a second level peak temperature of 84°C at 3,000 years after waste placement. Modified temperatures for other selected points near the container are also obtained for a million years to obtain a better estimate of temperature in the near-field of a finite repository. It should be noted that to correct the near-field (i.e., a DGR with infinite horizontal extent) modelling results to be representative of a DGR of finite horizontal extent, the two far-field models (i.e., infinite and finite horizontal extent) must be run for the specific repository conditions and dimensions.

It is recommended that the HOTROK program, which provides an exact solution for a single rock material and conservative estimates for the inclusion of sealing materials, be employed to conduct a rapid and independent thermal analysis of deep geological repository using an in-floor borehole placement method, for comparison with the modified temperatures shown in this report.

A coupled near-field thermal-mechanical model is also conducted for the first 100 years after waste placement. The stability of the rock mass is evaluated using the Hoek and Brown empirical failure criterion. Excavation of the room tunnel would not cause any failure in the rock near the tunnel. However, drilling placement boreholes in the floor of the tunnel would cause the wall of the boreholes and the rock on the bottom of the tunnel between two adjacent boreholes to become unstable.

The greatest thermally induced stresses in the rock occur 3,600 years after waste placement when the DGR temperature is the highest. Further work will be required to determine how to model the thermally induced mechanical response for the near-field modelling beyond 800 years due to the numerical issues associated with applying boundary conditions for a finite repository in a near-field model.

ACKNOWLEDGEMENTS

AECL technical reviews from P. Baumgartner, A. Man and D. Priyanto and NWMO review from N. Chandler and G. Simmons are appreciated.

REFERENCES

- Acres Consulting Services Limited in conjunction with RE/SPEC Ltd. 1985. A feasibility study of the multilevel vault concept. Atomic Energy of Canada Limited Technical Report, TR-297. Chalk River, Ontario.
- Acres Consulting Services Ltd. 1993. A preliminary study of long-hole emplacement alternatives. Atomic Energy of Canada Limited Technical Report, TR-346. Chalk River, Ontario.
- Atomic Energy of Canada Limited (AECL). 1994. Environmental impact statement on the concept for disposal of Canada's nuclear fuel waste. Atomic Energy of Canada Limited Report, AECL-10711, COG-93-1. Chalk River, Ontario.
- Baumgartner, P., D.M. Bilinsky, C. Onofrei, Y. Ates, F. Bilsky, J.L. Crosthwaite and G.W. Kuzyk. 1995. The in-room emplacement method for a used fuel disposal facility – preliminary design considerations. AECL Technical Record TR-655, COG-94-533. Chalk River, Ontario.
- Birgersson, L., K. Pers and M. Wilborgh. 2001. Project jade: long-term function and safety comparison of repository systems prepared by Kemakta Konsult AB for Swedish Nuclear Fuel and Waste Management Company (SKB). SKB Technical Report TR-01-18. Stockholm, Sweden.
- CTECH. 2002. Deep geologic repository design update. CTECH Report 1106/MD18085/REP/01, Issue 1. (Available at www.nwmo.ca)
- Golder Associates Ltd. 1993. Used-fuel disposal vault far-field thermal and thermalmechanical analysis. Atomic Energy of Canada Limited Report, TR-M-015. Chalk River, Ontario.
- Hoek, E. and E.T. Brown. 1980. Underground Excavation In Rock. The Institute of Mining and Metallurgy, London.
- Hoek, E. and E.T. Brown. 1988. The Hoek-Brown failure criterion – a 1988 update. 15th Canadian Rock Mechanics Symposium, Toronto, Canada.
- Maak, P. 2006. Used fuel container requirements. OPG Document Number 06819-PDR-01110-10000 R02. Ontario Power Generation. Toronto, Ontario.
- Martin, C.D. 1993. The strength of massive Lac du Bonnet granite around underground openings. Ph.D. Thesis, Department of Civil and Geotechnical Engineering, University of Manitoba, Winnipeg, Manitoba, Canada.
- Mathers, W.G. 1985. HOTROK, A program for calculating the transient temperature field from an underground nuclear waste disposal vault. Atomic Energy of Canada Limited Technical Record, TR-336. Chalk River, Ontario.

- NRCan (Natural Resources Canada). 2007. Canada's nuclear future: Clean, safe responsible. Natural Resources Canada news release 2007/50, June 14, 2007. (Available at www.nrcan-rncan.gc.ca/media/newsrelease/2007/200750.e.htm).
- NWMO. 2005. Choosing a way forward. The future management of Canada's used nuclear fuel. Final study. Nuclear Waste Management Organization . (Available at www.nwmo.ca).
- Olivella, S., A. Gens, J. Carrera and E.E. Alonso. 1996. Numerical modelling for a simulator (CODE_BRIGHT) for the coupled analysis of saline media. *In* Engineering Computations, Vol. 13, No. 7, pp. 87-112.
- RWE NUKEM Limited. 2003a. Deep geologic repository in-floor borehole emplacement – Design changes from the in-room emplacement concept. RWE NUKEM Report 89125/REP/02.
- RWE NUKEM Limited. 2003b. Deep geologic repository in-floor borehole design update – Finite Element Analyses. RWE NUKEM Report 80115/REP/01.
- Tsai, A. 1986. Far-field thermal transient analyses for a used fuel disposal vault. Report No. GHED-DR-8612, Geotechnical and Hydraulic Engineering Dept., Ontario Hydro. Toronto, Ontario.
- Tsui, K.K., and A. Tsai. 1982. Near-field thermal and stress analyses for immobilized waste and irradiated fuel disposal vaults in crystalline hard rock. Ontario Hydro Report No. 82575. Toronto, Ontario.
- Tsui, K.K. and A. Tsai. 1985. Thermal analyses for different options of nuclear fuel waste placement. Atomic Energy of Canada Limited Report, AECL-7823. Chalk River, Ontario.
- Tsui, K.K. and A. Tsai. 1994a. Three dimensional thermal and thermomechanical analyses for the near-field of a disposal vault with the borehole emplacement option. Ontario Hydro Nuclear, Report No: N-03788-940014 (UFMED). Toronto, Ontario.
- Tsui, K.K. and A. Tsai. 1994b. Three-dimensional thermal and thermomechanical analyses for the near-field of a disposal vault with an in-room emplacement option. Ontario Hydro Nuclear, Report No: N-03788-940015 (UFMED). Toronto, Ontario.
- Tsui, K.K. and A. Tsai. 1994c. The effects of sequential excavation during the construction of a disposal vault with the borehole emplacement option. Ontario Hydro Nuclear, Report No: N-03788-940016 (UFMED). Toronto, Ontario.
- Wai, R.S.C. and A. Tsai. 1995. Three-dimensional thermal and thermal-mechanical analyses for a used-fuel disposal vault with the in-room emplacement option. Ontario Hydro Report No. N-REP-03780-0083 R00 (UFMED). Toronto, Ontario.